

1 Rabies virus with a destabilization domain added to its nucleoprotein spreads between 2 neurons only if the domain is removed

3
4 Lei Jin¹, Makoto Matsuyama¹, Heather A. Sullivan¹, Mulangma Zhu¹, Thomas K. Lavin¹,
5 YuanYuan Hou¹, Nicholas E. Lea¹, Maxwell T. Pruner¹, María Lucía Dam Ferdínez¹, and Ian R.
6 Wickersham^{1*}

7
8 ¹McGovern Institute for Brain Research, Massachusetts Institute of Technology, Cambridge, MA
9

10 11 **ABSTRACT**

12
13 Monosynaptic tracing using rabies virus is an important technique in neuroscience, allowing brain-
14 wide labeling of neurons directly presynaptic to a targeted neuronal population. A 2017 article
15 reported development of a noncytotoxic version – a major advance – based on attenuating the
16 rabies virus by addition of a destabilization domain to the C-terminus of a viral protein. However,
17 this modification did not appear to hinder the ability of the virus to spread between neurons. We
18 analyzed two viruses provided by the authors and show here that both were mutants that had lost
19 the intended modification, explaining the paper's paradoxical results. We then made a virus that
20 actually did have the intended modification and found that it did not spread under the conditions
21 described in the original paper – namely, without an exogenous protease being expressed in
22 order to remove the destabilization domain – but that it did spread, albeit with relatively low
23 efficiency, if the protease was supplied. We conclude that the new approach is not robust but that
24 it may become a viable technique given further optimization and validation.
25

26 27 **SIGNIFICANCE STATEMENT**

28
29 Rabies virus, which spreads between synaptically connected neurons, has been one of the
30 primary tools used by neuroscientists to reveal the organization of the brain. A new modification
31 to rabies virus was recently reported to allow the mapping of connected neurons without adverse
32 effects on the cells' health, unlike earlier versions. Here we show that the conclusions of that study
33 were probably incorrect and based on having used viruses that had lost the intended modification
34 because of mutations. We also show that a rabies virus that does retain the intended modification
35 does not spread between neurons under the conditions reported previously; however, it does
36 spread between neurons under different conditions, suggesting that the approach may be
37 successful if refined further.
38

39 40 **INTRODUCTION**

41
42 Viruses have become important tools for neuroscience(1-16), and "monosynaptic tracing" based
43 on rabies virus (5) has become the primary method of labeling neurons directly presynaptic to
44 some targeted group of neurons (17-20). Its core components are, first, selective infection of the
45 targeted neuronal group with a recombinant rabies virus with a deleted gene (which in all work
46 published to date is the "G" gene encoding the glycoprotein that coats the viral envelope) and,
47 second, complementation of the deletion in the targeted starting neurons, by expression of the
48 deleted gene in *trans*. With all of its gene products therefore present in the starting cells, the virus
49 can fully replicate within them and spreads, as wild-type rabies virus does, to cells directly
50 presynaptic to the initially infected neurons. Assuming that G has not been provided in *trans* in
51 these presynaptic cells too, the deletion-mutant ("ΔG", denoting the deletion of G) virus is unable

52 to spread beyond them, resulting in labeling of just the neurons in the initially targeted population
53 and ones that are directly presynaptic to them (5).

54 A drawback of these ΔG (or "first-generation" (21)) rabies viruses is that they are cytotoxic
55 (4, 21, 22), which has spurred several labs to develop less toxic versions. Reardon, Murray, and
56 colleagues (22) showed that simply using ΔG rabies virus of a different parent strain — switching
57 from the original SAD B19 strain to the more neuroinvasive CVS N2c strain (23) — decreased
58 toxicity and increased the efficiency of transneuronal spread. Our own group has taken a more
59 drastic approach, recently introducing "second-generation" rabies viruses from which both G and
60 a second gene, "L", encoding the viral polymerase, have been deleted (21). Although in our
61 published work we have only shown that these second-generation, " ΔGL " viruses are efficient
62 means of direct retrograde targeting of projection neurons, it is at least theoretically possible for
63 ΔGL viruses to be used for monosynaptic tracing, if the second deleted gene were also expressed
64 in *trans*.

65 Taking a quite different approach, Ciabatti et al. (24) introduced "self-inactivating rabies"
66 ("SiR") viruses, which differed from simple first-generation (ΔG , SAD B19 strain) ones by the
67 addition of a destabilization domain to the C-terminus of one of the viral proteins, so that the
68 protein would be rapidly degraded soon after it was produced. Because the protein in question
69 (the nucleoprotein, encoded by the "N" gene) is essential for viral gene expression and replication,
70 its destabilization was intended to "silence" viral gene expression and prevent replication, making
71 the viruses nontoxic.

72 These SiR viruses were designed to be unable to replicate unless an exogenous protease
73 (tobacco etch virus protease, TEVP) was expressed in infected cells in order to remove the
74 destabilization (or "PEST" (25)) domain. However, the paper reported that they were able to
75 spread between neurons – which requires replication – just as efficiently as unmodified first-
76 generation viruses did, without the protease being provided at all.

77 We hypothesized that the viruses that were used for the reported transsynaptic tracing
78 experiments (24) were mutants with premature stop codons at or near the end of the native
79 nucleoprotein gene and before the sequence of the destabilization domain. Rhabdoviruses have
80 high mutation rates (26-31), and production of high-titer rabies virus stocks for *in vivo* injection
81 typically involves repeated passaging on complementing cell lines (32-34), which affords ample
82 opportunity for accumulation of mutants with a selective replication advantage.

83 Here we show that, in both of the two SiR virus samples that we analyzed, the great
84 majority of viral particles did have mutations in their genomes that caused the complete loss of
85 the intended C-terminal addition to the nucleoprotein, so that they were effectively just ordinary
86 first-generation ΔG rabies viral vectors. We also tested the SiR-CRE virus *in vivo* and found that
87 it was rapidly cytotoxic.

88 We also show that a ΔG virus that does have the intended modification to the
89 nucleoprotein does not spread transsynaptically *in vivo* in the absence of TEVP, but that it does
90 spread when TEVP is provided, although with lower efficiency than a virus without the
91 modification.

92
93

94 RESULTS

95
96 We analyzed samples of two viruses sent directly from the Tripodi lab to MIT two months
97 after their publication(24) and given directly to the Wickersham lab soon afterward, still frozen and
98 unopened, with express permission from Marco Tripodi by email on December 5, 2017:
99 "EnvA/SiR-CRE" (made from genome plasmid Addgene 99608, pSAD-F3-NPEST-iCRE-2A-
100 mCherryPEST) and "EnvA/SiR-FLPo" (made from genome plasmid Addgene 99609, pSAD-
101 F3-NPEST-FLPo-2A-mCherryPEST). Both had the SAD B19 strain of rabies virus as their parent

102 strain and had been packaged with the avian and sarcoma virus subgroup A envelope
103 glycoprotein ("EnvA") for targeted infection of cells expressing EnvA's receptor, TVA (5).

104 For comparison with the two SiR viruses, we made five control viruses in our own
105 laboratory: three first-generation vectors, RV Δ G-4Cre (21), RV Δ G-4FLPo (see Methods), and
106 RV Δ G-4mCherry (35), and two second-generation vectors, RV Δ GL-4Cre and RV Δ GL-4FLPo
107 (21). All of these viruses are on the SAD B19 background, like the SiR viruses. For each of the
108 four recombinase-expressing viruses from our laboratory, we made one preparation packaged
109 with the EnvA envelope protein and one preparation packaged with the native rabies virus (SAD
110 B19 strain) glycoprotein (denoted as "B19G"); RV Δ G-4mCherry (used only as a control for the
111 Sanger sequencing) was only packaged with the EnvA envelope protein.

113 Sequencing of viral genomes: Sanger sequencing

114
115 In order to directly test our hypothesis that the SiR viruses had developed premature stop
116 codons removing the PEST domain in a majority of viral particles, we sequenced the genomes of
117 a large number of individual viral particles using two different techniques.

118 First, we used ordinary Sanger sequencing to determine the sequence in the vicinity of
119 the end of the nucleoprotein gene for 50 to 51 individual viral particles of each of the two SiR
120 viruses and of a first-generation virus from our own laboratory, RV Δ G-4mCherry (Figure 1 and
121 Supplementary File S1). We ensured the isolation of individual viral genomes by using a primer
122 with a random 8-base index for the reverse transcription step, so that the cDNA copy of each RNA
123 viral genome would have a unique index. Following the reverse transcription step, we amplified
124 the genomes by standard PCR, cloned the amplicons into a generic plasmid, transformed this
125 library into E.coli and sequenced plasmids purified from individual colonies.

126 As shown in Figure 1, the results confirmed our hypothesis that SiR viruses are prone to
127 loss of the 3' addition to the nucleoprotein gene. Specifically, in the SiR-CRE sample, 100% of
128 the 51 sequenced viral particles had lost the PEST domain. Fifty out of the 51 had the same point
129 mutation in the linker between the end of the native nucleoprotein gene and the TEVP cleavage
130 site, converting a glycine codon (GGA) to a stop codon (TGA) so that the only modification to the
131 C-terminus of the nucleoprotein was the addition of two amino acids (a glycine and a serine). The
132 one sequenced viral particle that did not have this point mutation had a single-base insertion in
133 the second-to-last codon of the native nucleoprotein gene, frameshifting the rest of the sequence
134 and resulting in 15 amino acids of nonsense followed by a stop codon before the start of the PEST
135 domain sequence.

136 In the SiR-FLPo sample, the population was more heterogeneous: out of 50 sequenced
137 viral particles, 18 had the same stop codon that was found in almost all genomes in the Cre
138 sample, while another 28 had a different stop codon three amino acids upstream, immediately at
139 the end of the native nucleoprotein gene (converting a serine codon (TCA) to a stop codon (TGA)).
140 Four viral particles had no mutations in the sequenced region. Thus 46/50 (92%) of the SiR-FLPo
141 viral particles sequenced had lost the PEST domain.

142 In contrast, in the first-generation virus from our own lab, RV Δ G-4mCherry, none of the 50
143 viral particles sequenced had mutations in the sequenced region containing the end of the
144 nucleoprotein gene.

146 Sequencing of viral genomes: Single-molecule, real-time (SMRT) sequencing

147
148 As a second approach to analyzing the mutations present in the SiR viruses, we employed
149 a large-scale sequencing technology: single-molecule, real-time ("SMRT") sequencing, which
150 provides independent sequences of tens of thousands of individual single molecules in a sample
151 in parallel (Figure 2 and Supplementary File S2). The results from this advanced sequencing
152 method were quite consistent with the results from the Sanger sequencing presented above. As

153 with the sample preparation for Sanger sequencing, we included a random index (10 bases, in
154 this case) in the reverse transcription primer, so that again the cDNA copy of each RNA viral
155 genome molecule would be labeled with a unique index.

156 SMRT sequencing entails circularization of the DNA amplicons and multiple consecutive
157 passes around the resulting circular molecule, with the redundancy provided by this repeated
158 sequencing of each position increasing the signal to noise ratio and statistical significance of the
159 results. The numbers presented in Figure 2 and below use the default of including only clones
160 that had at least three reads of each base ("circular consensus sequence 3", or "CCS3" in
161 Supplementary File S2). Using the increasingly stringent criteria of requiring either five or eight
162 reads per base (CCS5 or CCS8) reduced the numbers of qualifying genomes in all cases and
163 changed the percentages slightly but gave very similar results overall. Because read accuracy for
164 SMRT sequencing is $\geq 98\%$ for circular consensus sequencing with 3 passes (see
165 [https://www.mscience.com.au/upload/pages/pacbio/technical-note---experimental-design-for-](https://www.mscience.com.au/upload/pages/pacbio/technical-note---experimental-design-for-targeted-sequencing.pdf)
166 [targeted-sequencing.pdf](https://www.mscience.com.au/upload/pages/pacbio/technical-note---experimental-design-for-targeted-sequencing.pdf)), we used a conservative threshold of 2% frequency of any given point
167 mutation position in order to screen out false positives. Also to be very conservative, for Figure 2
168 we ignored all apparent frame shifts caused by insertions and deletions, because insertions in
169 particular are prone to false positives with SMRT sequencing (36). See Supplementary File S2
170 for details, including details of frameshifts due to insertions; Supplementary Files S3-S5 contain
171 the sequences of the PCR amplicons that would be expected based on published sequences of
172 the three viruses, but to summarize here:

173 As a control, we used a virus from our own laboratory, RV Δ G-4Cre (21) (see Addgene
174 #98034 for reference sequence). Out of 17,978 sequenced genomes of this virus, we found no
175 mutations above threshold frequency at the end of N. We did find that 1,706 viral particles (9.49%)
176 had a nonsynonymous mutation (TCT (Ser) \rightarrow ACT (Thr)) farther up in N at amino acid position
177 419 (31 amino acids upstream of the end of the 450-aa native protein). We do not know if this
178 mutation is functionally significant, although it is not present in CVS N2c (37), HEP-Flury (38),
179 ERA (39), or Pasteur strains (Genbank GU992320), so these particles may effectively be N-
180 knockouts that were propagated by coinfection with virions with intact N (see Discussion for more
181 on such parasitic co-propagating mutants).

182 For the SiR-CRE virus, out of 22,205 viral genomes sequenced, 22,032 had the premature
183 stop codon (GGA \rightarrow TGA) in the linker between the native nucleoprotein gene and the TEVP
184 cleavage site sequence. In other words, even without including frameshifts, at least 99.22% of
185 the individual viral particles in the SiR-CRE sample were essentially first-generation Δ G vectors,
186 with the only modification of the nucleoprotein being an additional two amino acids at the C-
187 terminus.

188 For the SiR-FLPo virus, out of 17,086 viral genomes sequenced, 5,979 had the stop codon
189 (GGA \rightarrow TGA) in the linker, 8,624 had the stop codon (TCA \rightarrow TGA) at the end of N, and a further
190 28 had a different stop codon (TCA \rightarrow TAA) at the same position at the end of N. Of these, 305
191 viral particles had premature stop codons at both of these two positions, so that the total number
192 of viral particles with one or both stop codons immediately before the PEST domain was (8624 +
193 5979 + 28 - 305 = 14,326. In other words, again even without including frameshifts, at least
194 83.85% of the individual viral particles in the SiR-FLPo sample were essentially first-generation
195 Δ G vectors, with the only modification of the nucleoprotein being either two amino acids added
196 to, or one amino acid lost from, the C-terminus.

197 198 **Anti-nucleoprotein immunostaining**

199
200 We infected reporter cell lines with serial dilutions of the two EnvA-enveloped SiR viruses
201 as well as the eight recombinase-expressing ones from our own lab: Δ G vs. Δ GL, Cre vs. FLPo,
202 EnvA vs. B19G envelopes. Three days later, we immunostained the cells for rabies virus
203 nucleoprotein and imaged the cells with confocal microscopy.

204 As seen in Supplementary Figure S1, we found that the cells infected with the SiR viruses
205 looked very similar to those infected with the first-generation, ΔG viruses. Notably, the viral
206 nucleoprotein, which in the SiR viruses is intended to be destabilized and degrade rapidly in the
207 absence of TEVP, accumulated in the SiR-infected cells in clumpy distributions that looked very
208 similar to those in the cells infected with the first-generation, ΔG viruses. By contrast, the cells
209 infected with the second-generation, ΔGL viruses, which we have shown to be noncytotoxic (21),
210 did not show any such nucleoprotein accumulation, clumped or otherwise, only punctate labeling
211 presumably indicating isolated viral particles or post-infection uncoated viral particles
212 (ribonucleoprotein complexes) that are not replicating.

213

214 **Longitudinal two-photon imaging *in vivo***

215

216 To see whether the SiR viruses kill neurons in the brain, we conducted longitudinal two-
217 photon imaging *in vivo* of virus-labeled neurons in visual cortex of tdTomato reporter mice, as we
218 had done previously to demonstrate the nontoxicity of second-generation rabies virus (21) (Figure
219 3). Because the SiR viruses were EnvA-enveloped, we first injected a lentivirus expressing EnvA's
220 receptor TVA, then one week later we injected either SiR-CRE or one of two EnvA-enveloped
221 viruses made in our laboratory: the first-generation virus RV ΔG -4Cre(EnvA) or the second-
222 generation virus RV ΔGL -4Cre(EnvA). Beginning one week after rabies virus injection, we imaged
223 labeled neurons at the injection site every seven days for four weeks, so that we could track the
224 fate of individual neurons over time.

225 As we found in our previous work (21), our second-generation virus RV ΔGL -4Cre did not
226 kill neurons to any appreciable degree: all but a tiny handful of the neurons labeled by this virus
227 at seven days after injection were still present three weeks later in all mice. Also as we have found
228 previously (21), our first-generation virus RV ΔG -4Cre did kill neurons, but by no means all of them
229 (see the Discussion for possible reasons for this).

230 However, we found that the putatively nontoxic SiR-CRE caused a steep loss of neurons
231 much more pronounced than even our first-generation virus did. By 14 days after injection, 70%
232 of cells seen at seven days were dead; by 28 days, 81% were.

233 There is a possible confound from our use of the tdTomato reporter line Ai14 (which we
234 used primarily because we already had large numbers of mice of this line): because SiR-CRE is
235 actually "SiR-iCRE-2A-mCherryPEST", designed to coexpress mCherry (with an added C-
236 terminal PEST domain intended to destabilize it, as for the nucleoprotein) along with Cre, it is
237 conceivable that some of the SiR-CRE-labeled red cells at seven days were only expressing
238 mCherry and not tdTomato. If the destabilized mCherry were expressed only transiently, as
239 intended(24), and a significant fraction of SiR-CRE virions had mutations in the Cre gene so that
240 they did not express functioning Cre, then it is possible that some of the red cells seen at seven
241 days were labeled only with mCherry that stopped being visible by 14 days, so that it would only
242 look like those cells had died.

243 We viewed this alternative explanation as unlikely, because the designers of SiR-CRE
244 had injected it in an EYFP reporter line and found no cells labeled only with mCherry and not
245 EYFP at six days and nine days postinjection (see Figure S4 in Ciabatti et al. (24)). Nevertheless,
246 we addressed this potential objection in several ways.

247 First, we sequenced the transgene inserts (iCre-P2A-mCherryPEST) of 21 individual SiR-
248 CRE viral particles (see Supplementary File S6) and found that only two out of 21 had mutations
249 in the Cre gene, suggesting that there would not have been a large population of cells only labeled
250 by mCherry and not by tdTomato.

251 Second, we repeated some of the SiR-CRE injections and imaging in a different reporter
252 line: Ai35, expressing Arch-EGFP-ER2 after Cre recombination (40) (Jax 012735). Although we
253 found that the membrane-localized green fluorescence from the Arch-EGFP-ER2 fusion protein
254 was too dim and diffuse at seven days postinjection to be imaged clearly, we were able to obtain

255 clear images of a number of cells at 11 days postinjection. We found that 46% of them had
256 disappeared only three days later (see Supplementary Figure S2 and Supplementary Video S1),
257 and 86% had disappeared by 28 days postinjection, consistent with a rapid die-off. Furthermore,
258 we found that the red fluorescence in Ai35 mice, which was due only to the mCherry expressed
259 by the virus, was much dimmer than the red fluorescence in Ai14 mice at the same time point of
260 seven days postinjection and with the same imaging parameters (see Supplementary Figure S3):
261 the mean intensity was 45.86 (arbitrary units, or "a.u.") in Ai14 but only 16.29 a.u. in Ai35. This is
262 consistent with the published findings that tdTomato is a much brighter fluorophore than mCherry
263 (41), particularly with two-photon excitation (42), and it is also consistent with Ciabatti et al.'s
264 addition of a destabilization domain to mCherry's C-terminus. We therefore redid the counts of
265 labeled cells in our Ai14 datasets to include only cells with fluorescence at seven days of more
266 than 32.33 a.u., the midpoint of the mean intensities in Ai35 versus Ai14 mice, in order to exclude
267 neurons that might have been labeled with mCherry alone. As seen in Supplementary Figure S4,
268 restricting the analysis to the cells that were brightest at seven days (and therefore almost
269 certainly not labeled with just mCherry instead of either just tdTomato or a combination of both
270 mCherry and tdTomato) made no major difference: 70.0% of SiR-labeled neurons had
271 disappeared by 14 days, and 80.8% were gone by 21 days.

272 Although in theory it is possible that the disappearance of the infected cells could be due
273 to cessation of tdTomato or Arch-EGFP-ER2 expression rather than to the cells' deaths, because
274 of downregulation by rabies virus of host cell gene expression (43), we view this as highly unlikely.
275 Downregulation of host cell gene expression by rabies virus is neither total ("cells with high
276 expression of RbV transcripts retain sufficient transcriptional information for their classification
277 into a specific cell type." (43)) nor uniform (44); in practice, we saw no evidence of a decline in
278 reporter expression in the infected cells but in fact found the exact opposite. As can be seen in a
279 number of cells in Figures 3 and S4, the cells got brighter and brighter over time, unless they
280 abruptly disappeared. In our experience, including in this case, cells infected with rabies virus
281 increase in brightness until they die, often blebbing and coming apart into brightly labeled pieces,
282 regardless of whether the fluorophore is expressed from a reporter allele (as in this case) or
283 directly by the virus (see Chatterjee et al. 2018 for many more examples of this (21)).

284

285 **Construction and testing of a virus with an intact PEST domain**

286

287 We decided to directly test whether a rabies virus with an intact PEST domain fused to its
288 nucleoprotein can spread transsynaptically, with or without TEVP (Figure 4). Beginning with our
289 lab's first-generation virus RV Δ G-4Cre(21), we constructed a "self-inactivating" version, "RV Δ G-
290 NPEST-4Cre", by adding the coding sequence for the C-terminal addition from Ciabatti et al.(24)
291 to the 3' end of the nucleoprotein gene. To reduce the chance of the PEST domain being lost to
292 nonsense mutations during production of the virus, we made synonymous changes to five codons
293 near the junction of the end of the native nucleoprotein gene and the beginning of the addition,
294 so that those codons were no longer a single mutation away from being stop codons; apart from
295 these five synonymous changes, the nucleotide sequence of the addition was identical to that
296 used by Ciabatti et al.(24) (Figure 4A). We also made a matched "revertant" version, "RV Δ G-
297 N*PEST-4Cre", with exactly the same sequence as RV Δ G-NPEST-4Cre except with a stop codon
298 three codons into the linker, at the same location as the stop codon that we had found in the
299 overwhelming majority of viral particles in the original SiR-CRE. While the genomes of these two
300 new viruses only differed from each other by one codon, therefore, at the protein level one virus
301 (RV Δ G-NPEST-4Cre) had a full-length PEST domain on the end of its nucleoprotein, while the
302 other (RV Δ G-N*PEST-4Cre) had only a two-amino-acid (Gly-Ser) addition to the end of its
303 nucleoprotein and otherwise was an ordinary first-generation Δ G virus.

304 Following production of high-titer EnvA-enveloped virus (see Methods), we confirmed that
305 the final stocks retained the intended 3' additions to the nucleoprotein gene by extracting the

306 genomic RNA and used Sanger sequencing on the genomes of 32 viral particles for each virus.
307 All of the clones sequenced for each of the two viruses had the respective intended modifications
308 (Figure 4, panel A; details in Supplementary File S7), except for one N*PEST clone that had a
309 synonymous mutation in the PEST domain after the introduced stop codon (and that was
310 therefore irrelevant. We also found three other incidental mutations in one clone each: one
311 NPEST clone had a synonymous mutation in the nucleoprotein gene (at Ser437, from TCA to
312 TCG), one N*PEST clone had a different synonymous mutation in the nucleoprotein gene (at
313 Asn436, from AAC to AAT), and one NPEST clone had a single point mutation in the intergenic
314 region between the N and P genes).

315 Having verified that the NPEST and N*PEST viruses retained their respective
316 modifications, we tested their ability to spread transsynaptically *in vivo* in the absence of TEVP,
317 using corticostriatal neurons as the starting cells (Figure 4, panel B). We injected an AAV2-
318 retro(11) expressing FLPo into the dorsolateral striatum of three mice each of the tdTomato
319 reporter line Ai14(45), with a cocktail of two helper viruses (AAV1)(46-48) injected into the primary
320 somatosensory cortex (barrel field) in the same surgery. Corticostriatal neurons were therefore
321 coinfecting with all three viruses for expression of TVA (to allow infection by EnvA-enveloped RV)
322 and G (to allow spread of the Δ G viruses to presynaptic cells), as well as the fluorophores EGFP
323 (marking TVA expression) and mTagBFP2 (marking G expression). One week after AAV injection,
324 we injected either the NPEST or the N*PEST virus at equalized titers, then perfused the mice
325 either 12 days or 3 weeks after the rabies virus injections. Figure 4 and Supplementary Figure S5
326 show the results.

327 The N*PEST virus, which had only an additional two amino acids on the C-terminus of its
328 nucleoprotein, spread very efficiently (bottom rows of images in panels B and C, and rightmost
329 bar in each pair in the charts in panel E). We counted tdTomato-labeled neurons in ipsilateral
330 cortex as well as in thalamus and in contralateral cortex (note that we counted neurons only in
331 every sixth 50 μ m section (see Methods), so that the numbers of labeled neurons in the entire
332 brain of each mouse would be approximately six times the numbers given below and in the
333 figures). At 12 days, we found an average of 2,772 tdTomato-labeled neurons in ipsilateral cortex;
334 we also found an average of 12 labeled neurons in contralateral cortex and 40 in thalamus. At 3
335 weeks after rabies virus injection, a time point which is unusually long for a first-generation
336 virus(21) but which we included to match the duration used by Ciabatti et al.(24), the N*PEST
337 virus had spread to vastly more neurons: on average 13,070 in ipsilateral cortex, 253 in
338 contralateral cortex, and 507 in thalamus. Importantly, all this label was not due simply to leaky
339 TVA expression or residual RVG-enveloped virus, as control experiments without G resulted in
340 very minimal labeling (Supplementary Figure S7), but instead indicates efficient transsynaptic
341 spread of the N*PEST virus, consistent with our lab's prior experience with the parent virus RV Δ G-
342 4Cre(EnvA) as well as with other first-generation RV Δ G vectors.

343 In contrast, the NPEST virus, which had the intact PEST domain fused to its nucleoprotein,
344 showed no clear evidence of transsynaptic spread without TEVP at either time point examined
345 (top rows of images in panels C and D, and leftmost bar in each pair in the charts in panel E). At
346 12 days, we found averages of 10 labeled cells at the injection site, 2 in contralateral cortex, and
347 none at all in thalamus. At 3 weeks, the situation was not much different: we found averages of
348 30 labeled cells at the injection site, 0.333 in contralateral cortex, and still zero in thalamus. These
349 numbers were not significantly different from those in the matched controls without G, for which
350 the means at 12 days were 4.667, 0.667, and 0 (injection site, contralateral cortex, and thalamus,
351 respectively) and the means at 3 weeks were 12.333, 0, and 0. Single-factor ANOVAs were used
352 for all comparisons; all cell counts and results of statistical analyses are given in Supplementary
353 File S8.

354 We then tested the ability of the two viruses to spread when both TEVP and G are supplied
355 (Figure 5 and Supplementary Figure S6). These experiments were done in exactly the same way
356 as the ones without TEVP but with a third virus, AAV1-TREtight-H2b-emiRFP670-TEVP, included

357 in the helper virus mixture. This third helper virus was of the same design as the G-expressing
358 AAV (AAV1-TREtight-mTagBFP2-B19G) but expressed TEVP (S219V mutant) instead of G and
359 an H2b-fused near-infrared fluorescent protein (emiRFP670) instead of the blue fluorophore
360 mTagBFP2.

361 With both TEVP and G provided, the NPEST virus did show evidence of spread: at 12
362 days, there were on average 469 labeled cells in ipsilateral cortex, 5 in contralateral cortex, and
363 3 in thalamus; at 3 weeks, there were on average 1,257 in ipsilateral cortex, 4 in contralateral
364 cortex, and 18 in thalamus.

365 The N*PEST virus still labeled many more cells than the NPEST one did under these
366 conditions (panels C and D). At 12 days, the N*PEST virus had labeled on average 4.5 times as
367 many cells in ipsilateral cortex (2,090 cells), twice as many in contralateral cortex (10 cells), and
368 13.3 times as many in thalamus (40 cells); at 3 weeks, it had labeled 2.7 times as many cells in
369 ipsilateral cortex (3,397 cells), 9.3 times as many in contralateral cortex (37 cells), and 2.4 times
370 as many in thalamus (43 cells). While these differences were not found to be statistically
371 significant, the comparisons were presumably underpowered, due to the very low number of
372 subjects (n=3) we used per group, which was dictated by the limited availability of Ai14 mice.

373 Comparing the best conditions for the NPEST virus (that is, with TEVP provided) to the
374 best conditions for the N*PEST one (that is, without TEVP provided) gave very large and highly
375 significant differences for almost all comparisons (panels E and F). At 3 weeks, for example, the
376 N*PEST virus had labeled 10.3 times as many cells in ipsilateral cortex (averages of 13,070 vs
377 1,257; $p=0.000119$), 14.3 times as many in thalamus as the NPEST virus (252.6 vs 17.6;
378 $p=0.00433$), and 117.8 times as many cells in contralateral cortex (506.6 vs 4.3; $p=0.00550$).

379
380

381 DISCUSSION

382

383 Our transsynaptic tracing results using virus with an intact PEST domain contradict the earlier
384 claim that such a virus can spread between neurons in the absence of TEVP(24). Our findings
385 from sequencing the SiR viruses from the originating laboratory suggest that the reason for that
386 claim was that the viruses used in the original study had lost the intended modification.

387 While it is possible that the escape of the two SiR virus samples from the modification
388 intended to attenuate them was a fluke due to bad luck with those two batches, we view this as
389 unlikely, for three reasons. First, the reported finding that viral replication and spread occurred in
390 the absence of TEVP is difficult to understand in the absence of mutations but is easily explained
391 if the viral preparations used for those experiments harbored the kind of mutations that we found
392 in the two preparations to which we had access. Second, the two SiR virus samples that we
393 analyzed had independently developed mutations causing loss of the intended C-terminal addition
394 to the nucleoprotein; we know that the mutations were independent because the two samples
395 were of different viruses so did not both derive from a single compromised parental stock. Third,
396 the mutation profiles of the two viruses were very different: whereas the SiR-CRE sample had the
397 same point mutation in nearly 100% of its viral particles, only a minority of the SiR-FLPo particles
398 had that particular mutation, with the majority having a different point mutation three codons away
399 that had the same result. This suggests that any of the many opportunities for removing the C-
400 terminal addition — creation of a premature stop codon at any one of a number of sites, or a
401 frameshift mutation anywhere in the vicinity — can be exploited by a given batch of virus, greatly
402 increasing the probability of such mutants arising.

403 While it is clearly possible to make virus with the intended modification to the
404 nucleoprotein, because we have done so here (and the authors of the original paper also report
405 doing so, in a recent preprint (49) in response to our own preprint of an earlier version of this
406 paper), our findings suggest that the approach in its current form is vulnerable to being
407 undermined by viral mutation. Although a number of groups have made recombinant rabies

408 viruses — as well as other rhabdoviruses and other nonsegmented negative-strand RNA viruses
409 — encoding fusions of exogenous proteins to viral proteins (50-60), most of these groups have
410 found that the additions significantly impaired function, and some have found that the viruses
411 rapidly lost C-terminal additions to viral proteins. For example, an attempt to make SAD B19
412 rabies virus with EGFP fused to the C-terminus of the nucleoprotein was unsuccessful, suggesting
413 that large C-terminal additions make the nucleoprotein dysfunctional; the authors of that paper
414 resorted instead to making virus encoding the fusion protein in addition to the wild-type
415 nucleoprotein (53). A vesicular stomatitis virus with GFP fused to the C-terminus of the
416 glycoprotein gene lost the modification within a single passage of the virus because of a point
417 mutation creating a premature stop codon (50). Relatedly, a VSV with its glycoprotein gene
418 replaced with that of a different virus was found to quickly develop a premature stop codon
419 causing loss of the last 21 amino acids of the exogenous glycoprotein, conferring a marked
420 replication advantage to the mutants bearing the truncated version (61).
421 Generalizing from these prior examples as well as our findings here, we suggest that any attempt
422 to attenuate a virus by addition to the C-terminus of a viral protein will be vulnerable to loss of the
423 modification, and that any such virus will therefore need to be monitored very carefully.

424 It is unclear whether further improvements to the design of the viruses can be made to
425 make loss of the PEST domain less likely. Although the synonymous mutations that we made to
426 five codons near the junction of N and the 3' addition are a good start, there are numerous other
427 codons in the immediate vicinity that are also one point mutation away from being stop codons
428 but that do not have synonyms that are not. Furthermore, no such changes would protect against
429 frameshifts.

430 If the viruses used for the transsynaptic tracing experiments in the original paper were
431 actually de facto first-generation, ΔG viruses like the SiR samples that we analyzed, how could
432 the authors have found, in postmortem tissue, cells labeled by SiR-CRE that had survived for
433 weeks? The answer may simply be that, as we have shown in Chatterjee et al. (21) and again
434 here (Figure 3), and as the original authors also report in their new preprint (49), a preparation of
435 first-generation rabies viral vector expressing Cre can leave a large fraction of labeled cells alive
436 for at least months, in contrast to similar ones encoding tdTomato (21) or EGFP (4). Similarly,
437 Gomme et al. found long-term survival of some neurons following infection by a replication-
438 competent rabies virus expressing Cre (62)). Our results with the "revertant" control virus RV ΔG -
439 N*PEST-4Cre (Figures 4 and 5, and Supplementary Figures S5-S7), showing thousands of
440 labeled neurons three weeks after rabies virus injection, are consistent with this as well.

441 One reason, in turn, why a preparation of a simple ΔG rabies virus encoding Cre can leave
442 many cells alive may be that not all the virions are in fact first-generation viral particles, because
443 of the high mutation rate that we have highlighted in this paper. We have shown in Chatterjee et
444 al. (21) that a second-generation (ΔGL) rabies virus, which has both its glycoprotein gene G and
445 its polymerase gene L deleted, leaves cells alive for the entire four months that we followed them.
446 However, any first-generation (ΔG) virus that contains a frameshift or point mutation knocking out
447 L will in practice be a ΔGL virus. Indeed, a stop codon or frameshift mutation in any of several
448 other viral genes is likely to have a similar effect as one in L (and it might be that the Ser419Thr
449 mutation that we found in 9.49% of our RV ΔG -4Cre virions is just such a knockout mutation of N).
450 Together with the high mutation rate of rabies virus, this means that, within every preparation of
451 first-generation rabies virus there is almost guaranteed to be a population of de facto second-
452 generation variants mixed in with the intended first-generation population and propagated in the
453 producer cells by complementation by the first-generation virions. Any rabies virus preparation
454 (whether made in the laboratory or occurring naturally) can be expected to contain a population
455 of such knockout (whether by substitution, frameshift, or deletion) mutants (related to the classic
456 phenomenon of "defective interfering particles", or mutants with a marked replication advantage
457 (63-65), and the higher the multiplicity of infection when passaging the virus, the higher the
458 proportion of such freeloading viral particles typically will be. This would not necessarily be noticed

459 in the case of a virus encoding a more common transgene product such as a fluorophore, because
460 the expression levels of these by the knockout mutants would be too low to label cells clearly (see
461 Figure 1 in Chatterjee et al. (21)). However, with Cre as the payload, any "second-generation"
462 particles would be able to label neurons but not kill them, because second-generation rabies viral
463 vectors do not kill cells for at least months (21). This explanation would predict that the percentage
464 of neurons surviving infection with a rabies virus encoding Cre will depend on the particular viral
465 preparation that is injected, with some having a greater fraction of knockout particles than others.

466 This could explain why the SiR-CRE virus sample killed cells faster than our own RV Δ G-
467 4Cre (Figure 3). This analysis would also presumably apply to first-generation (Δ G) viruses
468 expressing FLPo: while we found that the FLPo-expressing version that we made did not leave
469 as many cells alive as the Cre-expressing version did (Supplementary Figure S8), that preparation
470 may simply have had fewer mutants with knockout of genes essential for replication.

471 On a positive note, we found that virus with an intact PEST domain does spread
472 between neurons when TEVP is supplied. This suggests that such viruses could in fact become
473 the basis for monosynaptic tracing systems with reduced toxicity. Our finding is complementary
474 to those of the original authors in their recent preprint (49) that an intact SiR virus did not kill
475 labeled neurons for five months: that study was of neurons directly infected by B19G-enveloped
476 virus (i.e., without using EnvA-enveloped virus, expression of TVA to mediate its selective
477 infection, expression of G to complement the Δ G virus, or expression of TEVP to remove the C-
478 terminal addition to the nucleoprotein); they did not show that their intact virus could spread
479 between neurons or that it is nontoxic as it does so. Conversely, we showed here that an intact
480 NPEST virus can spread between neurons, but we did not assay toxicity during this process. It
481 remains to be seen to what degree an NPEST or SiR virus that spreads transsynaptically is
482 cytotoxic, not only to transsynaptically-labeled cells but also to the starting cells, which need to
483 express both G and TEVP to allow replication and spread of the virus. This is not a trivial point,
484 as G is toxic when overexpressed (66), and the original authors' finding that cultured cells
485 rapidly lost TEVP activity (49) suggests that TEVP expressed at sufficient levels may be toxic as
486 well.

487 Although we found that the "intact" NPEST virus spread considerably less than that of
488 the "revertant" control virus, there may be room for improvement: the TEVP expression levels
489 that we engineered are unlikely to happen to be optimal, and the numbers of labeled neurons
490 could increase further with longer survival times. On the other hand, if overexpression of TEVP
491 causes toxicity (see above), increasing it beyond what we achieved could be deleterious.
492 Another consideration is the nine additional amino acids that are unavoidably left on the C-
493 terminus of the nucleoprotein after the rest of the addition is removed by TEVP: while these
494 additional amino acids may not much impair the function of the protein, they are unlikely to help
495 it.

496 It is also unclear to what degree a minority population of revertant mutants that did arise
497 in stocks of otherwise-intact virus would pose a problem for monosynaptic tracing studies. If, for
498 example, ~5% of the virions in a given preparation were revertant mutants (e.g., as the original
499 authors report obtaining after six passages in cells highly expressing TEVP (49)), one might
500 expect the same percentage of labeled presynaptic neurons to be labeled by those mutants and
501 therefore to experience the toxicity of infection by a first-generation, Δ G virus. However, because
502 the process of infecting the starter cells, replicating within them (if provided with G), and spreading
503 to other cells is comparable to an additional passage in cell culture, the percentage of presynaptic
504 cells labeled by the revertant mutants could be higher, and would presumably depend on the level
505 of TEVP expression in each starter cell.

506 In summary, our results suggest that rabies virus with a PEST domain added to its
507 nucleoprotein only spreads between neurons if the PEST domain is removed, whether by
508 expression of TEVP or by mutation. Our finding that virus with an intact PEST domain can spread
509 when TEVP is provided, as the designers had presumably originally intended, raises the

510 possibility that further optimization and validation could make the SiR approach a viable option
511 for monosynaptic tracing with reduced toxicity.

512

513

514 **SUMMARY OF METHODS (see Supplementary Methods for details)**

515

516 **Cloning**

517 The following novel plasmids were made using standard cloning techniques (see Supplementary
518 Methods): pLV-CAG-FLEX-BFP-(mCherry)' (Addgene 115234), pLV-CAG-F14F15S-BFP-
519 (mCherry)' (Addgene 115235), pLV-U-TVA950 (Addgene 115236), pRV Δ G-4FLPo (Addgene
520 122050), pAAV-synP-F14F15S-splitTVA-EGFP-tTA (Addgene 136917), pB-CAG-TEVP-IRES-
521 mCherry (Addgene 174377), pAAV-synP-FLPo (Addgene 174378), pAAV-TREtight-H2b-
522 emiRFP670-TEVP (Addgene 174379), pRV Δ G-NPEST-4Cre (Addgene 174380), pRV Δ G-
523 N*PEST-4Cre (Addgene 174381), pCAG-hypBase. All of the above novel plasmids have been
524 deposited with Addgene and can be obtained from there, except for pCAG-hypBase, the
525 distribution of which is not permitted due to intellectual property constraints.

526

527 **Production of lentiviral and adeno-associated viral vectors**

528 Lentiviral vectors were made as described (67) but using a vesicular stomatitis virus envelope
529 expression plasmid pMD2.G for most vectors except for LV-U-TVA950(B19G), which was made
530 using the rabies virus envelope expression plasmid pCAG-B19GVSVGCD (67).

531

532 AAV1-synP-F14F15S-splitTVA-EGFP-tTA was packaged as serotype 1 by the UNC vector core
533 (and can be purchased from there as well as from Addgene (catalog # 136917)).

534

535 AAV1-TREtight-mTagBFP2-B19G (which we have described previously(46, 47)), was packaged
536 as serotype 1 by Addgene (catalog # 100798-AAV1).

537

538 AAV1-TREtight-H2b-emiRFP670-P2A-TEVP and AAV2-retro-synP-FLPo were made by standard
539 techniques (see Supplementary Methods).

540

541 **Production of titering cell lines**

542 Reporter cell lines 293T-FLEX-BC and 293T-F14F15S-BC were made using lentiviral vectors
543 made from pLV-CAG-FLEX-BFP-(mCherry)' and pLV-CAG-F14F15S-BFP-(mCherry)', described
544 above. TVA-expressing versions, 293T-FLEX-BC-TVA and 293T-F14F15S-BC-TVA, were made
545 by infecting the above lines with LV-U-TVA950(VSVG) (described above).

546

547 **Production of TEVP-expressing cell line**

548 293T-TEVP was made by transfecting HEK 293T/17 cells with pCAG-hypBase and pB-CAG-
549 TEVP-IRES-mCherry, then sorting.

550

551 **Production and titering of rabies viruses**

552 RV Δ G-4Cre, RV Δ GL-4Cre, RV Δ G-NPEST-4Cre, and RV Δ G-N*PEST-4Cre were produced
553 mostly as described (21, 34) (see Supplementary Methods); titering was as described (32) but
554 using the 293T-FLEX-BC and 293T-F14F15S-BC lines used for B19G-enveloped viruses and the
555 293T -FLEX-BC-TVA and 293T-F14F15S-BC-TVA used for the EnvA-enveloped viruses.

556

557 **Extraction of viral genomic RNA and preparation for Sanger sequencing**

558 RNA viral genomes were extracted from virus samples using a Nucleospin RNA kit (Macherey-
559 Nagel, Germany), then converted to cDNA by RT-PCR (Agilent Technologies, USA) with a
560 barcoded primer. cDNA sequences were amplified using Platinum SuperFi Green Master Mix

561 (Invitrogen (Thermo Fisher), USA) and cloned into pEX-A (Eurofins Genomics, USA) using an In-
562 Fusion HD Cloning Kit (Takara Bio, Japan). Sequencing data was collected for over fifty clones
563 per sample.

564

565 **Single-molecule, real-time (SMRT) sequencing**

566 Double-stranded DNA samples for SMRT sequencing were prepared similarly to the above,
567 except that that the clones generated from each of the three virus samples were tagged with one
568 of the standard PacBio barcode sequences to allow identification of each clone's sample of origin
569 following multiplex sequencing. This was in addition to the random index (10 nucleotides in this
570 case) that was again included in the RT primers in order to uniquely tag each individual genome.

571

572 **Surgeries and virus injections for two-photon imaging**

573 All experimental procedures using mice were conducted according to NIH guidelines and were
574 approved by the MIT Committee for Animal Care (CAC). Mice were housed 1-4 per cage under a
575 normal light/dark cycle for all experiments.

576

577 Adult mice of Cre-dependent reporter strains Ai14 (68) (Jackson Laboratory #007908) or Ai35D
578 (40) (Jackson Laboratory # 012735) mice were injected in V1 with LV-U-TVA950(B19G), then
579 implanted with a glass window. Seven days later, windows were removed and one of the three
580 EnvA-enveloped rabies viral vectors (with equalized titers) was injected at the same coordinates,
581 then coverslips were reapplied.

582

583 ***In vivo* two-photon imaging and image analysis**

584 Beginning seven days after injection of each rabies virus and continuing every seven days up to
585 a maximum of four weeks following rabies virus injection, the injection sites were imaged on a
586 two-photon microscope. One field of view was chosen in each mouse in the area of maximal
587 fluorescent labelling. Cell counting was performed with the ImageJ Cell Counter plugin.

588

589 **Monosynaptic tracing experiments: surgeries and virus injections**

590 The three helper AAV1s were combined at final titers of 3.6E10 gc/ml for AAV1-synP-F14F15S-
591 splitTVA-EGFP-tTA and 6.60E11 gc/ml for AAV1-TREtight-mTagBFP2-B19G and/or AAV1-
592 TREtight-H2b-emiRFP670-P2A-TEVP. 250 nl of helper virus mixture was injected into layer 5 of
593 barrel cortex of Ai14 mice; in the same surgery, 300 nl of AAV2-retro-synP-FLPo (1.16E13 gc/ml)
594 was injected into dorsolateral striatum. 7 days after AAV injection, 300nl of RVΔG-NPEST-
595 4Cre(EnvA) (1.86E9 iu/ml) or RVΔG-N*PEST-4Cre(EnvA) (diluted to 1.86E9 iu/ml) was injected
596 in barrel cortex at the same site as the helper AAV mixtures.

597

598 **Monosynaptic tracing experiments: perfusions and histology**

599 12 days or 3 weeks after injection of rabies virus, mice were perfused; Brains were postfixed
600 overnight and cut into 50 μm coronal sections on a vibrating microtome. Sections were
601 immunostained as described(47) with a chicken anti-GFP (Aves Labs GFP-1020) 1:500 and
602 donkey anti-chicken Alexa Fluor 488 (Jackson Immuno 703-545-155) 1:200.

603

604 **Monosynaptic tracing experiments: cell counts and microscopy**

605 tdTomato-labeled neurons in contralateral cortex and thalamus were counted manually with the
606 Cell Counter plugin in ImageJ. Cells at the injection site were counted either manually or (when
607 dense) using the Analyze Particle function in ImageJ. Only one of the six series of sections (i.e.,
608 every sixth section: see above) was counted for each mouse. Images for figures were taken on a
609 confocal microscope (Zeiss, LSM 900).

610

611

612 **ACKNOWLEDGEMENTS**

613 We thank Ernesto Ciabatti and Marco Tripodi for sharing samples of EnvA/SiR-CRE and
614 EnvA/SiR-FLPo and for comments on the manuscript. We thank Ed Callaway, Sean Whelan,
615 Ayano Matsushima, and Kim Ritola for helpful discussion and Jun Zhuang, Soumya Chatterjee,
616 and Ali Cetin for helpful discussion and sharing their own results with SiR viruses. We thank
617 Stuart Levine, Noelani Kamelamela, and Huiming Ding of the MIT BioMicro Center for
618 assistance with SMRT sequencing and bioinformatic data analysis and Sara Beach for helpful
619 feedback on the manuscript. Research reported in this publication was supported by the
620 following BRAIN Initiative awards from the National Institute of Mental Health: U01MH106018
621 (Wickersham) RF1MH120017 (Wickersham), U01MH114829 (Dong), and U19MH114830
622 (Zeng).

623

624

625 **REFERENCES**

626

- 627 1. Ugolini G, Kuypers HG, & Strick PL (1989) Transneuronal transfer of herpes virus from
628 peripheral nerves to cortex and brainstem. *Science* 243(4887):89-91.
- 629 2. Ugolini G (1995) Specificity of rabies virus as a transneuronal tracer of motor networks:
630 transfer from hypoglossal motoneurons to connected second-order and higher order
631 central nervous system cell groups. *J Comp Neurol* 356(3):457-480.
- 632 3. Kelly RM & Strick PL (2000) Rabies as a transneuronal tracer of circuits in the central
633 nervous system. *J Neurosci Methods* 103(1):63-71.
- 634 4. Wickersham IR, Finke S, Conzelmann KK, & Callaway EM (2007) Retrograde neuronal
635 tracing with a deletion-mutant rabies virus. *Nature Methods* 4(1):47-49.
- 636 5. Wickersham IR, *et al.* (2007) Monosynaptic restriction of transsynaptic tracing from
637 single, genetically targeted neurons. *Neuron* 53(5):639-647.
- 638 6. Atasoy D, Aponte Y, Su HH, & Sternson SM (2008) A FLEX switch targets
639 Channelrhodopsin-2 to multiple cell types for imaging and long-range circuit mapping.
640 *The Journal of neuroscience : the official journal of the Society for Neuroscience*
641 28(28):7025-7030.
- 642 7. Beier KT, *et al.* (2011) Anterograde or retrograde transsynaptic labeling of CNS neurons
643 with vesicular stomatitis virus vectors. *P Natl Acad Sci USA*.
- 644 8. Lo L & Anderson DJ (2011) A Cre-dependent, anterograde transsynaptic viral tracer for
645 mapping output pathways of genetically marked neurons. *Neuron* 72(6):938-950.
- 646 9. Schwarz LA, *et al.* (2015) Viral-genetic tracing of the input-output organization of a
647 central noradrenaline circuit. *Nature*.
- 648 10. Deverman BE, *et al.* (2016) Cre-dependent selection yields AAV variants for widespread
649 gene transfer to the adult brain. *Nat Biotechnol* 34(2):204-209.
- 650 11. Tervo DG, *et al.* (2016) A Designer AAV Variant Permits Efficient Retrograde Access to
651 Projection Neurons. *Neuron* 92(2):372-382.
- 652 12. Dimidschstein J, *et al.* (2016) A viral strategy for targeting and manipulating
653 interneurons across vertebrate species. *Nat Neurosci* 19(12):1743-1749.
- 654 13. Zeng WB, *et al.* (2017) Anterograde monosynaptic transneuronal tracers derived from
655 herpes simplex virus 1 strain H129. *Mol Neurodegener* 12(1):38.
- 656 14. Luo L, Callaway EM, & Svoboda K (2018) Genetic Dissection of Neural Circuits: A Decade
657 of Progress. *Neuron* 98(4):865.

- 658 15. Ravindra Kumar S, *et al.* (2020) Multiplexed Cre-dependent selection yields systemic
659 AAVs for targeting distinct brain cell types. *Nat Methods* 17(5):541-550.
- 660 16. Mich JK, *et al.* (2021) Functional enhancer elements drive subclass-selective expression
661 from mouse to primate neocortex. *Cell Rep* 34(13):108754.
- 662 17. Augustine V, *et al.* (2018) Hierarchical neural architecture underlying thirst regulation.
663 *Nature* 555(7695):204-209.
- 664 18. Kohl J, *et al.* (2018) Functional circuit architecture underlying parental behaviour. *Nature*
665 556(7701):326-331.
- 666 19. Evans DA, *et al.* (2018) A synaptic threshold mechanism for computing escape decisions.
667 *Nature* 558(7711):590-594.
- 668 20. Kaelberer MM, *et al.* (2018) A gut-brain neural circuit for nutrient sensory transduction.
669 *Science* 361(6408).
- 670 21. Chatterjee S, *et al.* (2018) Nontoxic, double-deletion-mutant rabies viral vectors for
671 retrograde targeting of projection neurons. *Nat Neurosci* 21(4):638-646.
- 672 22. Reardon TR, *et al.* (2016) Rabies Virus CVS-N2c(DeltaG) Strain Enhances Retrograde
673 Synaptic Transfer and Neuronal Viability. *Neuron* 89(4):711-724.
- 674 23. Morimoto K, Hooper DC, Spitsin S, Koprowski H, & Dietzschold B (1999) Pathogenicity of
675 different rabies virus variants inversely correlates with apoptosis and rabies virus
676 glycoprotein expression in infected primary neuron cultures. *J Virol* 73(1):510-518.
- 677 24. Ciabatti E, Gonzalez-Rueda A, Mariotti L, Morgese F, & Tripodi M (2017) Life-Long
678 Genetic and Functional Access to Neural Circuits Using Self-Inactivating Rabies Virus. *Cell*
679 170(2):382-392 e314.
- 680 25. Rogers S, Wells R, & Rechsteiner M (1986) Amino acid sequences common to rapidly
681 degraded proteins: the PEST hypothesis. *Science* 234(4774):364-368.
- 682 26. Steinhauer DA & Holland JJ (1987) Rapid evolution of RNA viruses. *Annu Rev Microbiol*
683 41:409-433.
- 684 27. Steinhauer DA, de la Torre JC, & Holland JJ (1989) High nucleotide substitution error
685 frequencies in clonal pools of vesicular stomatitis virus. *J Virol* 63(5):2063-2071.
- 686 28. Holland JJ, De La Torre JC, & Steinhauer DA (1992) RNA virus populations as
687 quasispecies. *Curr Top Microbiol Immunol* 176:1-20.
- 688 29. Holmes EC, Woelk CH, Kassis R, & Bourhy H (2002) Genetic constraints and the adaptive
689 evolution of rabies virus in nature. *Virology* 292(2):247-257.
- 690 30. Jenkins GM, Rambaut A, Pybus OG, & Holmes EC (2002) Rates of molecular evolution in
691 RNA viruses: a quantitative phylogenetic analysis. *J Mol Evol* 54(2):156-165.
- 692 31. Combe M & Sanjuan R (2014) Variation in RNA virus mutation rates across host cells.
693 *PLoS Pathog* 10(1):e1003855.
- 694 32. Wickersham IR, Sullivan HA, & Seung HS (2010) Production of glycoprotein-deleted
695 rabies viruses for monosynaptic tracing and high-level gene expression in neurons.
696 *Nature protocols* 5(3):595-606.
- 697 33. Osakada F & Callaway EM (2013) Design and generation of recombinant rabies virus
698 vectors. *Nat Protoc* 8(8):1583-1601.
- 699 34. Wickersham IR & Sullivan HA (2015) Rabies viral vectors for monosynaptic tracing and
700 targeted transgene expression in neurons. *Cold Spring Harb Protoc* 2015(4):375-385.

- 701 35. Weible AP, *et al.* (2010) Transgenic targeting of recombinant rabies virus reveals
702 monosynaptic connectivity of specific neurons. *The Journal of neuroscience : the official*
703 *journal of the Society for Neuroscience* 30(49):16509-16513.
- 704 36. Carneiro MO, *et al.* (2012) Pacific biosciences sequencing technology for genotyping and
705 variation discovery in human data. *BMC Genomics* 13:375.
- 706 37. Wirblich C & Schnell MJ (2011) Rabies virus (RV) glycoprotein expression levels are not
707 critical for pathogenicity of RV. *J Virol* 85(2):697-704.
- 708 38. Tao L, *et al.* (2010) Molecular basis of neurovirulence of flury rabies virus vaccine strains:
709 importance of the polymerase and the glycoprotein R333Q mutation. *J Virol*
710 84(17):8926-8936.
- 711 39. Prehaud C, Lay S, Dietzschold B, & Lafon M (2003) Glycoprotein of nonpathogenic rabies
712 viruses is a key determinant of human cell apoptosis. *J Virol* 77(19):10537-10547.
- 713 40. Madisen L, *et al.* (2012) A toolbox of Cre-dependent optogenetic transgenic mice for
714 light-induced activation and silencing. *Nature neuroscience* 15(5):793-802.
- 715 41. Shaner NC, *et al.* (2004) Improved monomeric red, orange and yellow fluorescent
716 proteins derived from *Discosoma* sp. red fluorescent protein. *Nat Biotechnol*
717 22(12):1567-1572.
- 718 42. Drobizhev M, Makarov NS, Tillo SE, Hughes TE, & Rebane A (2011) Two-photon
719 absorption properties of fluorescent proteins. *Nat Methods* 8(5):393-399.
- 720 43. Huang KW & Sabatini BL (2020) Single-Cell Analysis of Neuroinflammatory Responses
721 Following Intracranial Injection of G-Deleted Rabies Viruses. *Front Cell Neurosci* 14:65.
- 722 44. Prosniak M, Hooper DC, Dietzschold B, & Koprowski H (2001) Effect of rabies virus
723 infection on gene expression in mouse brain. *Proc Natl Acad Sci U S A* 98(5):2758-2763.
- 724 45. Madisen L, *et al.* (2015) Transgenic mice for intersectional targeting of neural sensors
725 and effectors with high specificity and performance. *Neuron* 85(5):942-958.
- 726 46. Liu K, *et al.* (2017) Lhx6-positive GABA-releasing neurons of the zona incerta promote
727 sleep. *Nature* 548(7669):582-587.
- 728 47. Lavin TK, Jin L, & Wickersham IR (2019) Monosynaptic tracing: a step-by-step protocol. *J*
729 *Chem Neuroanat*:101661.
- 730 48. Lavin TK, Jin L, Lea NE, & Wickersham IR (2020) Monosynaptic Tracing Success Depends
731 Critically on Helper Virus Concentrations. *Front Synaptic Neurosci* 12:6.
- 732 49. Ciabatti E, *et al.* (2020) Genomic stability of Self-inactivating Rabies.
733 *bioRxiv*:2020.2009.2019.304683.
- 734 50. Dalton KP & Rose JK (2001) Vesicular stomatitis virus glycoprotein containing the entire
735 green fluorescent protein on its cytoplasmic domain is incorporated efficiently into virus
736 particles. *Virology* 279(2):414-421.
- 737 51. Duprex WP, Collins FM, & Rima BK (2002) Modulating the function of the measles virus
738 RNA-dependent RNA polymerase by insertion of green fluorescent protein into the open
739 reading frame. *J Virol* 76(14):7322-7328.
- 740 52. Finke S, Brzozka K, & Conzelmann KK (2004) Tracking fluorescence-labeled rabies virus:
741 enhanced green fluorescent protein-tagged phosphoprotein p supports virus gene
742 expression and formation of infectious particles. *J Virol* 78(22):12333-12343.
- 743 53. Koser ML, *et al.* (2004) Rabies virus nucleoprotein as a carrier for foreign antigens. *Proc*
744 *Natl Acad Sci U S A* 101(25):9405-9410.

- 745 54. Brown DD, *et al.* (2005) Rational attenuation of a morbillivirus by modulating the activity
746 of the RNA-dependent RNA polymerase. *J Virol* 79(22):14330-14338.
- 747 55. Das SC, Nayak D, Zhou Y, & Pattnaik AK (2006) Visualization of intracellular transport of
748 vesicular stomatitis virus nucleocapsids in living cells. *J Virol* 80(13):6368-6377.
- 749 56. Klingen Y, Conzelmann KK, & Finke S (2008) Double-labeled rabies virus: live tracking of
750 enveloped virus transport. *Journal of virology* 82(1):237-245.
- 751 57. Das SC, Panda D, Nayak D, & Pattnaik AK (2009) Biarsenical labeling of vesicular
752 stomatitis virus encoding tetracysteine-tagged m protein allows dynamic imaging of m
753 protein and virus uncoating in infected cells. *J Virol* 83(6):2611-2622.
- 754 58. Marriott AC & Hornsey CA (2011) Reverse genetics system for Chandipura virus: tagging
755 the viral matrix protein with green fluorescent protein. *Virus Res* 160(1-2):166-172.
- 756 59. Soh TK & Whelan SP (2015) Tracking the Fate of Genetically Distinct Vesicular Stomatitis
757 Virus Matrix Proteins Highlights the Role for Late Domains in Assembly. *J Virol*
758 89(23):11750-11760.
- 759 60. Nikolic J, Civas A, Lama Z, Lagaudriere-Gesbert C, & Blondel D (2016) Rabies Virus
760 Infection Induces the Formation of Stress Granules Closely Connected to the Viral
761 Factories. *PLoS Pathog* 12(10):e1005942.
- 762 61. Case JB, *et al.* (2020) Replication-competent vesicular stomatitis virus vaccine vector
763 protects against SARS-CoV-2-mediated pathogenesis. *bioRxiv*.
- 764 62. Gomme EA, Wirblich C, Addya S, Rall GF, & Schnell MJ (2012) Immune clearance of
765 attenuated rabies virus results in neuronal survival with altered gene expression. *PLoS*
766 *Pathog* 8(10):e1002971.
- 767 63. Wiktor TJ, Dietzschold B, Leamson RN, & Koprowski H (1977) Induction and biological
768 properties of defective interfering particles of rabies virus. *J Virol* 21(2):626-635.
- 769 64. Kawai A & Matsumoto S (1977) Interfering and noninterfering defective particles
770 generated by a rabies small plaque variant virus. *Virology* 76(1):60-71.
- 771 65. Clark HF, Parks NF, & Wunner WH (1981) Defective interfering particles of fixed rabies
772 viruses: lack of correlation with attenuation or auto-interference in mice. *J Gen Virol*
773 52(Pt 2):245-258.
- 774 66. Faber M, *et al.* (2002) Overexpression of the rabies virus glycoprotein results in
775 enhancement of apoptosis and antiviral immune response. *J Virol* 76(7):3374-3381.
- 776 67. Wickersham IR, *et al.* (2015) Lentiviral vectors for retrograde delivery of recombinases
777 and transactivators. *Cold Spring Harb Protoc* 2015(4):368-374.
- 778 68. Madisen L, *et al.* (2010) A robust and high-throughput Cre reporting and
779 characterization system for the whole mouse brain. *Nature neuroscience* 13(1):133-140.
780

FIGURES

Figure 1: Single-molecule Sanger sequencing of individual viral genomes revealed that most SiR virions had lost the intended C-terminal modification to the nucleoprotein.

(A) Schematic of the RT-PCR workflow. In the reverse transcription (RT) step, the RT primer, containing a random 8-nucleotide sequence, anneals to the 3' rabies virus leader, adding a unique random index to the 5' end of the cDNA molecule corresponding to each individual viral particle's RNA genome. In the PCR step, the forward PCR primer anneals to the RT primer sequence and the reverse PCR primer anneals within the viral phosphoprotein gene P. Both PCR primers have 15-base sequences homologous to those flanking an insertion site in a plasmid used for sequencing, allowing the amplicons to be cloned into the plasmid using a seamless cloning method before transformation into bacteria. The resulting plasmid library consists of plasmids containing up to 4^8 different index sequences, allowing confirmation that the sequences of plasmids purified from individual picked colonies correspond to the sequences of different individual rabies viral particles' genomes.

(B) Representative Sanger sequencing data of the 8-bp index and the TEV-PEST sequence. Mutations are highlighted in red.

(C) Mutation variants and their frequencies in each viral vector sample based on Sanger sequencing data. No unmutated genomes were found in the SiR-CRE sample: 50 out of 51 had a substitution creating an opal stop codon just before the TEV cleavage site, and the 51st genome contained a frameshift which also removed the C-terminal addition. In the SiR-FLPo sample, only 4 out of 50 clones had an intact sequence of the C-terminal addition; the other 46 out of 50 had one of two *de novo* stop codons at the end of N or the beginning of the TEV cleavage site. In the sample of RV Δ G-4mCherry, a virus from our laboratory included as a control to distinguish true mutations on the rabies genomes from mutations due to the RT-PCR process, none of the 51 clones analyzed had mutations in the sequenced region.

Figure 1

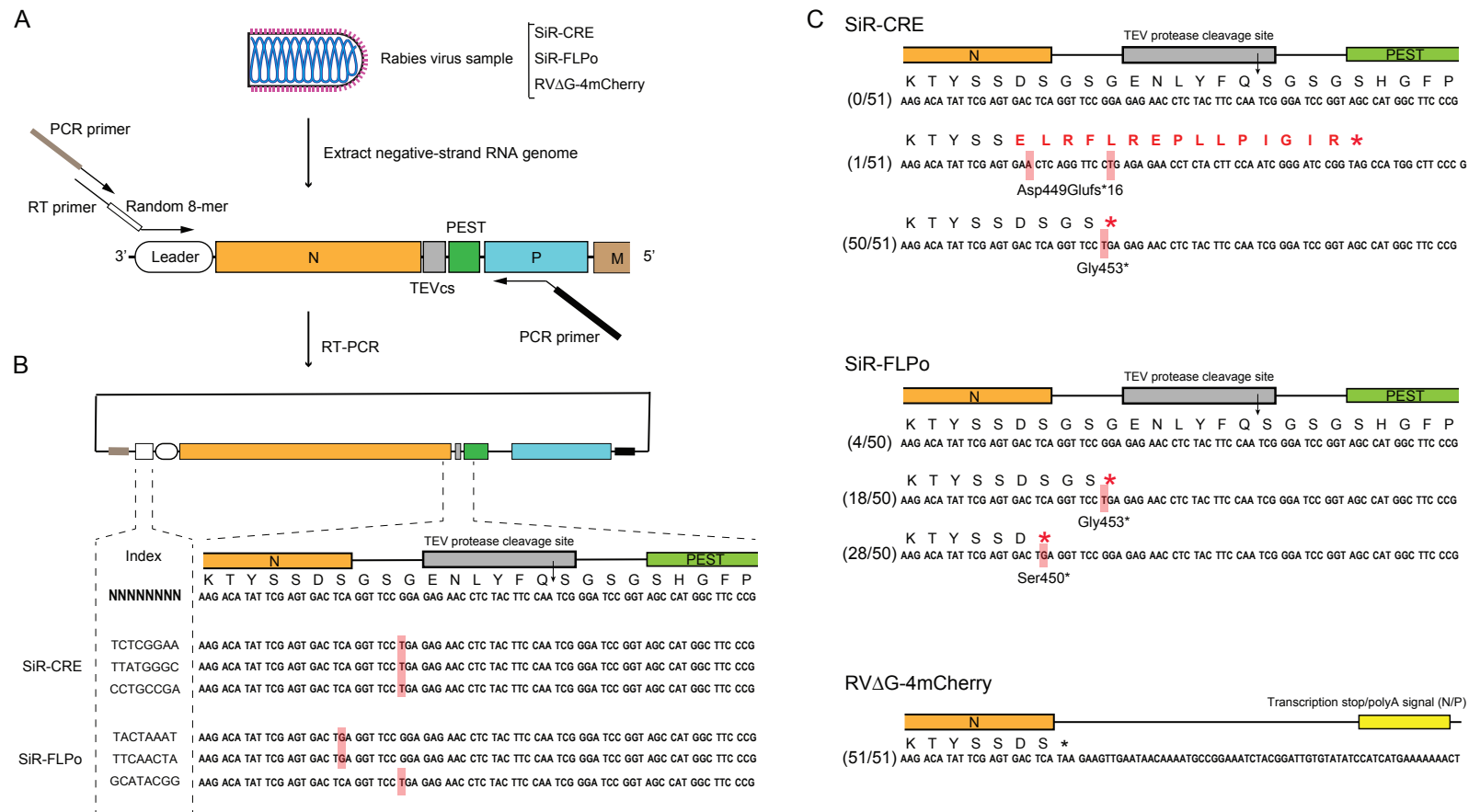


Figure 2: Single-molecule, real-time (SMRT) sequencing of thousands of barcoded viral genomes confirmed that most SiR virions had lost the intended C-terminal modification to the nucleoprotein.

(A) Schematic of workflow for SMRT sequencing. An RT primer with a random 10-nucleotide sequence anneals to the leader sequence on the negative-sense single-stranded RNA genome. Forward and reverse PCR primers have distinct SMRT barcodes at their 5' ends for the three different virus samples. After RT-PCR, each amplicon library consists of amplicons each containing a SMRT barcode to identify the sample of origin as well as the 10-nucleotide index (i.e., with a potential diversity of 4^{10} different indices) to uniquely label the individual genome of origin. SMRT "dumbbell" adaptors are then ligated to the amplicons' ends, making circular templates which are then repeatedly traversed by a DNA polymerase, resulting in long polymerase reads each containing multiple reads of the positive and negative strands. The individual subreads for a given molecule are combined to form circular consensus sequence (CCS) reads.

(B) High-frequency (>2%) point mutations found in the rabies vector samples based on SMRT sequencing. Horizontal axis represents nucleotide position along the reference sequences (see text); vertical axis represents variant frequency. Total number of CCS3 reads (i.e., with at least 3 subreads for each position) are 22,205 for SiR-CRE, 17,086 reads for SiR-FLPo, and 17,978 reads for RV Δ G-4Cre. The great majority of SiR-CRE and SiR-FLPo genomes have point mutations creating premature stop codons at or just after the end of N and before the C-terminal addition. The only frequent (>2%) mutation found in the control virus, RV Δ G-4Cre, was a single amino acid substitution at position 419 in 9.49% of virions. Insertions and deletions are not shown here (see text).

(C) Summary of results. In the SiR virus samples, 99.22% of SiR-CRE virions and 83.85% of SiR-FLPo virions had point mutations creating premature stop codons that completely removed the intended C-terminal addition to the nucleoprotein, making them simply first-generation (Δ G) rabies viral vectors. This does not include any insertions or deletions causing frameshifts (see text), which would further increase the percentage of first-generation-type virions in these samples. In the RV Δ G-4Cre sample, there were no premature stop codons at or near the end of the nucleoprotein gene.

Figure 2

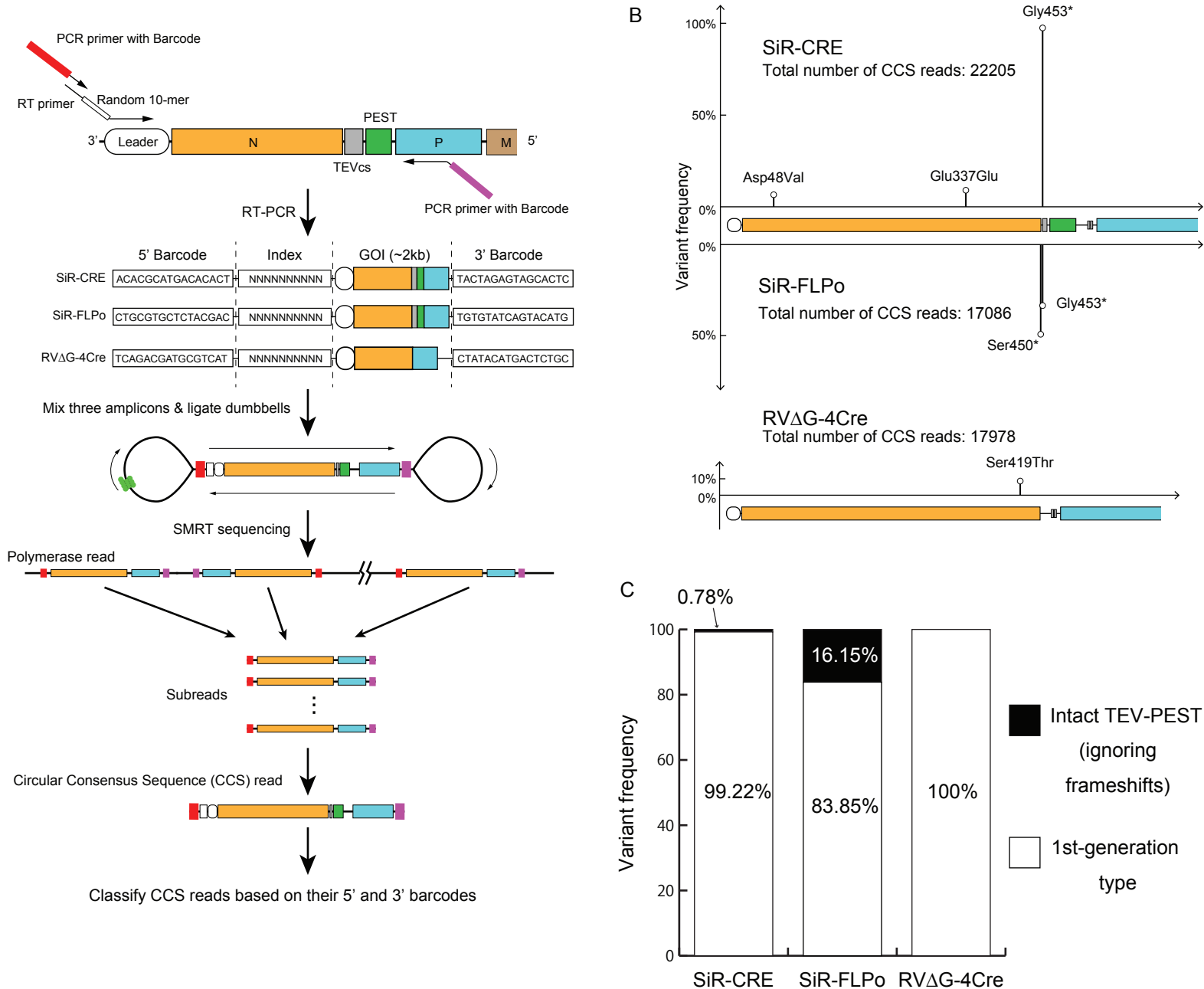


Figure 3: Longitudinal two-photon imaging *in vivo* showed that SiR virus killed approximately 80% of infected neurons *in vivo* within 2-4 weeks.

A) Representative fields of view (FOVs) of visual cortical neurons labeled with RV Δ G-4Cre (top row), RV Δ GL-4Cre (middle row), or SiR-CRE (bottom row) in Ai14 mice (Cre-dependent expression of tdTomato). Images within each row are of the same FOV imaged at the four different time points in the same mouse. Circles indicate cells that are present at 7 days postinjection but no longer visible at a subsequent time point. Scale bar: 50 μ m, applies to all images.

B-D) Numbers of cells present at week 1 that were still present in subsequent weeks. While very few cells labeled with RV Δ GL-4Cre were lost, and RV Δ G-4Cre killed a significant minority of cells, SiR-CRE killed the majority of labeled neurons within 14 days following injection.

E) Percentages of cells present at week 1 that were still present in subsequent imaging sessions. By 28 days postinjection, an average of only 20.5% of cells labeled by SiR-CRE remained.

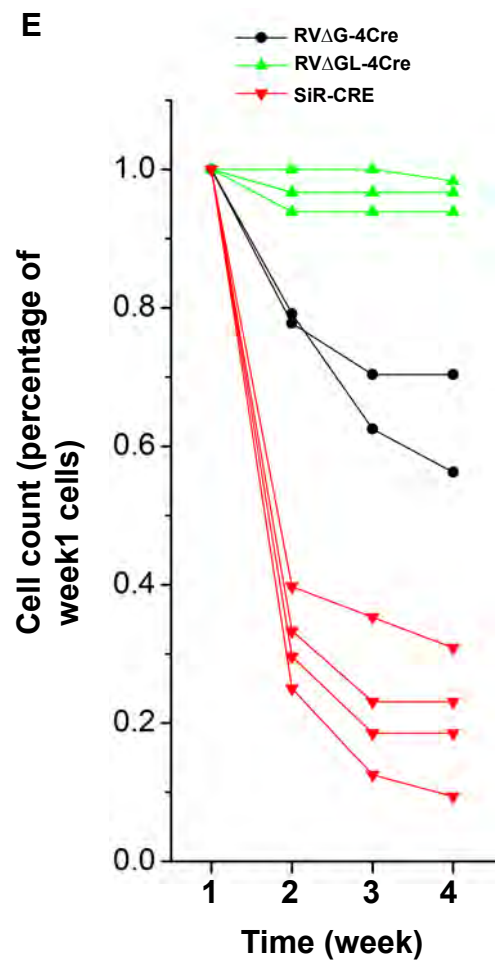
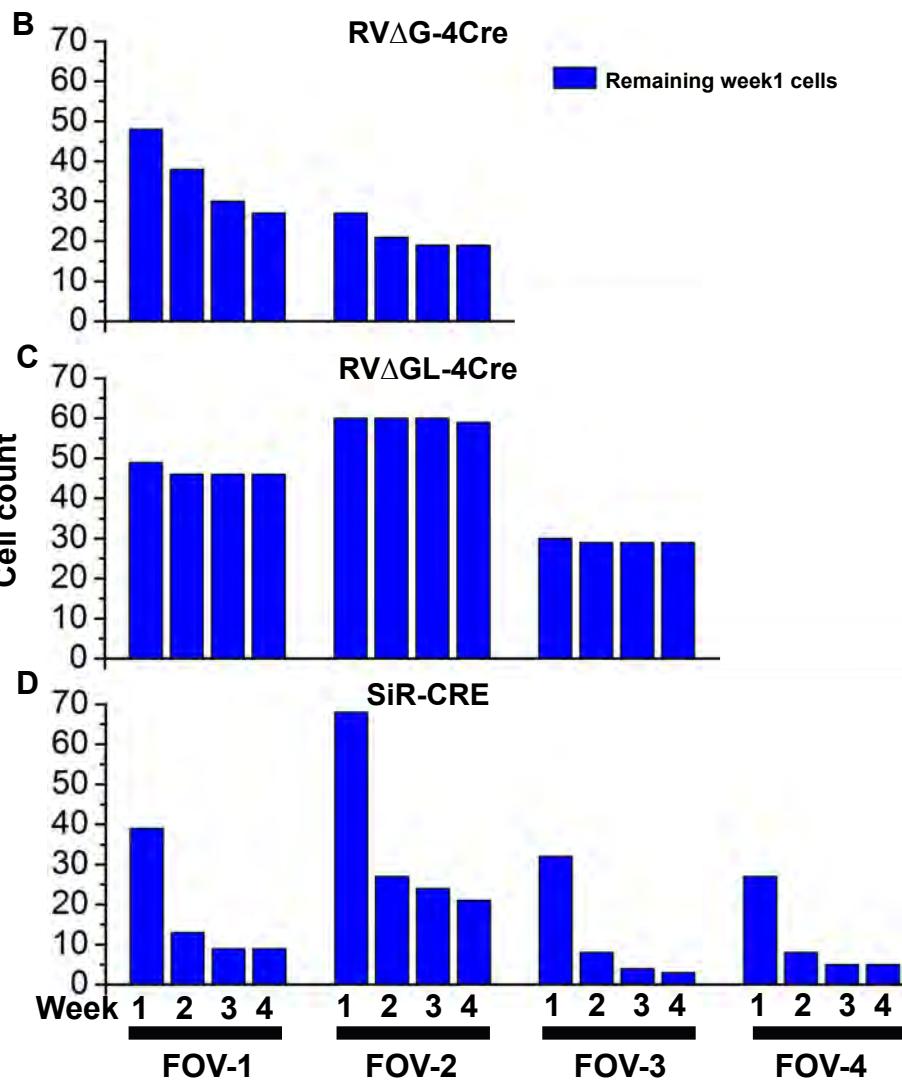
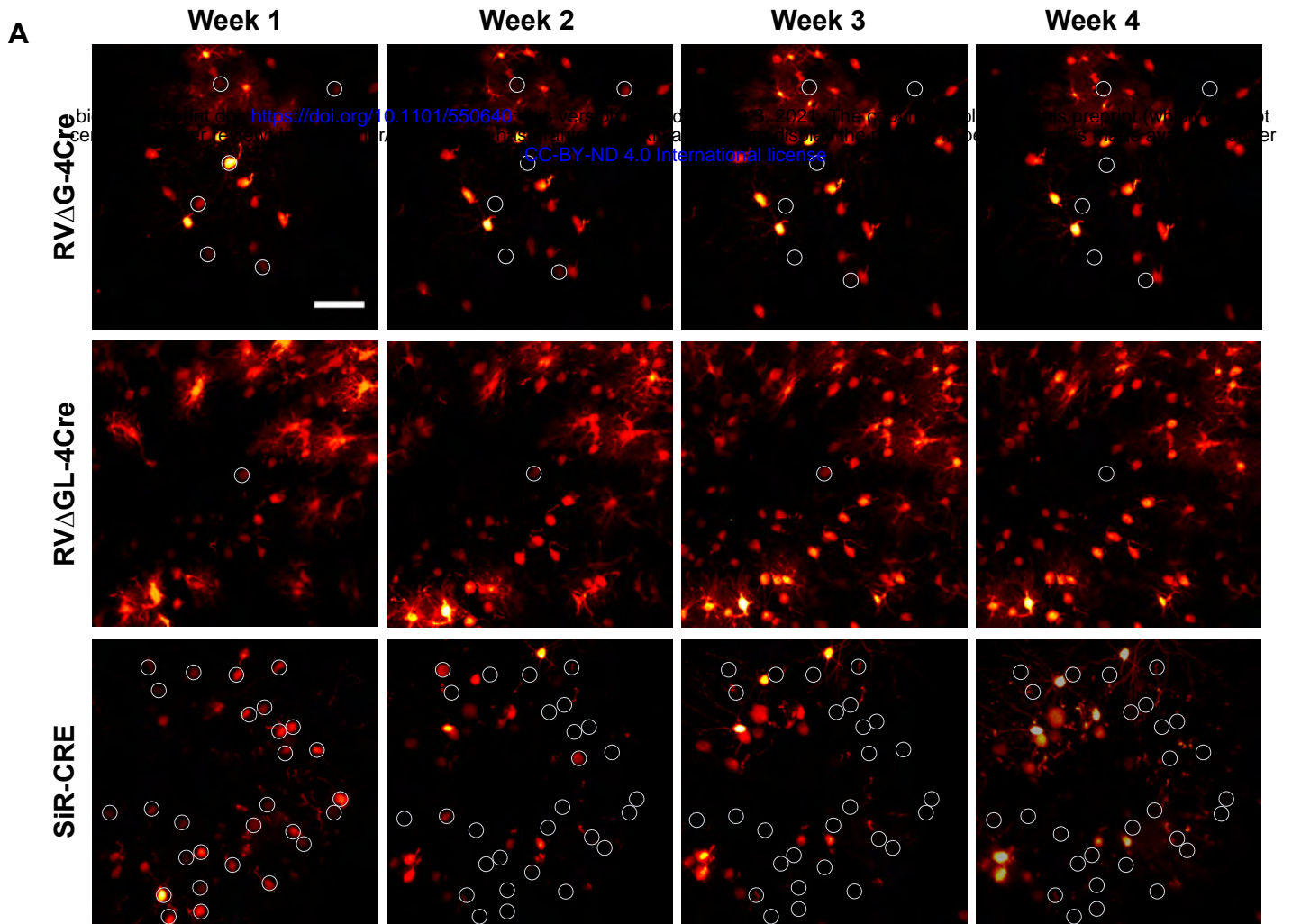


Figure 4: Rabies virus with an intact PEST domain does not spread in the absence of TEVP.

A) Sequences of the region of the junction between the nucleoprotein gene N and its 3' addition in SiR-CRE (intended sequence) as well as in our two new viruses RV Δ G-NPEST-4Cre and RV Δ G-N*PEST-4Cre. Apart from synonymous mutations we made in five codons (highlighted in green) to make them less likely to mutate to stop codons, RV Δ G-NPEST-4Cre has exactly the same 3' addition to N as was intended for SiR. RV Δ G-N*PEST-4Cre has exactly the same sequence as RV Δ G-NPEST-4Cre apart from a stop codon that we deliberately introduced at the same location as the nonsense mutation that we had found in almost every SiR-CRE virion, so that the only modification to the native nucleoprotein is an additional two amino acids (Gly-Ser) on its C-terminus. Sanger sequencing of 32 viral particles of each virus confirmed that the intended additions were still present in the final stocks.

B) Diagram of virus injections for monosynaptic tracing experiments. An AAV2-retro expressing FLPo was injected in dorsolateral striatum, and a FLP-dependent helper virus combination was injected into barrel cortex to express TVA and G in corticostriatal cells. Rabies virus was injected seven days later at the same location in barrel cortex, and mice were perfused either 12 days or 21 days after rabies virus injection.

C) At 12 days after injection, the NPEST virus (top row), with an intact PEST domain, shows no evidence of spread, whereas the N*PEST virus (bottom row), without the PEST domain, has labeled thousands of neurons in ipsilateral cortex (shown here) and also spread to contralateral cortex and thalamus (see Supplementary Figure S5 for images). For all panels in this figure as well as Figure 5 and the related supplementary figures, the red channel shows tdTomato, reporting Cre expression from the rabies viruses; the green channel shows EGFP, coexpressed with TVA (and tTA) by the first helper virus; the blue channel shows mTagBFP2, coexpressed with G by the second helper virus. Scale bar: 200 μ m, applies to all images.

D) At 21 days after injection, the N*PEST virus again shows no evidence of spread, while the N*PEST virus has labeled many thousands of neurons. Scale bar: 200 μ m, applies to all images.

E) Counts of labeled neurons in ipsilateral cortex (left), contralateral cortex (center), and thalamus (right) at 12 days and 21 days for the two viruses. Each dot indicates the total number of labeled cells found in a given mouse brain when examining every sixth 50 μ m section (see Methods). All differences in numbers of cells labeled by the two viruses are highly significant for all conditions (see Supplementary File S8 for all counts and statistical analyses), except for the numbers of contralateral cells at 12 days.

SIR-CRE
 AAG ACA TAT **AGT** AGT GAC **GGT** TCC **GG** GAG AAC CTC TAC TTC CAA **GGC** TCC GGT AGC CAT GGC TTC CCG

RVΔG-NPEST-4Cre (32/32)
 AAG ACA TAT **AGT** AGT GAC **AGT** GGT TCC **GGC** GAG AAC CTC TAC TTC CAA **AGT** GGC TCC GGT AGC CAT GGC TTC CCG

RVΔG-N*PEST-4Cre (32/32)
 AAG ACA TAT **AGT** AGT GAC **AGT** GGT TCC **TGA** GAG AAC CTC TAC TTC CAA **AGT** GGC TCC GGT AGC CAT GGC TTC CCG

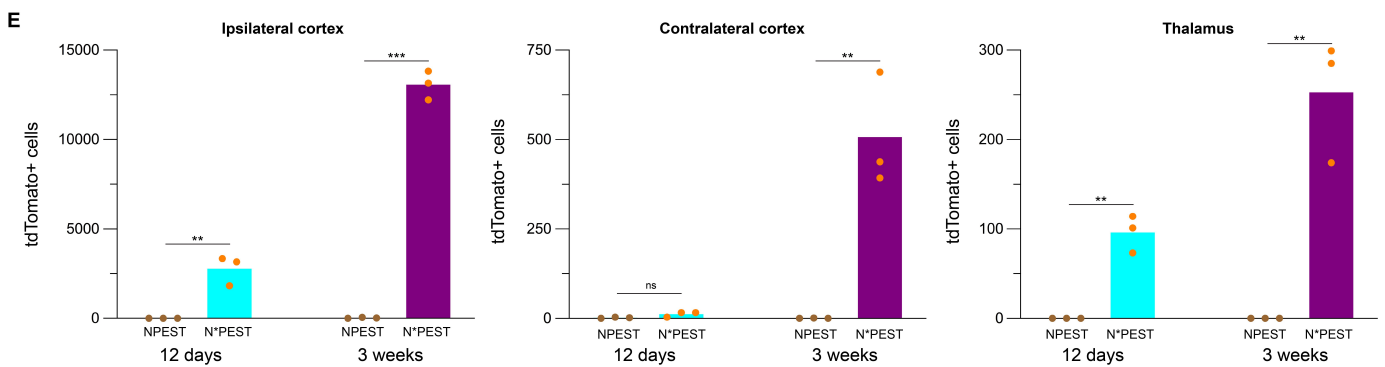
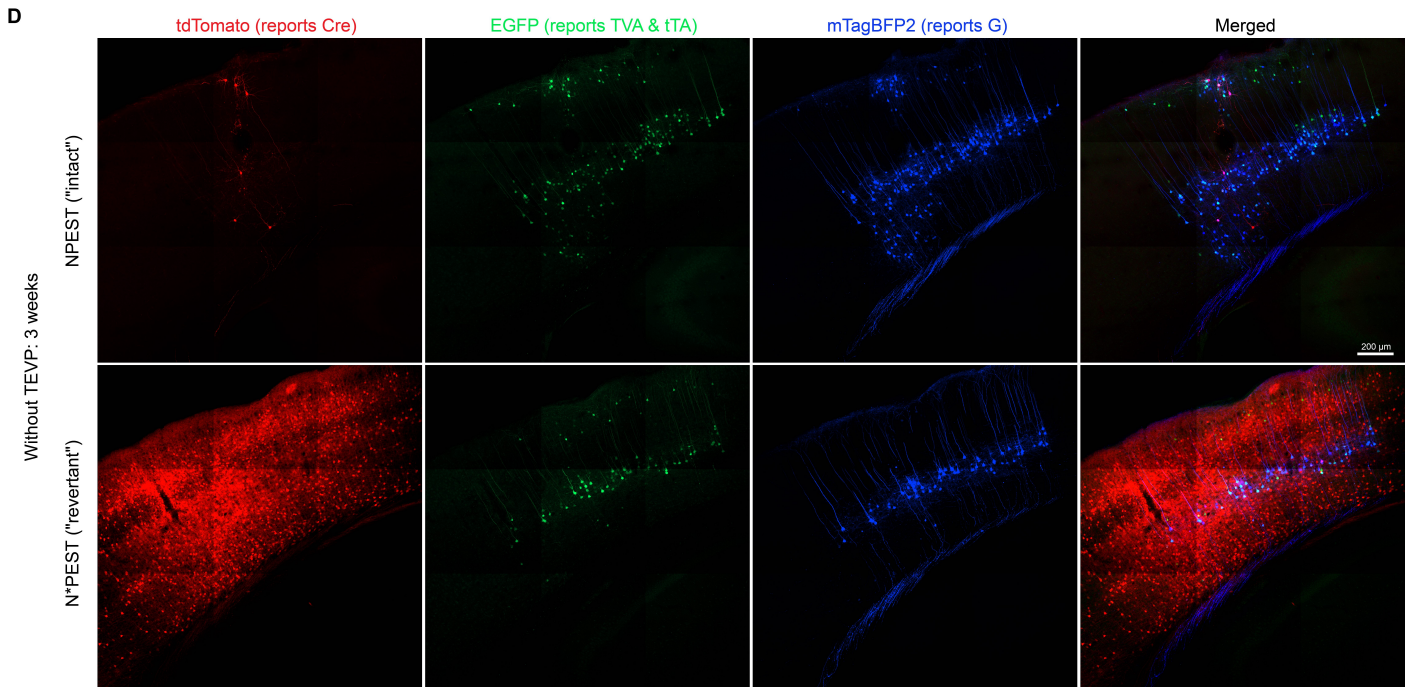
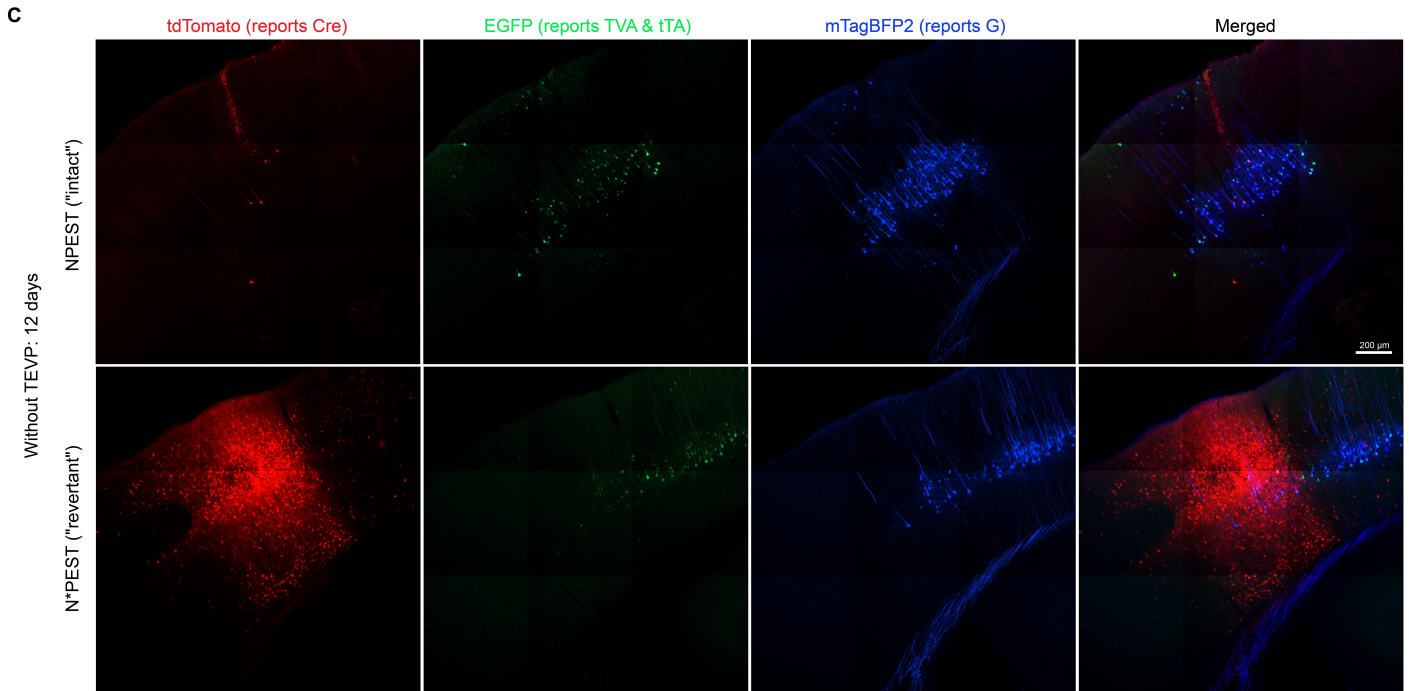
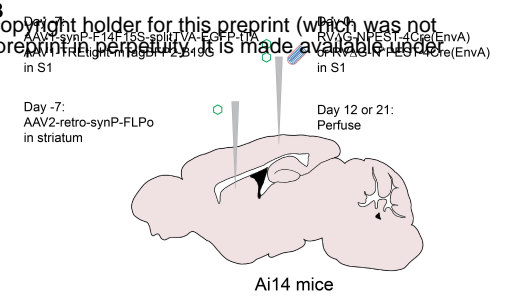


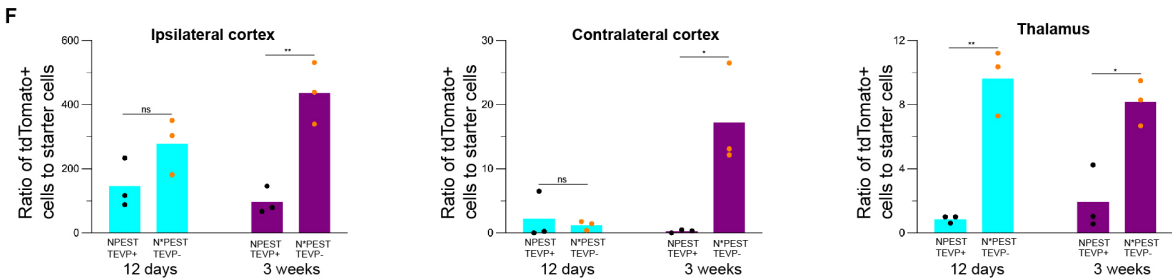
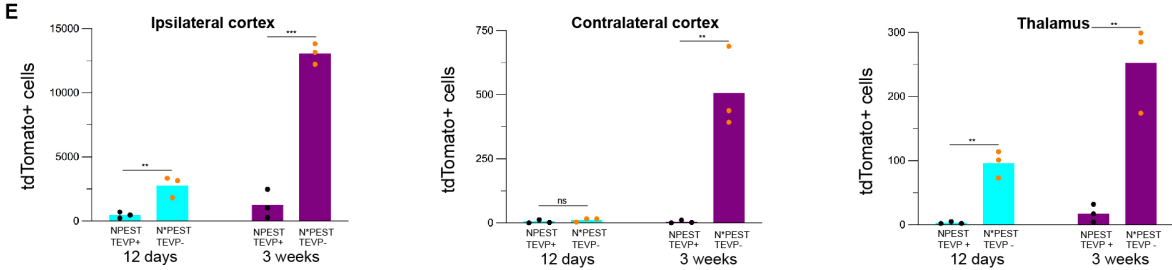
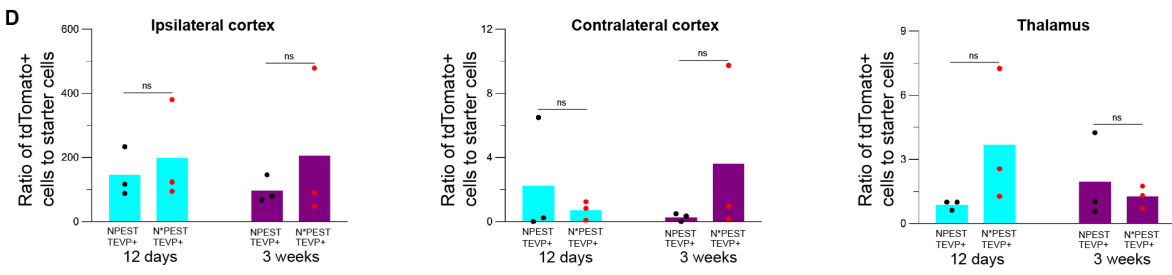
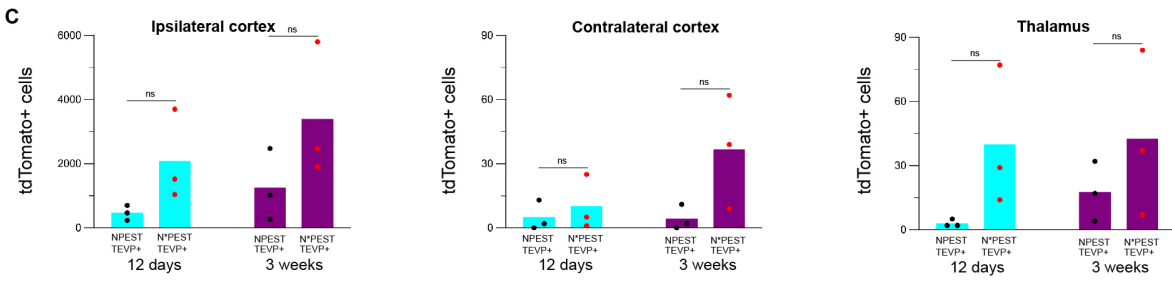
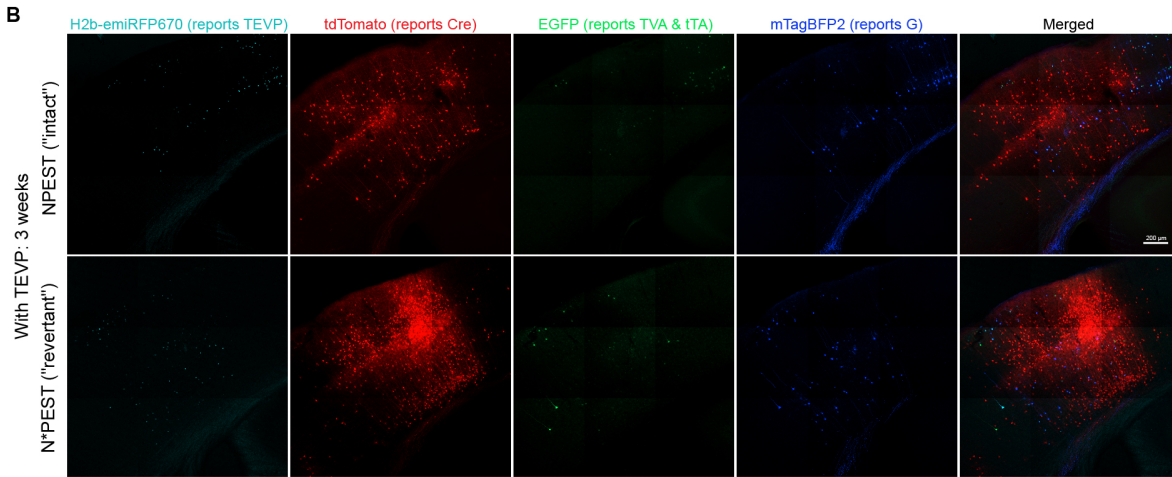
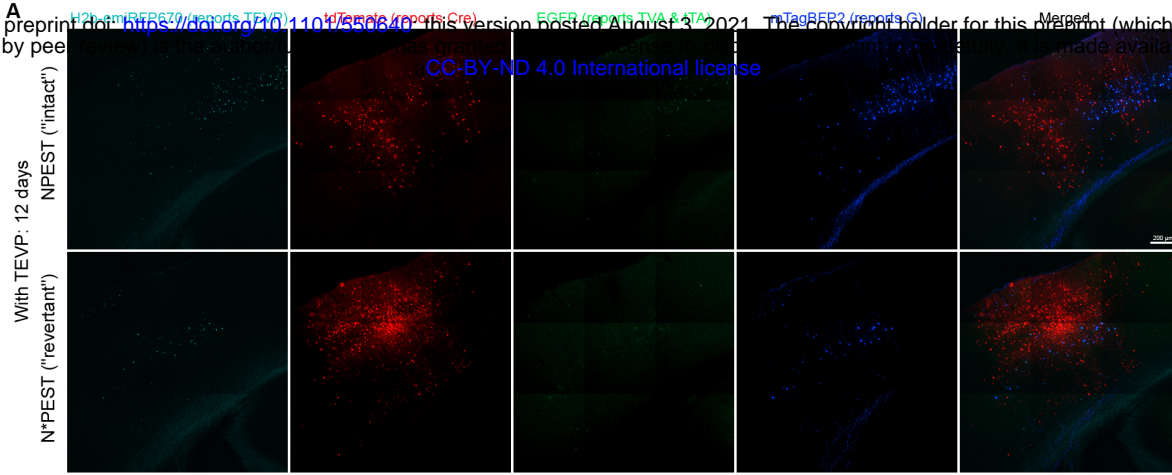
Figure 5: Rabies virus with an intact PEST domain does spread when TEVP is supplied, although with lower efficiency than virus without a PEST domain.

With the experimental design exactly the same as shown in Figure 4, Panel B but with a TEVP-expressing AAV included in the helper virus mixture, the NPEST virus did spread transsynaptically, but to a more limited degree than the N*PEST one.

A, B) At both 12 (A) and 21 (B) days after injection, both NPEST (top row) and N*PEST (bottom row) viruses have labeled many cells in ipsilateral cortex (shown here), although many more cells are labeled by the NPEST virus. Both viruses have also spread to contralateral cortex and thalamus (see Supplementary Figure S6 for images).

C - D) Counts of tdTomato+ cells (C) and ratios (D) of number of tdTomato+ cells to number of "starter cells", defined here as cells coexpressing tdTomato, mTagBFP2, and emiRFP670, with TEVP supplied for both viruses (in cases in which TEVP is not supplied (see below), starter cells are defined as cells coexpressing tdTomato and mTagBFP2). Both the absolute numbers and the ratios are higher (in all cases except for contralateral cortex at 12 days) for the N*PEST virus than for the NPEST one, although the differences were not significant with the small size of each group (see text). Note that the inclusion of TEVP reduced the spread of the N*PEST virus considerably (cf. Figure 4; all counts and statistical comparisons are in Supplementary File S8).

E - F) Comparison of the best condition for the NPEST virus (with TEVP; same data as in panel C and D above) to the best condition for the N*PEST one (without TEVP; same data as in Figure 4) gives highly significant differences for most comparisons, with the advantage of the N*PEST virus over the NPEST version increasing between 12 days and 3 weeks.



SUPPLEMENTARY METHODS

Cloning

Lentiviral transfer plasmids were made by cloning, into pCSC-SP-PW-GFP (1) (Addgene #12337), the following components:

the CAG promoter (2) and a Cre-dependent "FLEX" (3) construct consisting of pairs of orthogonal lox sites flanking a back-to-back fusion of the gene for mTagBFP2 (4) immediately followed by the reverse-complemented gene for mCherry (5), to make the Cre reporter construct pLV-CAG-FLEX-BFP-(mCherry)' (Addgene 115234);

the CAG promoter (2) and a Flp-dependent "FLEX" (3) construct consisting of pairs of orthogonal FRT sites (6) flanking a back-to-back fusion of the gene for mTagBFP2 (4) immediately followed by the reverse-complemented gene for mCherry (5), to make the Flp reporter construct pLV-CAG-F14F15S-BFP-(mCherry)' (Addgene 115235);

the ubiquitin C promoter from pUB-GFP (7) (Addgene 11155) and the long isoform of TVA (8) to make the TVA expression vector pLV-U-TVA950 (Addgene 115236).

The first-generation vector genome plasmid pRV Δ G-4FLPo (Addgene 122050) was made by cloning the FLPo gene (9) into pRV Δ G-4Cre.

pAAV-synP-F14F15S-splitTVA-EGFP-tTA (Addgene 136917) is a FLP-dependent version of the Cre-dependent helper virus genome plasmid pAAV-synP-FLEX-splitTVA-EGFP-tTA (Addgene 52473) with orthogonal FRT sites(6) instead of orthogonal lox sites.

pCAG-hypBase was made by synthesizing the 1785-bp gene for an improved version of piggyBac transposase (10) and cloning it into the EcoRI and NotI sites of pCAG-GFP (7) (Addgene 11150).

pB-CAG-TEVP-IRES-mCherry (Addgene 174377) was made by cloning the CAG promoter (2), a mammalian codon-optimized version (11, 12) of the TEVP gene (S219V mutant) (13), the EMCV IRES (14), and the mCherry gene (5) into pB-CMV-MCS-EF1-Puro (System Biosciences #PB510B-1).

pAAV-synP-FLPo (Addgene 174378) was made by cloning the FLPo gene(9) into the EcoRI and AcclII sites of pAAV-synP-FLEX-EGFP-B19G (Addgene 59333).

pAAV-TREtight-H2b-emiRFP670-TEVP (Addgene 174379) was made by cloning an H2b-emiRFP670 fusion gene (15) (sequence from Addgene 136571 but with the internal kozak sequence replaced by a short GSG linker to prevent translation of fluorophore unfused to H2b), followed by a P2A sequence and the above-described TEVP gene, into the EcoRI and NheI sites of pAAV-TREtight-mTagBFP2-B19G (16) (Addgene 100799).

pRV Δ G-NPEST-4Cre (Addgene 174380) was made by cloning a synthesized fragment containing the 3' addition from Ciabatti et al. '17, with synonymous changes to 5 codons (17) in the immediate vicinity of the junction between the nucleoprotein gene and the 3' addition so that more than a single point mutation would be required to convert them to stop codons, into the PmlI and BstI sites of pRV Δ G-4Cre(18) (Addgene 98034).

pRV Δ G-N*PEST-4Cre (Addgene 174381) was made identically to the above except that the glycine codon in position 453 was replaced with a stop codon (TGA).

All of the above novel plasmids have been deposited with Addgene, with the accession numbers given above, and can be purchased from there except for pCAG-hypBase, the distribution of which is not permitted due to intellectual property constraints.

Production of lentiviral and adeno-associated viral vectors

Lentiviral vectors were made by transfection of HEK-293T/17 cells (ATCC 11268) as described (19) but using the vesicular stomatitis virus envelope expression plasmid pMD2.G (Addgene 12259) for all vectors except for LV-U-TVA950(B19G), which was made using the rabies virus envelope expression

plasmid pCAG-B19GVSVC (19). Lentiviral vectors expressing fluorophores were titered as described (20); titers of LV-U-TVA950(VSVG) and LV-U-TVA950(B19G) were assumed to be approximately the same as those of the fluorophore-expressing lentiviral vectors produced in parallel.

AAV1-synP-F14F15S-splitTVA-EGFP-tTA was packaged as serotype 1 by the UNC vector core (and can be purchased from there as well as from Addgene (catalog # 136917)).

AAV1-TREtight-mTagBFP2-B19G (which we have described previously(16, 21)), was packaged as serotype 1 by Addgene (catalog # 100798-AAV1).

AAV1-TREtight-H2b-emiRFP670-P2A-TEVP and AAV2-retro-synP-FLPo were made by transfecting HEK 293T/17 cells with the respective genome plasmid along with pHelper (Cellbiolabs VPK-421) and either pAAV-RC1 (Cellbiolabs VPK-421) or "rAAV2-retro helper" (Addgene 81070)(22), using Xfect Transfection Reagent (Takara 631318) according to the manufacturer's protocol, with collection of supernatant (and replacement with fresh media) at 3 days after transfection and collection of supernatant as well as the transfected cells at 5 days after transfection. Virus was pelleted from supernatants using PEG 8000; cells were lysed by four freeze-thaw cycles. Pelleted virus and cell lysate were pooled and treated with benzonase, purified on an iodixanol gradient, then concentrated in an Amicon Ultra-15 centrifugal filter unit (Millipore Sigma UFC9100).

Production of titering cell lines

To make reporter cell lines, HEK-293T/17 cells were infected with either pLV-CAG-FLEX-BFP-(mCherry)' or pLV-CAG-F14F15S-BFP-(mCherry)' at a multiplicity of infection of 100 in one 24-well plate well each. Cells were expanded to 2x 15cm plates each, then sorted on a FACS Aria to retain the top 10% most brightly blue fluorescent cells. After sorting, cells were expanded again to produce the cell lines 293T-FLEX-BC and 293T-F14F15S-BC, reporter lines for Cre and FLPo activity, respectively. TVA-expressing versions of these two cell lines were made by infecting one 24-well plate well each with LV-U-TVA950(VSVG) at an MOI of approximately 100; these cells were expanded to produce the cell lines 293T-FLEX-BC-TVA and 293T-F14F15S-BC-TVA.

Production of TEVP-expressing cell line

The 293T-TEVP cell line was made by transfecting HEK 293T/17 (ATCC CRL-11268) cells with pCAG-hypBase and pB-CAG-TEVP-IRES-mCherry in a 15 cm plate (293T/17) or one well each of a 24 well plate (BHK-B19G2 and BHK-EnvA2) using Lipofectamine 2000 (Thermo Fisher 11668019) according to the manufacturer's instructions, then expanding and sorting the cells on a FACS Aria (BD Biosciences) for the brightest 20% of red fluorescent cells, then expanding and freezing the sorted cells.

Production and titering of rabies viruses

RV Δ G-4Cre and RV Δ GL-4Cre were produced as described (18, 23), with EnvA-enveloped viruses made by using cells expressing EnvA instead of G for the last passage. Titering and infection of cell lines with serial dilutions of viruses was as described (24), with the 293T-TVA-FLEX-BC and 293T-TVA-F14F15S-BC lines used for B19G-enveloped viruses and the 293T-TVA-FLEX-BC and 293T-TVA-F14F15S-BC used for the EnvA-enveloped viruses. For the *in vivo* injections, the three EnvA-enveloped, Cre-encoding viruses were titered side by side, and the two higher-titer viruses were diluted so that the final titer of the injected stocks of all three viruses were approximately equal at 1.39E9 infectious units per milliliter.

The two new rabies viruses RV Δ G-NPEST-4Cre and RV Δ G-N*PEST-4Cre were produced as described(18, 23) but with only one amplification passage (P1) between the rescue transfection step and the final passage on EnvA-expressing cells. For the NPEST version, the following additional modifications were made: for the rescue transfection, the new cell line 293T-TEVP (see above) was used instead of HEK 293T-17, and pB-CAG-TEVP-IRES-mCherry (10 μ g per 15 cm plate) was included in the plasmid mix. Because pilot testing showed no clear advantage of the 293T-TEVP line over transfected 293Ts for passaging, the P1 passage was on HEK 293T/17 cells transfected with equal amounts of pCAG-B19G and pB-CAG-TEVP-IRES-mCherry (32 μ g of each plasmid per 15 cm plate). The final passage was on BHK-EnvA2 cells(24) transfected with pB-CAG-TEVP-IRES-mCherry. Lipofectamine 2000 (Thermo Fisher 11668019) was used for all transfections, following the manufacturer's protocol.

The final stocks of RV Δ G-NPEST-4Cre(EnvA) and RV Δ G-N*PEST-Cre(EnvA) were titered side by side as described(24) series on 293T-FLEX-BC-TVA cells (see above) in two-fold dilution series. Final titers of the viruses were determined to be 1.86e9 iu/ml for RV Δ G-NPEST-4Cre(EnvA) and 2.41e10 iu/mL (normalized) for

RVΔG-NEPEST-4Cre(EnvA). Prior to injection *in vivo* (see below), the N*PEST virus was diluted 12.96-fold in DPBS to match the titer of the NPEST version.

Immunostaining and imaging of cultured cells

Reporter cells (see above) plated on coverslips coated in poly-L-lysine (Sigma) were infected with serial dilutions of RVΔG-4Cre and RVΔGL-4Cre as described (24). Three days after infection, cells were fixed with 2% paraformaldehyde, washed repeatedly with blocking/permeabilization buffer (0.1% Triton-X (Sigma) and 1% bovine serum albumin (Sigma) in PBS), then labeled with a blend of three FITC-conjugated anti-nucleoprotein monoclonal antibodies (Light Diagnostics Rabies DFA Reagent, EMD Millipore 5100) diluted 1:100 in blocking buffer for 30 minutes, followed by further washes in blocking buffer, then finally briefly rinsed with distilled water and air-dried before mounting the coverslips onto microscope slides with Prolong Diamond Antifade (Thermo P36970) mounting medium. Images of wells at comparable multiplicities of infection (~0.1) were collected on a Zeiss 710 confocal microscope.

Extraction of viral genomic RNA and preparation for Sanger sequencing

RNA viral genomes were extracted from two Tripodi lab (EnvA/SiR-CRE and EnvA/SiR-FLPo) and three Wickersham lab (RVΔG-4mCherry, RVΔG-NPEST-4Cre(EnvA), and RVΔG-N*PEST-Cre(EnvA)) rabies virus samples using a Nucleospin RNA kit (Macherey-Nagel, Germany) and treated with DNase I (37°C for 1 hour, followed by 70°C for 5 minutes). Extracted RNA genomes were converted to complementary DNA using an AccuScript PfuUltra II RT-PCR kit (Agilent Technologies, USA) at 42°C for 2 hours with the following barcoded (so that individual viral particles' genomes would be marked with distinct barcodes) primer annealing to the rabies virus leader sequence:

Adapter_N8_leader_fp: TCAGACGATGCGTCATGCNNNNNNNACGCTTAACAACCAGATC

cDNA sequences from the leader through the first half of the rabies virus P gene were amplified using Platinum SuperFi Green Master Mix (Invitrogen (Thermo Fisher), USA) with cycling conditions as follows: denaturation at 98°C for 30 seconds, followed by 25 cycles of amplification (denaturation at 98°C for 5 seconds and extension at 72°C for 75 seconds), with a final extension at 72°C for 5 minutes, using the following primers:

pEX_adapter_fp: CAGCTCAGACGATGCGTCATGC

Barcode2_P_rp: GCAGAGTCATGTATAGCTTCTTGAGCTCTCGGCCAG

The ~2kb PCR amplicons were extracted from an agarose gel, purified with Nucleospin Gel and PCR Clean-up (Macherey-Nagel, Germany), and cloned into pEX-A (Eurofins Genomics, USA) using an In-Fusion HD Cloning Kit (Takara Bio, Japan). The cloned plasmids were transformed into Stellar competent cells (Takara Bio, Japan), and 200 clones per rabies virus sample were isolated and purified for sequencing. For each clone, the index and the 3' end of the N gene were sequenced until sequencing data was collected for over fifty clones per sample: 51 clones from SiR-CRE(EnvA), 50 from SiR-FLPo(EnvA), and 51 from RVΔG-4mCherry(EnvA). Although viral samples may contain plasmid DNA, viral mRNA, and positive-sense anti-genomic RNA, this RT-PCR procedure can amplify only the negative-sense RNA genome: the reverse transcription primer is designed to anneal to the leader sequence of the negative-strand genome so that cDNA synthesis can start from the negative-sense RNA genome, with no other possible templates. Additionally, the PCR amplifies the cDNA, not any plasmids which were transfected into producer cell lines during viral vector production, because the forward PCR primer anneals to the primer used in the reverse transcription, rather than any viral sequence. This RT-PCR protocol ensures that only negative-sense RNA rabies viral genomes can be sequenced.

Sanger sequencing of transgenes in SiR viruses

The procedure for sequencing the transgene inserts was the same as above, but with the RT primer being Adaptor_N8_M_fp (see below), annealing to the M gene and again with a random 8-nucleotide index to tag each clone, and with PCR primers pEX_adapter_fp (see above) and Barcode2_L_rp (see below), to amplify the sequences from the 3' end of the M gene to the 5' end of the L gene, covering the iCre-P2A-mCherryPEST (or FLPo-P2A-mCherryPEST) sequence.

Primers for RT and PCR for Sanger sequencing were as follows:

Adaptor_N8_M_fp:

TCAGACGATGCGTCATGCNNNNNNNCAACTCCAACCCTTGGGAGCA

Barcode2_L_rp:

GCAGAGTCATGTATAGTTGGGGACAATGGGGGTTCC

Sanger sequencing analysis of PEST region in SiR and control viruses

Alignment and mutation detection were performed using SnapGene 4.1.9 (GSL Biotech LLC, USA). Reference sequences of the viral samples used in this study were based on deposited plasmids in Addgene: pSAD-F3-NPEST-iCRE-2A-mCherryPEST (Addgene #99608), pSAD-F3-NPEST-FLPo-2A-mCherryPEST (Addgene #99609), and pRVΔG-4mCherry (Addgene #52488). Traces corresponding to indices and mutations listed in Figure 1 and Supplementary File S1 were also manually inspected and confirmed.

Single-molecule, real-time (SMRT) sequencing

Double-stranded DNA samples for SMRT sequencing were prepared similarly to the above, except that the clones generated from each of the three virus samples were tagged with one of the standard PacBio barcode sequences to allow identification of each clone's sample of origin following multiplex sequencing (see <https://www.pacb.com/wp-content/uploads/multiplex-target-enrichment-barcoded-multi-kilobase-fragments-probe-based-capture-technologies.pdf> and <https://github.com/PacificBiosciences/Bioinformatics-Training/wiki/Barcoding-with-SMRT-Analysis-2.3>). This was in addition to the random index (10 nucleotides in this case) that was again included in the RT primers in order to uniquely tag each individual genome.

RNA viral genomes were extracted from two Tripodi lab (SiR-CRE and Sir-FLPo) and one Wickersham lab (RVΔG-4Cre (18); see Addgene #98034 for reference sequence) virus samples using a Nucleospin RNA kit (Macherey-Nagel, Germany) and treated with DNase I (37°C for 1 hour, followed by 70° for 5 minutes). Primers for RT and PCR are listed below. PCR cycling conditions were as follows: denaturation at 98°C for 30 seconds, followed by 20 cycles of amplification (denaturation at 98°C for 5 seconds and extension at 72°C for 75 seconds), with a final extension at 72°C for 5 minutes. This left each amplicon with a 16bp barcode at each of its ends that indicated which virus sample it was derived from, in addition to a 10-nt index sequence that was unique to each genome molecule.

Primers for RT and PCR for SMRT sequencing were as follows:

RVΔG-4Cre:

RT:

Barcode1_cagc_N10_leader_fp:

TCAGACGATGCGTCATCAGCNNNNNNNNNACGCTTAACAACCAGATC

PCR:

Barcode1_cagc_fp: TCAGACGATGCGTCAT-CAGC

Barcode2_P_rp (see above)

SiR-CRE:

RT:

Barcode5_cagc_N10_leader_fp:

ACACGCATGACACACTCAGCNNNNNNNNNACGCTTAACAACCAGATC

PCR:

Barcode5_cagc_fp: ACACGCATGACACACT-CAGC

Barcode3_P_rp: GAGTGCTACTCTAGTACTTCTTGAGCTCTCGGCCAG

SiR-FLPo:

RT:

Barcode9_cagc_N10_leader_fp:

CTGCGTGCTCTACGACCAGCNNNNNNNNNACGCTTAACAACCAGATC

PCR:

Barcode9_cagc_fp: CTGCGTGCTCTACGAC-CAGC

Barcode4_P_rp: CATGTA CTGACTGATACACTTCTTGAGCTCTCGGCCAG

After the amplicons were extracted and purified from an agarose gel, the three were mixed together at 1:1:1 molar ratio. The amplicons' sizes were confirmed on the Fragment Analyzer (Agilent Technologies, USA), then hairpin loops were ligated to both ends of the mixed amplicons to make circular SMRTbell templates for Pacbio Sequel sequencing. SMRTbell library preparation used the PacBio Template Preparation Kit v1.0 and Sequel

Chemistry v3. Samples were then sequenced on a PacBio Sequel system running Sequel System v.6.0 (Pacific Biosciences, USA), with a 10-hour movie time.

Bioinformatics for PacBio sequence analysis

For the ~2kb template, the DNA polymerase with a strand displacement function can circle around the template and hairpins multiple times; the consensus sequence of multiple passes yields a CCS (circular consensus sequence) read for each molecule. Raw sequences were initially processed using SMRT Link v.6.0 (Pacific Biosciences, USA). Sequences were filtered for a minimum of read length 10 bp, pass 3, and read score 65. 127,178 CCS reads were filtered through passes 3 and Q10; 89,188 CCS reads through passes 5 and Q20; 29,924 CCS reads through passes 8 and Q30. Downstream bioinformatics analysis was performed using BLASR V5.3.2 for the alignment, bcftools v.1.6 for variant calling. Mutations listed in Figure 2 and Supplementary File S2 were also manually inspected and confirmed using Integrative Genomics Viewer 2.3.32 (software.broadinstitute.org/software/igv/). Analysis steps included the following: 1. Exclude CCS reads under 1000 bases, which may have been derived from non-specific reverse transcription or PCR reactions. 2. Classify the CCS reads to the three samples, according to the PacBio barcodes on the 5' ends. 3. For any CCS reads that contain the same 10-nucleotide random index, select only one of them, to avoid double-counting of clones derived from the same cDNA molecule. 4. Align the reads to the corresponding reference sequence (see Supplementary Files S3-S5). 5. Count the number of mutations at each nucleotide position of the reference sequences.

Surgeries and virus injections for two-photon imaging

All experimental procedures using mice were conducted according to NIH guidelines and were approved by the MIT Committee for Animal Care (CAC). Mice were housed 1-4 per cage under a normal light/dark cycle for all experiments.

Adult (>9 weeks, male and female) Cre-dependent tdTomato reporter Ai14 (25) (Jackson Laboratory #007908) or Arch-EGFP reporter Ai35D (26) (Jackson Laboratory # 012735) mice were anesthetized with isoflurane (4% in oxygen) and ketamine/xylazine (100mg/kg and 10mg/kg respectively, i.p.). Mice were given buprenorphine (0.1 mg/kg s.q.) and meloxicam (2 mg/kg s.q.) as preemptive analgesics, as well as eye ointment (Puralube); the scalp was then shaved, depilated with Nair, and thoroughly rinsed before the mice were mounted on a stereotaxic instrument (Stoelting Co.) with a hand warmer (Heat Factory) underneath the animal to maintain body temperature. The scalp was then disinfected with povidone-iodine, and an incision was made at the appropriate location (see below).

A 3 mm craniotomy was opened over primary visual cortex (V1). 300 nl of LV-U-TVA950(B19G) (see above) was injected into V1 (-2.70 mm AP, 2.50 mm LM, -0.26 mm DV; AP and LM stereotaxic coordinates are with respect to bregma; DV coordinate is with respect to brain surface) using a custom injection apparatus comprised of a hydraulic manipulator (MO-10, Narishige) with headstage coupled via custom adaptors to a wire plunger advanced through pulled glass capillaries (Wiretrol II, Drummond) back-filled with mineral oil and front-filled with virus solution. Glass windows composed of a 3mm-diameter glass coverslip (Warner Instruments CS-3R) glued (Optical Adhesive 61, Norland Products) to a 5mm-diameter glass coverslip (Warner Instruments CS-5R) were then affixed over the craniotomy with Metabond (Parkell). Seven days after injection of the lentiviral vector, the coverslips were removed and 300 nl of one of the three EnvA-enveloped rabies viral vectors (with equalized titers as described above) was injected at the same stereotaxic coordinates. Coverslips were reapplied and custom stainless steel headplates (eMachineShop) were affixed to the skulls around the windows.

***In vivo* two-photon imaging and image analysis**

Beginning seven days after injection of each rabies virus and continuing every seven days up to a maximum of four weeks following rabies virus injection, the injection sites were imaged on a Prairie/Bruker Ultima IV In Vivo two-photon microscope driven by a Spectra Physics Mai-Tai Deep See laser with a mode locked Ti:sapphire laser emitting at a wavelength of 1020 nm for tdTomato and mCherry or 920 nm for EGFP. Mice were reanesthetized and mounted via their headplates to a custom frame, again with ointment applied to protect their eyes and with a handwarmer maintaining body temperature. One field of view was chosen in each mouse in the area of maximal fluorescent labelling. The imaging parameters were as follows: image size 512 X 512 pixels (282.6 μm x 282.6 μm), 0.782 Hz frame rate, dwell time 4.0 μs , 2x optical zoom, Z-stack step size 1 μm . Image acquisition was controlled with Prairie View 5.4 software. Laser power exiting the 20x water-immersion objective

(Zeiss, W plan-apochromat, NA 1.0) varied between 20 and 65 mW depending on focal plane depth (Pockel cell value was automatically increased from 450 at the top section of each stack to 750 at the bottom section). For the example images of labeled cells, maximum intensity projections (stacks of 150-400 μm) were made with Fiji software. Cell counting was performed with the ImageJ Cell Counter plugin. When doing cell counting, week 1 tdTomato labelled cells were defined as a reference; remaining week 1 cells were the same cells at later time point that align with week 1 reference cells but the not-visible cells at week 1 (the dead cells). Plots of cell counts were made with Origin 7.0 software (OriginLab, Northampton, MA). For the thresholded version of this analysis (Supplementary Figure S4), in order to exclude cells that could possibly have been labeled only with mCherry in the SiR-CRE group, only cells with fluorescence intensity greater than the average of the mean red fluorescence intensities of cells imaged in Ai35 versus Ai14 mice at the same laser power at 1020 nm at 7 days postinjection (32.33 a.u.) were included in the population of cells tracked from 7 days onward.

Monosynaptic tracing experiments: Sanger sequencing of viral genomic RNA

Sanger sequencing of RV Δ G-NPEST-4Cre(EnvA) and RV Δ G-N*PEST-4Cre(EnvA) was as described above but with the following modifications. The following barcoded primer was used for RT-PCR.

Adaptor-UMI-N_fp_57:

```
ACACTCTTTCCCTACACGACGCTCTTCCGATCTNNNNNNNNNNNNNNNNNNNNNAGAAAGTCCGGAGGCTG  
TTTAT
```

cDNA sequences from the nucleoprotein gene through the first half of the rabies virus P gene were amplified using Platinum SuperFi Green Master Mix (Invitrogen (Thermo Fisher), USA) with cycling conditions as follows: denaturation at 98°C for 30 seconds, followed by 21 cycles of amplification (denaturation at 98°C for 5 seconds, annealing at 60°C for 10 seconds and extension at 72°C for 21 seconds), with a final extension at 72°C for 5 minutes, using the following primers:

i5-anchor_CTAGCGCT_fp_56:

```
AATGATACGGCGACCACCGAGATCTACACCTAGCGCTACACTCTTTCCCTACACGAC
```

P_Sanger_rp_56:

```
CAAGCAGAAGACGGCACGATTTTCCATCATCCAGGTG
```

The 700bp PCR amplicons for RV Δ G-NPEST-4Cre (EnvA) or RV Δ G-N*PEST-4Cre (EnvA) virus were cloned into pEX-A (Eurofins Genomics, USA) using an In-Fusion HD Cloning Kit (Takara Bio, Japan) as above. The plasmids were transformed into Stellar competent cells (Takara Bio, Japan), and 32 clones from each rabies virus sample were isolated and purified for sequencing.

Monosynaptic tracing experiments: surgeries and virus injections

Following preparation of mice as described above ("Surgeries and virus injections for two-photon imaging") the three helper AAV1s were combined at final titers of

3.6E10 gc/ml for AAV1-synP-F14F15S-splitTVA-EGFP-tTA and 6.60E11 gc/ml for AAV1-TREtight-mTagBFP2-B19G (when included) and AAV1-TREtight-H2b-emiRFP670-P2A-TEVP (when included) in DPBS (Fisher, 14-190-250). 250 nl of helper virus mixture was injected into layer 5 of barrel cortex (AP -1.55 mm w.r.t. bregma, LM 3.00 mm w.r.t. bregma, -DV 0.75 mm w.r.t. brain surface) of Ai14 mice; in the same surgery, 300 nl of AAV2-retro-synP-FLPo (1.16E13 gc/ml) was injected into dorsolateral striatum (AP 0.74 mm w.r.t. bregma, LM 2.25 mm w.r.t. bregma, DV -2.30 mm w.r.t. the brain surface). 7 days after AAV injection, 300nl of RV Δ G-NPEST-4Cre(EnvA) (1.86E9 iu/ml) or RV Δ G-N*PEST-4Cre(EnvA) (diluted 12.96-fold in DPBS from 2.41E10 iu/ml to 1.86E9 iu/ml) was injected in barrel cortex at the same site as the helper AAV mixtures.

Monosynaptic tracing experiments: perfusions and histology

12 days or 3 weeks (depending on experiment; see main text) after injection of rabies virus, mice were transcardially perfused with 4% paraformaldehyde in phosphate-buffered saline. Brains were postfixed overnight in 4% paraformaldehyde in PBS on a shaker at 4°C and cut into 50 μm coronal sections on a vibrating microtome (Leica, VT-1000S). Sections were collected anterior to posteriorly into 6 tubes containing cryoprotectant. Collection goes on for 15 rounds so that each tube contains a sixth of the collected tissue (15 sections in each tube). Sections were immunostained as described(21) with a chicken anti-GFP primary antibody (Aves Labs GFP-1020) 1:500 and donkey anti-chicken Alexa Fluor 488 secondary antibody (Jackson Immuno 703-545-155) 1:200. Sections were mounted with Prolong Diamond Antifade mounting medium (Thermo Fisher P36970).

Monosynaptic tracing experiments: cell counts and microscopy

Coronal sections between 1.2mm and -3.3mm relative to bregma were examined under an epifluorescence microscope (Zeiss, Imager.Z2). When necessary due to high density of labeled cells, images were taken with the same microscope for cell counting. tdTomato-labeled neurons in contralateral cortex and thalamus were counted manually with the Cell Counter plugin in ImageJ. For cells at the injection site, when tdTomato expressing cells were few and sparse (usually less than 100 per section), cells coexpressing mTagBFP2 or H2b-emiRFP670 alongside were counted manually adding separate labels to each and then looking for overlapping cells. When tdTomato expressing cells were dense, tdTomato labeled cells were first counted using the Analyze Particle function in ImageJ (size in micron²: 20-400; circularity: 0.20-1.00). The outline of these cells was then merged on top of images of mTagBFP2 and H2b-emiRFP670 labeled cells for the counting of the overlapping cells. Only one of the six series of sections (i.e., every sixth section: see above) was counted for each mouse.

Images for figures were taken on a confocal microscope (Zeiss, LSM 900). So that the confocal images of brain tissue included in the figures in this paper are representative of each group, the images were taken after the counts were conducted (see above), in each case using the mouse with the middle number of labeled neurons in that group (i.e., neither the highest nor the lowest in the group of 3 mice used for each condition).

REFERENCES FOR SUPPLEMENTARY METHODS

1. Marr RA, *et al.* (2004) Neprilysin regulates amyloid Beta peptide levels. *J Mol Neurosci* 22(1-2):5-11.
2. Niwa H, Yamamura K, & Miyazaki J (1991) Efficient selection for high-expression transfectants with a novel eukaryotic vector. *Gene* 108(2):193-199.
3. Atasoy D, Aponte Y, Su HH, & Sternson SM (2008) A FLEX switch targets Channelrhodopsin-2 to multiple cell types for imaging and long-range circuit mapping. *The Journal of neuroscience : the official journal of the Society for Neuroscience* 28(28):7025-7030.
4. Subach OM, Cranfill PJ, Davidson MW, & Verkhusha VV (2011) An enhanced monomeric blue fluorescent protein with the high chemical stability of the chromophore. *PLoS One* 6(12):e28674.
5. Shaner NC, *et al.* (2004) Improved monomeric red, orange and yellow fluorescent proteins derived from *Discosoma* sp. red fluorescent protein. *Nat Biotechnol* 22(12):1567-1572.
6. Turan S, Kuehle J, Schambach A, Baum C, & Bode J (2010) Multiplexing RMCE: versatile extensions of the Flp-recombinase-mediated cassette-exchange technology. *J Mol Biol* 402(1):52-69.
7. Matsuda T & Cepko CL (2004) Electroporation and RNA interference in the rodent retina in vivo and in vitro. *P Natl Acad Sci USA* 101(1):16-22.
8. Bates P, Young JA, & Varmus HE (1993) A receptor for subgroup A Rous sarcoma virus is related to the low density lipoprotein receptor. *Cell* 74(6):1043-1051.
9. Raymond CS & Soriano P (2007) High-efficiency FLP and PhiC31 site-specific recombination in mammalian cells. *PLoS One* 2(1):e162.
10. Yusa K, Zhou L, Li MA, Bradley A, & Craig NL (2011) A hyperactive piggyBac transposase for mammalian applications. *Proc Natl Acad Sci U S A* 108(4):1531-1536.
11. Gray DC, Mahrus S, & Wells JA (2010) Activation of specific apoptotic caspases with an engineered small-molecule-activated protease. *Cell* 142(4):637-646.
12. Yang CF, *et al.* (2013) Sexually dimorphic neurons in the ventromedial hypothalamus govern mating in both sexes and aggression in males. *Cell* 153(4):896-909.
13. Kapust RB, *et al.* (2001) Tobacco etch virus protease: mechanism of autolysis and rational design of stable mutants with wild-type catalytic proficiency. *Protein Eng* 14(12):993-1000.
14. Gallardo HF, Tan C, & Sadelain M (1997) The internal ribosomal entry site of the encephalomyocarditis virus enables reliable coexpression of two transgenes in human primary T lymphocytes. *Gene Ther* 4(10):1115-1119.
15. Matlashov ME, *et al.* (2020) A set of monomeric near-infrared fluorescent proteins for multicolor imaging across scales. *Nat Commun* 11(1):239.
16. Liu K, *et al.* (2017) Lhx6-positive GABA-releasing neurons of the zona incerta promote sleep. *Nature* 548(7669):582-587.

17. Ciabatti E, Gonzalez-Rueda A, Mariotti L, Morgese F, & Tripodi M (2017) Life-Long Genetic and Functional Access to Neural Circuits Using Self-Inactivating Rabies Virus. *Cell* 170(2):382-392 e314.
18. Chatterjee S, *et al.* (2018) Nontoxic, double-deletion-mutant rabies viral vectors for retrograde targeting of projection neurons. *Nat Neurosci* 21(4):638-646.
19. Wickersham IR, *et al.* (2015) Lentiviral vectors for retrograde delivery of recombinases and transactivators. *Cold Spring Harb Protoc* 2015(4):368-374.
20. Sullivan HA & Wickersham IR (2015) Concentration and purification of rabies viral and lentiviral vectors. *Cold Spring Harb Protoc* 2015(4):386-391.
21. Lavin TK, Jin L, & Wickersham IR (2019) Monosynaptic tracing: a step-by-step protocol. *J Chem Neuroanat*:101661.
22. Tervo DG, *et al.* (2016) A Designer AAV Variant Permits Efficient Retrograde Access to Projection Neurons. *Neuron* 92(2):372-382.
23. Wickersham IR & Sullivan HA (2015) Rabies viral vectors for monosynaptic tracing and targeted transgene expression in neurons. *Cold Spring Harb Protoc* 2015(4):375-385.
24. Wickersham IR, Sullivan HA, & Seung HS (2010) Production of glycoprotein-deleted rabies viruses for monosynaptic tracing and high-level gene expression in neurons. *Nature protocols* 5(3):595-606.
25. Madisen L, *et al.* (2010) A robust and high-throughput Cre reporting and characterization system for the whole mouse brain. *Nature neuroscience* 13(1):133-140.
26. Madisen L, *et al.* (2012) A toolbox of Cre-dependent optogenetic transgenic mice for light-induced activation and silencing. *Nature neuroscience* 15(5):793-802.

Supplementary File S1: Sanger sequencing data of all clones shown in Figure 1.

51 clones derived from SiR-CRE, 50 from SiR-FLPo, and 51 from RV Δ G-4mCherry are identified by their unique indices. All of the indices as well as the sequences corresponding to the 3' end of the nucleoprotein gene are shown.

Supplementary File S1

bioRxiv preprint doi: <https://doi.org/10.1101/550640>; this version posted August 3, 2021. The copyright holder for this preprint (which was not certified by peer review) is the author/funder, who has granted bioRxiv a license to display the preprint in perpetuity. It is made available under aCC-BY-ND 4.0 International license.

Random 8-nucleotide index

N gene, tobacco etch virus protease cleavage site, PEST, transcription stop/polyA signal, mutation

Gly453* in N-TEV-PEST of SiR-CRE (50/51 clones)

TCTCGGAA, TTATGGGC, CCTGCCGA, CGTCGTTG, ACTCTAGT, GATCCGGT, ATTATGTA, TATTATCC, ATGCTAGA, GTTGTTTC, GAGTCGAC, GTCGACCT, CAAGAGTA, CGAAGCCA, GCGTGATA, CGTCCAGA, CTTGGTCC, GGGGTTTT, GTCCATAC, GTTTAATA, CAAAATCC, GTGGAGGC, CGGAAGGT, AGGACGGG, CCTCGGGA, GCATTTGC, TGGTTCGG, ATTTAGTC, ATGGGTAA, CTACGGGG, CCTGGTAC, GCATTTCA, AGTGTAGG, CGCATAGA, GTCACAAT, GTATGCTT, TCGGGTTT, ATGTTGTC, CAGCCGTA, GAGTGGCC, GGCCATT, GGATTTCC, GTACAAGC, GAAGATAT, AAACAGAT, AAGGCCTT, CGTTCGTC, AAAGACTA, ACTGAAAG, TGGGGATA

ATCATCAAGCCCCTCCAAACTCATTGCGCCGAGTTTCTAAACAAGACATATTCGAGTGACTCAAGTTCCGAGAGA
ACCTCTACTTCCAATCGGGATCCGGTAGCCATGGCTTCCCGCCGGAGGTGGAGGAGCAGGATGATGGCACGCT
GCCCATGTCTTGTGCCAGGAGAGCGGGATGGACCGTACCCTGCAGCCTGTGCTTCTGCTAGGATCAATGTGT
AAGAAGTTGAATAACAAAATGCCGAAATCTACGGATTGTGTATATCCATCATGAAAAAAA

Asp449Glufs*16 in N-TEV-PEST of SiR-CRE (1/51 clones)

AGGCTAAC

ATCATCAAGCCCCTCCAAACTCATTGCGCCGAGTTTCTAAACAAGACATATTCGAGTGAACTCAAGTTCCGAGAGA
AACCTCTACTTCCAATCGGGATCCGGTAGCCATGGCTTCCCGCCGGAGGTGGAGGAGCAGGATGATGGCACGCT
TGCCCATGTCTTGTGCCAGGAGAGCGGGATGGACCGTACCCTGCAGCCTGTGCTTCTGCTAGGATCAATGTGT
TAAAGAAGTTGAATAACAAAATGCCGAAATCTACGGATTGTGTATATCCATCATGAAAAAAA

No mutations in sequenced region of N-TEV-PEST of SiR-FLPo (4/50 clones)

TCATTAT, AAGTCGAA, TGAATACA, TATACAGC

ATCATCAAGCCCCTCCAAACTCATTGCGCCGAGTTTCTAAACAAGACATATTCGAGTGACTCAAGTTCCGGAGAGA
ACCTCTACTTCCAATCGGGATCCGGTAGCCATGGCTTCCCGCCGGAGGTGGAGGAGCAGGATGATGGCACGCT
GCCCATGTCTTGTGCCAGGAGAGCGGGATGGACCGTACCCTGCAGCCTGTGCTTCTGCTAGGATCAATGTGT
AAGAAGTTGAATAACAAAATGCCGAAATCTACGGATTGTGTATATCCATCATGAAAAAAA

Gly453* in N-TEV-PEST of SiR-FLPo (18/50 clones)

GAGGCCGC, CTTATCAC, TCAGTTTT, CTTAGCA, TTACTTTT, AAAATAAG, CCATTTCT, GTCACATT, GCATACGG, AGTATTAA, CCGGGTTG, GGTAATAA, CAGGGAGA, CATTTTTT, TGACAAAT, TCGTATAT, TAGGGATT, GATCCCCG

ATCATCAAGCCCCTCCAAACTCATTGCGCCGAGTTTCTAAACAAGACATATTCGAGTGACTCAAGTTCCGAGAGA
ACCTCTACTTCCAATCGGGATCCGGTAGCCATGGCTTCCCGCCGGAGGTGGAGGAGCAGGATGATGGCACGCT
GCCCATGTCTTGTGCCAGGAGAGCGGGATGGACCGTACCCTGCAGCCTGTGCTTCTGCTAGGATCAATGTGT
AAGAAGTTGAATAACAAAATGCCGAAATCTACGGATTGTGTATATCCATCATGAAAAAAA

Ser450* in N-TEV-PEST of SiR-FLPo (28/50 clones)

TACTAAAT, TTCAACTA, TAATAGGC, CGCGGGTC, AGGGTGCC, TTGCTGAC, CGGCCCTT, TACAGCGA, GAGTAGGA, GTAAACGC, CTATGGGT, TTGATTGA, AGGATTCT, GAGGTTTG, TACTTAGC, CCTGTAGT, GGGGTGGA, TTAAGTTG, CTCAATGA, CAGATCTG, GTCTGGTA, GCGTTGGG, TAAACGAG, TACTTGAG, CGGGGTGT, CGATCCCG, TGGGTGTC, GCCACGAT

ATCATCAAGCCCCTCCAAACTCATTGCGCCGAGTTTCTAAACAAGACATATTCGAGTGACTCAAGTTCCGGAGAGA
ACCTCTACTTCCAATCGGGATCCGGTAGCCATGGCTTCCCGCCGGAGGTGGAGGAGCAGGATGATGGCACGCT
GCCCATGTCTTGTGCCAGGAGAGCGGGATGGACCGTACCCTGCAGCCTGTGCTTCTGCTAGGATCAATGTGT
AAGAAGTTGAATAACAAAATGCCGAAATCTACGGATTGTGTATATCCATCATGAAAAAAA

No mutations in sequenced region of RVΔG-4mCherry (51/51 clones)

CGCCCCGC, GCCAATCT, GGCGGAAT, TGTGGAAC, GGAGGGAT, CGTAGTGT, AGAATCTC, TGTCTGGC, GCCTTTTA, TGGAAATCT, TTGTAATG, AGGCCTGT, CGGATATA, AATCCAAA, AAGGAAAA, GAATCAT, GCCGCTTC, CTTTGCCG, CGCAACCT, TCGGGCAT, GGGCGACT, AACTGGAT, TCGTCCG, TCAAAGCG, CGAGGCC, ATGTAGGA, AGATACGT, TGGCTTCG, ATTTCTA, TCGTCCG, TCGGAGCG, CTGTTATA, TACCGTTC, CGAATGTC, CCCTTTT, TGAGTGGG, TGTAATA, AAGGAGTC, ATTACCCT, TCCCTGAC, TGGTAAA, ACTATCTC, CCGGAAGC, CTTGGAGG, GCAACAAT, ATTACCGT, AATAGCAG, ACCATAGT, GGGTTGGT, CATTATT, GGGTACAC

ATCATCAAGCCCCTCCAAACTCATTGCGCCGAGTTTCTAAACAAGACATATTCGAGTGACTCATAAAGAAGTTGAATA
ACAAAATGCCGAAATCTACGGATTGTGTATATCCATCATGAAAAAAA

Supplementary File S2: Summary tables of SMRT sequencing data. These tables show all mutations occurring at positions mutated at greater than 2% frequency in the three virus samples analyzed. Position numbers in these tables refer to the sequences in the three Genbank files below (Supplementary Files S3-S5).

SINGLE-MOLECULE, REAL-TIME SEQUENCING RESULTS

Frameshifts and insertions

Position numbers in this file refer to the reference sequences included as Supplementary Files S4-S5. A "frameshift" is included in Tables 1a-2b if the number of deleted bases in positions 1439-1492 (the vicinity of the junction of the end of the N gene and the intended 3' addition) is not an integer multiple of 3, with insertions ignored. "Any error" includes either the apparent frameshifts, or the new TAA/TAG/TGA stop codons, or both, with insertions ignored. The number of "frameshifts" increases considerably if insertion mutations are included in the calculation, indicating that there is a much higher insertion rate as compared to that of deletion; however, previous studies have found that spurious insertions are high with SMRT (see main text), so we ignore insertions in this paper apart from summarizing the data below.

SiR-CRE				
Position	Mutation	CCS3	CCS5	CCS8
# Sequences		22205	866	239
243	GAT (reference)	20273	784	209
	GCT	3	0	0
	GGT	5	0	0
	GTT	1856	79	29
	DEL	68	3	1
1111	GAA (reference)	19807	760	197
	GAC	1	0	0
	GAG	2396	105	42
	GAT	0	0	0
	DEL	1	1	0
1457	AGA	6	0	0
	CGA	1	0	0
	GGA (reference)	140	5	1
	TGA	22032	858	237
	DEL	26	3	1
[1439, 1492]	Frame shift (#DELs not an integer multiple of 3, Insertion ignored)	507	13	3
[1439, 1492]	Any error (insertion ignored)	22104	864	239
% mutation in [1439, 1492]		100%	100%	100%

Table 1a. All mutations in the SiR-CRE sample at positions mutated at >2% frequency at all stringencies (CCS3, CCS5, CCS8), as well as frameshift mutations found in the C-terminal region of N.

SiR-CRE				
Position	Mutation	CCS3	CCS5	CC8
[1439, 1492]	Number of frame shifts due to DEL (number of DELs not an integer multiple of 3, insertion ignored)	507	13	3
[1439, 1492]	Number of frame shifts due to either DEL or INS or both (Sequence length not an integer multiple of 3)	2504	89	14
[1439, 1492]	Any error (insertion included)	22174	865	239

Table 1b. Frameshift mutations in the C-terminal region of N in the SiR-CRE sample at positions mutated at >2% frequency at all stringencies (CCS3, CCS5, CCS8).

SiR-FLPo				
Position	Mutation	CCS3	CCS5	CCS8
#Sequences		17086	695	210
1449	TAA	28	1	0
	TCA (reference)	8405	333	94
	TGA	8624	360	115
	TTA	3	0	0
	DEL	26	1	1
1457	AGA	3	0	0
	CGA	0	0	0
	GGA (reference)	11088	462	139
	TGA	5979	233	71
	DEL	16	0	0
[1439, 1492]	Frameshifts (#DELS not an integer multiple of 3, Insertion ignored)	448	11	3
[1439, 1492]	Any error (insertion ignored)	14444	589	180
% of mutation		85%	85%	86%

Table 2a. All mutations in the SiR-FLPo sample at positions mutated at >2% frequency at all stringencies (CCS3, CCS5, CCS8), as well as frameshift mutations found in the C-terminal region of N.

SiR-FLPo				
Position	Mutation	CCS3	CCS5	CCS8
[1439, 1492]	Number of frame shifts due to DEL (number of DELs not an integer multiple of 3, insertion ignored)	448	11	3
[1439, 1492]	Number of frame shifts due to either DEL or INS or both (Sequence length not an integer multiple of 3)	3562	121	24
[1439, 1492]	Any error (insertion included)	15818	642	196

Table 2b. Frameshift mutations in the C-terminal region of N in the SiR-FLPo sample at positions mutated at >2% frequency at all stringencies (CCS3, CCS5, CCS8).

RV Δ G-4Cre				
Position	Mutation	CCS3	CCS5	CC8
# Sequences		17978	757	254
1355	ACT	1706	84	28
	CCT	3	0	0
	GCT	1	1	1
	TCT (reference)	16139	667	224
	DEL	129	5	1
Total				

Table 3. All mutations in the SiR-FLPo sample at positions mutated at >2% frequency at all stringencies (CCS3, CCS5, CCS8).

Tables of all mutations above 2% frequency threshold

Table 4a to 4c list all single-nucleotide substitutions and deletions at positions mutated at >2% threshold frequency. The percentage of mutations is calculated based on the total number of single nucleotide and deletion mutations divided by the total number of reads aligned, when insertion mutations are ignored. Deletion mutations dominate in the medium-frequency range between 2% and 5%.

	Reference	Position	A	C	G	T	DEL	Un-mutated	Mutated (SNP/DEL)	% Mutation (SNP/DEL)
CCS3	G	1457	6	1	140	22032	26	140	22065	99.4
	A	1111	19807	1	2396	0	1	19807	2398	10.8
	A	243	20273	3	5	1856	68	20273	1932	8.7
	T	615	4	0	2	21229	970	21229	976	4.4
	G	1124	5	0	21356	7	837	21356	849	3.8
	A	81	21358	9	2	0	836	21358	847	3.8
	A	31	21381	0	0	0	824	21381	824	3.7
	T	713	1	2	4	21487	711	21487	718	3.2
	T	338	0	0	9	21498	698	21498	707	3.2
	A	1665	21544	1	4	0	656	21544	661	3.0
	A	53	21606	0	0	1	598	21606	599	2.7
	C	411	8	21683	0	1	513	21683	522	2.4
A	838	21718	1	0	1	485	21718	487	2.2	
CCS5	G	1457	0	0	5	858	3	5	861	99.4
	A	1111	760	0	105	0	1	760	106	12.2
	A	243	784	0	0	79	3	784	82	9.5
	A	31	828	0	0	0	38	828	38	4.4
	G	1124	0	0	831	0	35	831	35	4.0
	T	615	0	0	0	834	32	834	32	3.7
	A	81	837	1	1	0	27	837	29	3.3
	T	338	0	0	1	840	25	840	26	3.0
	T	713	0	0	1	841	24	841	25	2.9
	C	411	0	843	0	0	23	843	23	2.7
	A	53	846	0	0	0	20	846	20	2.3
CCS8	G	1457	0	0	1	237	1	1	238	99.6
	A	1111	197	0	42	0	0	197	42	17.6
	A	243	209	0	0	29	1	209	30	12.6
	A	31	228	0	0	0	11	228	11	4.6
	T	615	0	0	0	232	7	232	7	2.9
	G	1124	0	0	232	0	7	232	7	2.9
	C	411	0	233	0	0	6	233	6	2.5

Table 4a. SiR-CRE: substitutions and deletions at positions mutated at >2% frequency at all stringencies (CCS3, CCS5, CCS8).

	Reference	Position	A	C	G	T	DEL	Un-mutated	Mutated (SNP/DEL)	% Mutation (SNP/DEL)
CCS3	C	1449	28	8405	8624	3	26	8405	8681	50.8
	G	1457	3	0	11088	5979	16	11088	5998	35.1
	T	615	4	0	0	16322	760	16322	764	4.5
	A	81	16410	4	2	5	665	16410	676	4.0
	G	1124	0	0	16410	3	673	16410	676	4.0
	T	713	1	0	2	16500	583	16500	586	3.4
	A	1665	16536	1	1	0	548	16536	550	3.2
	A	31	16547	0	0	0	539	16547	539	3.2
	T	338	0	1	4	16582	499	16582	504	2.9
	A	53	16672	2	2	0	410	16672	414	2.4
	C	411	6	16683	1	0	396	16683	403	2.4
	A	838	16696	0	0	0	390	16696	390	2.3
G	208	301	0	16739	44	2	16739	347	2.0	
CCS5	C	1449	1	333	360	0	1	333	362	52.1
	G	1457	0	0	462	233	0	462	233	33.5
	A	81	665	0	0	0	30	665	30	4.3
	T	615	1	0	0	668	26	668	27	3.9
	A	1665	669	0	1	0	25	669	26	3.7
	T	713	0	0	0	671	24	671	24	3.5
	T	338	0	0	0	673	22	673	22	3.2
	C	411	0	676	0	0	19	676	19	2.7
	G	1124	0	0	676	0	19	676	19	2.7
	A	838	679	0	0	0	16	679	16	2.3
	G	346	0	0	680	0	15	680	15	2.2
	A	31	681	0	0	0	14	681	14	2.0
CCS8	C	1449	0	94	115	0	1	94	116	55.2
	G	1457	0	0	139	71	0	139	71	33.8
	T	713	0	0	0	203	7	203	7	3.3
	A	53	205	0	0	0	5	205	5	2.4
	A	81	205	0	0	0	5	205	5	2.4

Table 4b. SiR-FLPo: substitutions and deletions at positions mutated at >2% frequency at all stringencies (CCS3, CCS5, CCS8).

	Reference	Position	A	C	G	T	DEL	Un-mutated	Mutated (SNP/DEL)	% Mutation (SNP/DEL)
CCS3	T	1355	1706	3	1	16139	129	16139	1839	10.2
	A	31	16732	0	0	0	1246	16732	1246	6.9
	T	615	2	0	1	17266	709	17266	712	4.0
	A	81	17300	4	2	1	671	17300	678	3.8
	G	1124	0	0	17379	4	595	17379	599	3.3
	T	713	0	1	1	17469	507	17469	509	2.8
	T	338	1	0	2	17503	472	17503	475	2.6
	A	1506	17520	0	0	0	458	17520	458	2.5
CCS5	A	53	17579	1	2	1	395	17579	399	2.2
	T	1355	84	0	1	667	5	667	90	11.9
	A	31	703	0	0	0	54	703	54	7.1
	A	81	717	0	0	0	40	717	40	5.3
	T	615	0	0	0	729	28	729	28	3.7
	G	1124	0	0	738	0	19	738	19	2.5
	A	53	739	0	0	0	18	739	18	2.4
	T	713	0	0	0	740	17	740	17	2.2
CCS8	A	1506	740	0	0	0	17	740	17	2.2
	T	1355	28	0	1	224	1	224	30	11.8
	A	31	241	0	0	0	13	241	13	5.1
	T	615	0	0	0	248	6	248	6	2.4

Table 4c. RVΔG-4Cre: substitutions and deletions at positions mutated at >2% frequency at all stringencies (CCS3, CCS5, CCS8).

Supplementary File S3: SiR-CRE amplicon reference sequence. This Genbank-format file contains the expected (i.e., based on the published sequence: Addgene #99608) sequence of amplicons obtained from SiR-CRE for SMRT sequencing.

Supplementary File S3

LOCUS Exported 2183 bp ds-DNA linear SYN
07-JAN-2019
DEFINITION synthetic linear DNA.
ACCESSION .
VERSION .
KEYWORDS .
SOURCE synthetic DNA construct
ORGANISM synthetic DNA construct
REFERENCE 1 (bases 1 to 2183)
AUTHORS Trial User
TITLE Direct Submission
JOURNAL Exported Jan 7, 2019 from SnapGene 4.1.9
<http://www.snapgene.com>

FEATURES Location/Qualifiers
source 1..2183
/organism="PCR product"
/mol_type="other DNA"
primer_bind 1..48
/label=Barcode5_cagc_N10_leader_fp
primer_bind 1..20
/label=Barcode5_cagc_fp
gap 21..30
/estimated_length=10
5'UTR 31..100
/label=RV leader
/note="SPBN leader"
CDS 101..1450
/codon_start=1
/locus_tag="N"
/label=N
/note="N"
/
translation="MDADKIVFKVNNQVVSLKPEIIVDQY EYKYP AIKDLKKPCITLGK
APDLNKAYKSVLSGMSAAKLNPDVCSYLAAMQFFEGT CPEDWTSYGIVIARKGDKIT
PGSLVEIKRTDVEGNWALTGGMELTRDPTVPEHASLVGLLLSLYRLSKISGQNTGNYKT
NIADRIEQIFETAPFVKIVEHHTLMTTHKMCANWSTIPNFRFLAGTYDMFFSRIEHLYS
AIRVGT VVTAYEDCSGLVSFTGFIKQINLTAREAILYFFHKNFEEEIRRMFEPGQETAV
PHSYFIHFRSLGLSGKSPYSSNAVGHVFNL IHFVGCYMGQVRSLNATVIAACAPHEMSV
LGGYLGEFFGKGT FERRFFRDEKELQEYEAELTKTDVALADDGTVNSDDEDYFSGET
RSPEAVYTRIMNGGRLKRSHIRRYVSVSSNHQARPNSFAEFLNKTYSSDS"
CDS 1460..1480
/codon_start=1
/locus_tag="TEV site"

```

        /label=TEV site
        /note="TEV site"
        /translation="ENLYFQS"
CDS      1490..1609
        /codon_start=1
        /locus_tag="ECFP destabilized by fusion to
residues 422-461
        of mouse ornithine decarboxylase, giving an in
vivo(1)"
        /product="ECFP destabilized by fusion to residues
422-461
        of mouse ornithine decarboxylase, giving an in
vivo
        half-life of ~2 hours"
422-461
        /label=ECFP destabilized by fusion to residues
422-461...
        /label=ECFP destabilized by fusion to residues
422-461 of
        mouse ornithine decarboxylase, giving an in
vivo(1)
        /note="destabilization domain"
        /note="mammalian codon-optimized"
        /
translation="SHGFPPEVEEQDDGTLPMSCAQESGMDRHPAACASARINV"
CDS      1703..2167
        /codon_start=1
        /locus_tag="P"
        /label=P
        /note="P"
        /
translation="MSKIFVNPSAIRAGLADLEMAEETVDLINRNIEDNQAHLQGEPIE
VDNLPEDMGRHLHDDGKSPNHGEIAKVGEGKYREDFQMDEGEDPSFLFQSYLENVGVQI
VRQMRSGERFLKIWSQTVEEIISYVAVNFPNPPGKSSDKSTQTTGRELKK"
        primer_bind      complement(2148..2183)
        /label=Barcode3_P_rp
ORIGIN
      1 acacgcatga cacactcagc nnnnnnnnnn acgcttaaca accagatcaa
agaaaaaaca
      61 gacattgtca attgcaaagc aaaaatgtaa caccctaca atggatgccg
acaagattgt
     121 attcaaagtc aataatcagg tggctctctt gaagcctgag attatcgtgg
atcaatatga
     181 gtacaagtac cctgccatca aagatttgaa aaagccctgt ataaccctag
gaaaggctcc
     241 cgatttaa ataaagc ataca agtcagtttt gtcaggcatg agcgccgcca
aacttaatcc
```

Supplementary File S3

301 tgacgatgta tgttcctatt tggcagcggc aatgcagttt tttgagggga
catgtccgga
361 agactggacc agctatggaa ttgtgattgc acgaaaagga gataagatca
ccccaggttc
421 tctggtggag ataaaacgta ctgatgtaga agggaattgg gctctgacag
gaggcatgga
481 actgacaaga gaccccactg tccctgagca tgcgtcctta gtcggtcttc
tcttgagtct
541 gtataggttg agcaaaatat ccgggcaaaa cactggtaac tataagacaa
acattgcaga
601 caggatagag cagatTTTTG agacagcccc ttttgTtaaa atcgtggaac
accatactct
661 aatgacaact cacaaaatgt gtgctaattg gagtactata ccaaacttca
gatttttggc
721 cggaacctat gacatgtttt tctcccggat tgagcatcta tattcagcaa
tcagagtggg
781 cacagttgtc actgcttatg aagactgttc aggactggta tcatttactg
ggttcataaa
841 acaaatcaat ctaccgcta gagaggcaat actatatttc ttccacaaga
actttgagga
901 agagataaga agaatgtttg agccagggca ggagacagct gttcctcact
cttatttcat
961 ccacttccgt tcaactaggct tgagtgggaa atctccttat tcatcaaatg
ctgttggtca
1021 cgtgttcaat ctcaattcact ttgtaggatg ctatatgggt caagtccagat
ccctaaatgc
1081 aacggttatt gctgcatgtg ctctcatga aatgtctggt ctagggggct
atctgggaga
1141 ggaattcttc gggaaaggga catttgaaag aagattcttc agagatgaga
aagaacttca
1201 agaatacgag gcggtgaac tgacaaagac tgacgtagca ctggcagatg
atggaactgt
1261 caactctgac gacgaggact acttttcagg tgaaaccaga agtccggagg
ctgtttatac
1321 tcgaatcatg atgaatggag gtcgactaaa gagatctcac atacggagat
atgtctcagt
1381 cagttccaat catcaagccc gtccaaactc attcgccgag tttctaaaca
agacatattc
1441 gagtgactca ggttccggag agaacctcta cttccaatcg ggatccggta
gccatggctt
1501 cccgccggag gtggaggagc aggatgatgg cacgctgcc atgtcttgtg
cccaggagag
1561 cgggatggac cgtcaccctg cagcctgtgc ttctgctagg atcaatgtgt
aagaagttga
1621 ataacaaaat gccggaaatc tacggattgt gtatatccat catgaaaaaa
actaacaccc
1681 ctctttcga accatcccaa acatgagcaa gatctttgtc aatcctagtg
ctattagagc
1741 cggctctggcc gatcttgaga tggctgaaga aactgttgat ctgatcaata
gaaatatcga

Supplementary File S3

```
1801 agacaatcag gctcatctcc aaggggaacc catagaggtg gacaatctcc
ctgaggatat
1861 ggggcgactt cacctggatg atggaaaatc gcccaacat ggtgagatag
ccaaggtggg
1921 agaaggcaag tatcgagagg actttcagat ggatgaagga gaggatccta
gcttcctggt
1981 ccagtcatac ctggaaaatg ttggagtcca aatagtcaga caaatgaggt
caggagagag
2041 atttctcaag atatggtcac agaccgtaga agagattata tcctatgtcg
cggtcaactt
2101 tcccaaccct ccaggaaagt cttcagagga taaatcaacc cagactactg
gccgagagct
2161 caagaagtac tagagtagca ctc
//
```

Supplementary File S4: SiR-FLPo amplicon reference sequence. This Genbank-format file contains the expected (i.e., based on the published sequence: Addgene # 99609) sequence of amplicons obtained from SiR-FLPo for SMRT sequencing.

LOCUS Exported 2183 bp ds-DNA linear SYN
07-JAN-2019
DEFINITION synthetic linear DNA.
ACCESSION .
VERSION .
KEYWORDS .
SOURCE synthetic DNA construct
ORGANISM synthetic DNA construct
REFERENCE 1 (bases 1 to 2183)
AUTHORS Trial User
TITLE Direct Submission
JOURNAL Exported Jan 7, 2019 from SnapGene 4.1.9
<http://www.snapgene.com>
FEATURES Location/Qualifiers
source 1..2183
/organism="synthetic DNA construct"
/mol_type="other DNA"
primer_bind 1..48
/label=Barcode9_cagc_N10_leader_fp
primer_bind 1..20
/label=Barcode9_cagc_fp
gap 21..30
/estimated_length=10
5'UTR 31..100
/label=RV leader
/note="SPBN leader"
misc_feature 89..97
/label=Transcription start signal (N)
CDS 101..1450
/codon_start=1
/locus_tag="N"
/label=N
/note="N"
/
translation="MDADKIVFKVNNQVVSLKPEIIVDQY EYKYP A IKDLKKPCITL GK
APDLNKAYKSVLSGMSAAKLNPDVCSYLAAMQFFEGT CPEDWTSY GIVIARKGDKIT
PGSLVEIKRTDVEGNWALTGGMELTRDPTVPEHASLVGLLLSLYRLSKISGQNTGNYKT
NIADRIEQIFETAPFVKIVEHHTLMTTHKMCANWSTIPNFRFLAGTYDMFFSRIEHLYS
AIRVGT VVTAYEDCSGLVSFTGFIKQINLTAREAILYFFHKNFEEEIRRMFEPGQETAV
PHSYFIHFRSLGLSGKSPYSSNAVGHVFNL IHFVGCYMGQVRSLNATVIAACAPHEMSV
LGGYLGEFFGKGT FERRFFRDEKELQEYEA AELTKTDVALADDGTVNSDDEDYFSGET
RSPEAVYTRIMMNGGRLKRSHIRRYVSVSSNHQARPNSFAEFLNKTYSSDS"
CDS 1460..1480

Supplementary File S4

```

/codon_start=1
/product="tobacco etch virus (TEV) protease
recognition and
cleavage site"
/label=TEV site
/translation="ENLYFQS"
CDS
1490..1609
/codon_start=1
/locus_tag="ECFP destabilized by fusion to
residues 422-461
of mouse ornithine decarboxylase, giving an in
vivo(1)"
/product="ECFP destabilized by fusion to residues
422-461
of mouse ornithine decarboxylase, giving an in
vivo
half-life of ~2 hours"
/label=PEST
/label=ECFP destabilized by fusion to residues
422-461 of
mouse ornithine decarboxylase, giving an in
vivo(1)
/note="destabilization domain"
/note="mammalian codon-optimized"
/
translation="SHGFPPEVEEQDDGTLPMSCAQESGMDRHPAACASARINV"
misc_feature 1661..1671
/label=Transcription stop/pA signal (N/P & P/M))
misc_feature 1674..1682
/label=Transcription start signal (P)
misc_feature 1703..2167
/locus_tag="P"
/label=P
/note="P"
primer_bind complement(2148..2183)
/label=Barcode4_P_rp
ORIGIN
1 ctgcgtgctc tacgaccagc nnnnnnnnnn acgcttaaca accagatcaa
agaaaaaaca
61 gacattgtca attgcaaagc aaaaatgtaa caccctaca atggatgccg
acaagattgt
121 attcaaagtc aataatcagg tggctctctt gaagcctgag attatcgtgg
atcaatatga
181 gtacaagtac cctgccatca aagatttgaa aaagccctgt ataaccctag
gaaaggctcc
241 cgatttaa ataaagcataca agtcagtttt gtcaggcatg agcgccgcca
aactta atcc
301 tgacgatgta tgttcctatt tggcagcggc aatgcagttt tttgagggga
catgtccgga
361 agactggacc agctatggaa ttgtgattgc acgaaaagga gataagatca
```

Supplementary File S4

```
ccccaggttc
  421 tctggtggag ataaaacgta ctgatgtaga agggaattgg gctctgacag
gaggcatgga
  481 actgacaaga gaccccactg tccctgagca tgcgctccta gtcggtcttc
tcttgagtct
  541 gtataggttg agcaaaatat ccgggcaaaa cactggtaac tataagacaa
acattgcaga
  601 caggatagag cagatTTTTg agacagcccc ttttgTtaaa atcgtggaac
accatactct
  661 aatgacaact cacaaaatgt gtgctaattg gagtactata ccaaacttca
gatttttggc
  721 cggaacctat gacatgtttt tctcccggat tgagcatcta tattcagcaa
tcagagtggg
  781 cacagttgtc actgcttatg aagactgttc aggactggta tcatttactg
ggttcataaa
  841 acaaatcaat ctcaccgcta gagaggcaat actatatttc ttccacaaga
actttgagga
  901 agagataaga agaatgtttg agccagggca ggagacagct gttcctcact
cttatttcat
  961 ccacttccgt tctactaggct tgagtgggaa atctccttat tcatcaaatg
ctgttggtca
 1021 cgtgttcaat ctcattcact ttgtaggatg ctatatgggt caagtcagat
ccctaaatgc
 1081 aacggttatt gctgcatgtg ctctcatga aatgtctgtt ctagggggct
atctgggaga
 1141 ggaattcttc gggaaaggga catttgaaag aagattcttc agagatgaga
aagaacttca
 1201 agaatacgag gcggtgaac tgacaaagac tgacgtagca ctggcagatg
atggaactgt
 1261 caactctgac gacgaggact acttttcagg tgaaccaga agtccggagg
ctgtttatac
 1321 tcgaatcatg atgaatggag gtcgactaaa gagatctcac atacggagat
atgtctcagt
 1381 cagttccaat catcaagccc gtccaaactc attcgccgag tttctaaaca
agacatattc
 1441 gagtgactca ggttccggag agaacctcta cttccaatcg ggatccggta
gccatggctt
 1501 cccgccggag gtggaggagc aggatgatgg cacgctgcc atgtcttgtg
cccaggagag
 1561 cgggatggac cgtcaccctg cagcctgtgc ttctgctagg atcaatgtgt
aagaagttga
 1621 ataacaaaat gccggaaatc tacggattgt gtatatccat catgaaaaaa
actaacaccc
 1681 ctcctttcga accatcccaa acatgagcaa gatctttgtc aatcctagtg
ctattagagc
 1741 cggctctggcc gatcttgaga tggctgaaga aactgttgat ctgatcaata
gaaatatcga
 1801 agacaatcag gctcatctcc aagggaacc catagagggtg gacaatctcc
ctgaggatat
 1861 ggggcgactt cacctggatg atggaaaatc gcccaacat ggtgagatag
```

Supplementary File S4

```
ccaaggtggg
  1921 agaaggcaag tatcgagagg actttcagat ggatgaagga gaggatccta
gcttcctggt
  1981 ccagtcatac ctggaaaatg ttggagtcca aatagtcaga caaatgaggt
caggagagag
  2041 atttctcaag atatggtcac agaccgtaga agagattata tcctatgtcg
cggtcaactt
  2101 tcccaaccct ccaggaaagt cttcagagga taaatcaacc cagactactg
gccgagagct
  2161 caagaagtgt gtatcagtac atg
//
```

Supplementary File S5: RV Δ G-4Cre amplicon reference sequence. This Genbank-format file contains the expected (i.e., based on the published sequence: see Addgene #98034) sequence of amplicons obtained from RV Δ G-4Cre for SMRT sequencing.

LOCUS Exported 2024 bp ds-DNA linear SYN
07-JAN-2019
DEFINITION synthetic linear DNA.
ACCESSION .
VERSION .
KEYWORDS .
SOURCE synthetic DNA construct
ORGANISM synthetic DNA construct
REFERENCE 1 (bases 1 to 2024)
AUTHORS Trial User
TITLE Direct Submission
JOURNAL Exported Jan 7, 2019 from SnapGene 4.1.9
<http://www.snapgene.com>

FEATURES Location/Qualifiers
source 1..2024
/organism="synthetic DNA construct"
/mol_type="other DNA"
primer_bind 1..48
/label=Barcode1_cagc_N10_leader_fp
primer_bind 1..20
/label=Barcode1_cagc_fp
gap 21..30
/estimated_length=10
5'UTR 31..100
/label=RV leader
/note="SPBN leader"
misc_feature 89..97
/locus_tag="Transcriptional start (N)"
/label=Transcriptional start (N)
CDS 101..1450
/codon_start=1
/locus_tag="N"
/label=N
/note="N"
/
translation="MDADKIVFKVNNQVVSLKPEIIVDQYQYKYP AIKDLKKPCITLGK
APDLNKAYKSVLSGMSAAKLNPDVCSYLAAMQFFEGTCPEDWTSYGIVIARKGDKIT
PGSLVEIKRTDVEGNWALTGGMELTRDPTVPEHASLVGLLLSLYRLSKISGQNTGNYKT
NIADRIEQIFETAPFVKIVEHHTLMTTHKMCANWSTIPNFRFLAGTYDMFFSRIEHLYS
AIRVGTVVTAYEDCSGLVSFTGFIKQINLTAREAILYFFHKNFEEEIRRMFEPGQETAV
PHSYFIHFRSLGLSGKSPYSSNAVGHVFNLIHFVGCYMGQVRS LNATVIAACAPHEMSV
LGGYLGEFFGKGT FERRFRDEKELQEYEA AELTKTDVALADDGTVNSDDEDYFSGET
RSPEAVYTRIMMNGGRLKRSHIRRYVSVSSNHQARPNSFAEFLNKTYSSDS"

Supplementary File S5

```
misc_feature      1502..1512
                  /label=Transcription stop/pA signal (N/P & P/M))
misc_feature      1515..1523
                  /locus_tag="Transcriptional start (P)"
                  /label=Transcriptional start (P)
misc_feature      1544..2008
                  /locus_tag="P"
                  /label=P
                  /note="P"
primer_bind       complement(1989..2024)
                  /label=Barcode2_P_rp
```

ORIGIN

```
1 tcagacgatg cgatcatcagc nnnnnnnnnn acgcttaaca accagatcaa
agaaaaaaca
61 gacattgtca attgcaaagc aaaaatgtaa caccctaca atggatgccg
acaagattgt
121 attcaaagtc aataatcagg tggctctctt gaagcctgag attatcgtgg
atcaatatga
181 gtacaagtac cctgccatca aagatttgaa aaagccctgt ataaccctag
gaaaggctcc
241 cgatttaa ataaagcataca agtcagtttt gtcaggcatg agcgccgcca
aacttaatcc
301 tgacgatgta tgttcctatt tggcagcggc aatgcagttt tttgagggga
catgtccgga
361 agactggacc agctatggaa ttgtgattgc acgaaaagga gataagatca
ccccaggttc
421 tctggtggag ataaaacgta ctgatgtaga aggaattgg gctctgacag
gaggcatgga
481 actgacaaga gacccactg tccctgagca tgcgtcctta gtcggtcttc
tcttgagtct
541 gtataggttg agcaaatat ccgggcaaaa cactggtaac tataagacaa
acattgcaga
601 caggatagag cagatTTTTG agacagcccc ttttgTtaaa atcgtggaac
accatactct
661 aatgacaact cacaaaatgt gtgctaattg gactactata ccaaaactca
gatttttggc
721 cggaacctat gacatgtttt tctcccgat tgagcatcta tattcagcaa
tcagagtggg
781 cacagttgtc actgcttatg aagactgttc aggactggta tcatttactg
ggttcataaa
841 acaaatcaat ctcaccgcta gagaggcaat actatatttc ttccacaaga
actttgagga
901 agagataaga agaatgtttg agccagggca ggagacagct gttcctcact
cttatttcat
961 ccacttccgt tcactaggct tgagtgggaa atctccttat tcatcaaatg
ctgttggtca
1021 cgtgttcaat ctcatcact ttgtaggatg ctatatgggt caagtcagat
ccctaaatgc
1081 aacggttatt gctgcatgtg ctctcatga aatgtctggt ctagggggct
atctgggaga
```

Supplementary File S5

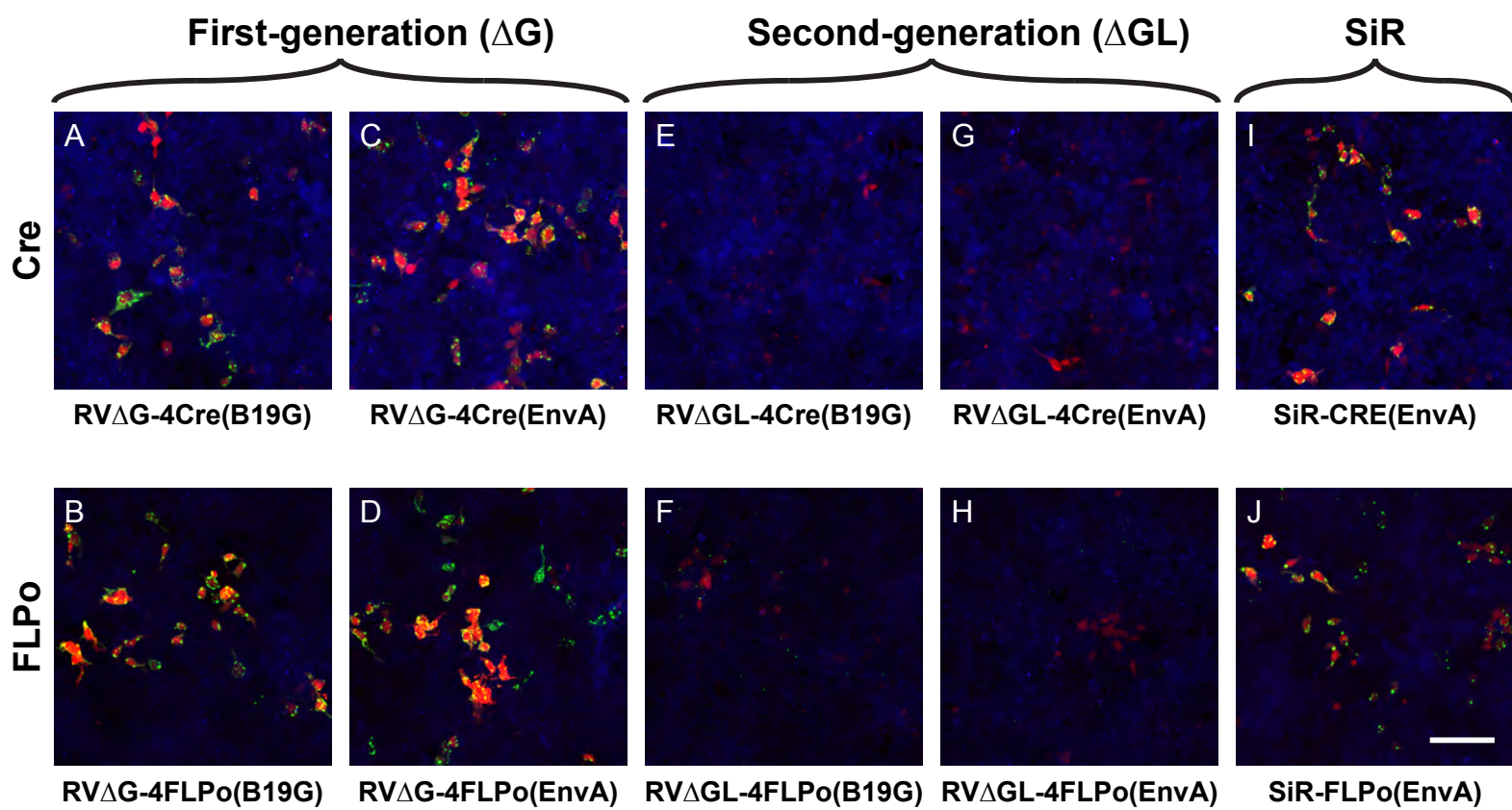
```
1141 ggaattcttc gggaaagga catttgaag aagattcttc agagatgaga
aagaacttca
1201 agaatacgag gcggctgaac tgacaaagac tgacgtagca ctggcagatg
atggaactgt
1261 caactctgac gacgaggact acttttcagg tgaaaccaga agtccggagg
ctgtttatac
1321 tcgaatcatg atgaatggag gtcgactaaa gagatctcac atacggagat
atgtctcagt
1381 cagttccaat catcaagccc gtccaaactc attcgccgag tttctaaaca
agacatatc
1441 gagtgactca taagaagttg aataacaaaa tgccggaat ctacggattg
tgtatatcca
1501 tcatgaaaaa aactaacacc cctcctttcg aaccatcca aacatgagca
agatctttgt
1561 caatcctagt gctattagag ccggtctggc cgatcttgag atggctgaag
aaactgttga
1621 tctgatcaat agaaatatcg aagacaatca ggctcatctc caaggggaac
ccatagaggt
1681 ggacaatctc cctgaggata tggggcgact tcacctggat gatggaaaat
cgcccaacca
1741 tggtagata gccaaggtgg gagaaggcaa gtatcgagag gactttcaga
tggatgaagg
1801 agaggatcct agcttcctgt tccagtcata cctggaaaat gttggagtcc
aaatagtcag
1861 acaaatgagg tcaggagaga gatttctcaa gatatgggtca cagaccgtag
aagagattat
1921 atcctatgtc gcgggtcaact ttccaaccc tccaggaaag tcttcagagg
ataaatcaac
1981 ccagactact ggccgagagc tcaagaagct atacatgact ctgc
//
```


Supplementary Figure S1: SiR viruses appeared to cause expression of viral nucleoprotein at levels similar to those of first-generation ΔG viruses.

(A-D) Reporter cells infected with first-generation, ΔG viruses show characteristic bright, clumpy anti-nucleoprotein staining (green), indicating high nucleoprotein expression and active viral replication. Red is mCherry expression, reporting expression of Cre or FLPO; blue is mTagBFP2, constitutively expressed by these reporter cell lines.

(E-H) Reporter cells infected with second-generation, ΔGL viruses show only punctate staining for nucleoprotein, indicating isolated individual viral particles or ribonucleoprotein complexes; these viruses do not replicate intracellularly (21). Reporter cassette activation takes longer from the lower recombinase expression levels of these viruses, so mCherry expression is dimmer than in cells infected with ΔG viruses at the same time point.

(I-J) Reporter cells infected with SiR viruses show clumps of nucleoprotein and rapid reporter expression indicating high expression of recombinases, similarly to cells infected with ΔG viruses. Scale bar: 100 μm , applies to all panels.



Supplementary File S6: >90% of SiR-CRE viral particles with the mCherry gene intact also have the Cre gene intact, suggesting that most of the SiR-CRE-infected cells that disappear over time in tdTomato reporter mice are dying rather than simply stopping expression of mCherry.

We sequenced the transgene inserts for 21 individual SiR-CRE clones (see Methods). 19 out of 21 had no mutations in the Cre gene, and two had one point mutation each (Ala88Val and Arg189Ile). All 21 had an intact mCherry gene. The lack of a large proportion of Cre-knockout mutants is one indication that the majority of red fluorescent neurons in SiR-CRE-injected Ai14 (tdTomato reporter) mice are not labeled only with mCherry, providing evidence that their disappearance is equivalent to their death.

Supplementary File S6

bioRxiv preprint doi: <https://doi.org/10.1101/550640>; this version posted August 3, 2021. The copyright holder for this preprint (which was not certified by peer review) is the author/funder, who has granted bioRxiv a license to display the preprint in perpetuity. It is made available under aCC-BY-ND 4.0 International license.



Random 8-nucleotide index
Cre gene, P2A, mCherry gene, PEST, and transcription stop/polyA signal, transcription start signal, L gene, mutation

No mutations in transgene insert of SiR-CRE (19/21 clones)

ACTTTCTA, AGCCAGT, TTATCAGG, AGGGCGTT, AGTGGGCA, GGGCCTTT, TCCCGCAA, GGTCGGGG, GGCCTATA, TGTCTCTC, CCTGTCCG, TAGCACAC, GATGTGG, TAAGCCT, CTCACAT, TTAGTCC, AACCCGAC, AGCGGCC, AGCGGGG
CAACTCCAACCCCTGGGAGCAATATAACAAAAACATGTTATGGTGCCATTAAACCGCTGCATTTTCATCAAAGTCA AGTTGATTACCTTTACATTTTGATCCTCTTGGATGTGAAAAAACTATTAAACATCCCTCAAAGGACCTGCAGGTACG CGGCCGGGTACCGCCACCATGGTGCCCAAGAAGAAGAGGAAAGTCTCCAACCTGCTGACTGTGCACCAAAAC CTGCCTGCCCTCCCTGTGGATGCCACCTCTGATGAAGTCAGGAAGAACCTGATGGACATGTTTCAGGGACAGGCA GGCCTTCTCTGAACACACCTGGAAGATGCTCCTGTCTGTGTGTCAGATCCTGGGCTGCCTGGTGCAAGCTGAACA ACAGGAAATGGTTCCTGCTGAACCTGAGGATGTGAGGGACTACCTCCTGTACCTGCAAGCAGAGGCTGGC TGTGAAGACCATCCAACAGCACCTGGGCCAGCTCAACATGCTGCACAGGAGATCTGGCCTGCCTCGCCCTTCT GACTCCAATGCTGTGTCCCTGGTGTGAGGAGAATCAGAAAGGAGAATGTGGATGCTGGGGAGAGAGCCAAAGC AGCCCTGGCCTTGAACGCACTGACTTTGACCAAGTCAGATCCCTGATGGAGAATCTGACAGATGCCAGGAC ATCAGGAACCTGGCCTTCTGGGCATTGCTTACAACACCTGCTGCGCATTGCCGAAATGCCAGAATCAGAGT GAAGGACATCTCCGCACCGATGGTGGGAGAATGCTGATCCACATTGGCAGGACCAAGACCCTGGTGTCCACA GCTGGTGTGGAGAAGGCCCTGTCCCTGGGGGTACCAAGCTGGTGGAGAGATGGATCCTGTGTCTGGTGTGG CTGATGACCCCAACAACACTACCTGTTCTGCCGGGTGAGGATGGGACGGCAGTGGAGGATCCGGAGCCACGAA CTGTCCACCCGGGCCCTGGAAGGGATCTTTGAGGCCACCCACCGCCTGATCTATGGTGCCAAGGATGACTCTG GGCAGAGATACCTGGCCTGGTCTGGCCACTCTGCCAGAGTGGGTGCTGCCAGGGACATGGCCAGGGCTGGTG TGCCATCCCTGAAATCATGCAGGCTGGTGGCTGGACCAATGTGAACATTGTGATGAACTACATCAGAAACCTGG ACTCTGAGACTGGGGCATGGTGGAGCTGCTCGAGGATGGGACGGCAGTGGAGGATCCGGAGCCACGAACT TCTCTCTGTAAAGCAAGCAGGAGACGTGGAAGAAAACCCCGGTCTACCGGTGTGAGCAAGGGCGAGGAGGA TAACATGGCCATCATCAAGGAGTTCATGCGCTTCAAGGTGCACATGGAGGGCTCCGTGAACGGCCACGAGTTCG AGATCGAGGGCGAGGGCGAGGGCCGCCCTACGAGGGCACCCAGACCAGCCAAAGCTGAAGGTGACCAAGGGT GGCCCTGCCCCTTCCCTGGACATCTGTCCCTCAGTTCATGTACGGCTCCAAGGCCTACGTGAAGCACC CCGCCGACATCCCCGACTACTTGAAGCTGTCTTCCCCGAGGGCTTCAAGTGGGAGCGCGTGTGAACTTCGA GGACGGCGCGGTGGTGAACCTGACCCAGGACTCCTCCCTGCAGGACGGCGAGTTCATCTACAAGGTGAAGCT GCGCGGCACCAACTTCCCTCCGACGGCCCCGTAATGCAGAAGAAGACCATGGGCTGGGAGGCCTCCTCCGA GCGGATGTGGCACGCTGCCCATGCTTGAAGGGCGAGTCAAGCAGAGGCTGAAGCTGAAGGACGGCGGCCA CTACGACGCTGAGGTCAAGACCACCTACAAGGCCAAGAAGCCCGTGCAGCTGCCGGCGCCTACAACGTCAAC ATCAAGTTGGACATCACCTCCACAACGAGGACTACACCATCGTGAACAGTACGAACCGCGCCGAGGGCCGCC ACTCCACCGGGCGCATGGACGAGCTGTACAAGGATATCTCAGCCATGGCTTCCCGCCGAGGTTGGAGGAGCA GGATGATGGCACGCTGCCCATGCTTGTGCCAGGAGAGCGGGATGGACCGTCAACCTGCAGCCTGTGCTTCT GCTAGGATCAATGTGTGACTCGAGGGCGCGCTACCCGCGGTAGCTTTTTCAGTCAAGAAAAAATCATTAGATCA GAAGAACAACCTGGCAACACTTCAACCTGAGACTTACTTCAAGATGCTCGATCCTGGAGAGGTCTATGATGACC CTATTGACCCAATCGAGTTAGAGGCTGAACCCAGAGGAACCCCATTTGTCCTCAAC

Ala88Val mutation in iCre gene of SiR-CRE (1/21 clones)

AGCTGGTT
CAACTCCAACCCCTGGGAGCAATATAACAAAAACATGTTATGGTGCCATTAAACCGCTGCATTTTCATCAAAGTCA AGTTGATTACCTTTACATTTTGATCCTCTTGGATGTGAAAAAACTATTAAACATCCCTCAAAGGACCTGCAGGTACG CGGCCGGGTACCGCCACCATGGTGCCCAAGAAGAAGAGGAAAGTCTCCAACCTGCTGACTGTGCACCAAAAC CTGCCTGCCCTCCCTGTGGATGCCACCTCTGATGAAGTCAGGAAGAACCTGATGGACATGTTTCAGGGACAGGCA GGCCTTCTCTGAACACACCTGGAAGATGCTCCTGTCTGTGTGTCAGATCCTGGGCTGCCTGGTGCAAGCTGAACA ACAGGAAATGGTTCCTGCTGAACCTGAGGATGTGAGGGACTACCTCCTGTACCTGCAAGTCAGAGCCTGGCT ACAGGAAATGGTTCCTGCTGAACCTGAGGATGTGAGGGACTACCTCCTGTACCTGCAAGTCAGAGCCTGGCT ACTCCAATGCTGTGTCCCTGGTGTGAGGAGAATCAGAAAGGAGAATGTGGATGCTGGGGAGAGAGCCAAGCA GGCCTGGCCTTGTGAACGCACTGACTTTGACCAAGTCAGATCCCTGATGGAGAATCTGACAGATGCCAGGACA TCAGGAACCTGGCTTCCCTGGGCATTGCTTACAACACCTGCTGCGCATTGCCGAAATGCCAGAATCAGAGTG AAGGACATCTCCCGCACCGATGGTGGGAGAATGCTGATCCACATTGGCAGGACCAAGACCCTGGTGTCCACAG CTGGTGTGGAGAAGGCCCTGTCCCTGGGGGTACCAAGCTGGTGGAGAGATGGATCCTGTGTCTGGTGTGGC TGATGACCCCAACAACACTACCTGTTCTGCCGGGTGAGGAGAATGGTGTGGCTGCCCTTCTGCCACCTCCCAAG TGTCACCCGGGCCCTGGAAGGGATCTTTGAGGCCACCCACCGCCTGATCTATGGTGCCAAGGATGACTCTGG GCAGAGATACCTGGCCTGGTCTGGCCACTTGCAGAGTGGTGTGCTGCCAGGGACATGGCCAGGCTGGTGT GTCCATCCCTGAAATCATGCAGGCTGGTGGCTGGACCAATGTGAACATTGTGATGAACTACATCAGAAACCTGGA

Supplementary File S6

bioRxiv preprint doi: <https://doi.org/10.1101/550640>; this version posted August 3, 2021. The copyright holder for this preprint (which was not certified by peer review) is the author/funder, who has granted bioRxiv a license to display the preprint in perpetuity. It is made available under aCC-BY-ND 4.0 International license.

```
CTCTGAGACTGGGGCCATGGTGAGGCTGCTCGAGGATGGGGACGGCAGTGGAGGATCCGGAGCCACGAACTT
CTCTCTGTAAAGCAAGCAGGAGACGTGGAAGAAAACCCCGGTCTTACCGGTGTGAGCAAGGGCGAGGAGGAT
AACATGGCCATCATCAAGGAGTTCATGCGCTTCAAGGTGCACATGGAGGGCTCCGTGAACGGCCACGAGTTCGA
GATCGAGGGCGAGGGCGAGGGCCGCCCTACGAGGGCACCCAGACCGCCAAGCTGAAGGTGACCAAGGGTG
GCCCCCTGCCCTTCGCCCTGGGACATCCTGTCCCTCAGTTTCATGTACGGCTCCAAGGCCACGTGAAGCACCC
CGCCGACATCCCGACTACTTGAAGCTGTCTTCCCGAGGGCTTCAAGTGGGAGCGCGTGATGAACTTCGAG
GACGGCGGCGTGGTGACCGTGACCCAGGACTCCTCCCTGCAGGACGGCGAGTTCATCTACAAGGTGAAGCTG
GACGGCACCAACTTCCCTCCGACGGCCCCGTAATGCAGAAGAAGACCATGGGCTGGGAGGCCTCCTCCGAG
CGGATGTACCCCGAGGACGGCGCCCTGAAGGGCGAGATCAAGCAGAGGCTGAAGCTGAAGGACGGCGGCCAC
TACGACGCTGAGGTCAAGACCACCTACAAGGCCAAGAAGCCCGTGCAGCTGCCGCGCCTACAACGTCAACA
TCAAGTTGGACATCACCTCCACAACGAGGACTACACCATCGTGAACAGTACGAACGCGCCGAGGGCCGCCA
CTCCACCGCGGCATGGACGAGCTGTACAAGGGATATCTCAGCCATGGCTTCCCGCCGGAGGTGGAGGAGCAG
GATGATGGCACGCTGCCCATGCTTGTGCCAGGAGAGCGGGATGGACCGTACCCTGCAGCCTGTGCTTCTG
CTAGGATCAATGTGTGACTCGAGGGCGCGCTACCCGCGGTAGCTTTTCAGTCTGAGAAAAAACATTAGATCAGA
AGAACAACTGGCAACACTTCTCAACCTGAGACTTACTTCAAGATGCTCGATCCTGGAGAGGTCTATGATGACCCT
ATTGACCCAATCGAGTTAGAGGCTGAACCCAGAGGAACCCCATGTCCCAAC
```

Arg189Ile mutation in iCre gene of SiR-CRE

```
AGCGGGGT
CAACTCCAACCTTGGGAGCAATATAACAAAAACATGTTATGGTGCCATTAAACCGCTGCATTTTCATCAAAGTCA
AGTTGATTACCTTTACATTTTATCCTCTTGGATTGTGAAAAAACTATTAACATCCCTCAAAGGACCTGCAGGTACG
CGGCCGCGGTACCGCACCATGGTGCCCAAGAAGAAGAGGAAAGTCTCCAACCTGCTGACTGTGCACCAAAAC
CTGCCTGCCCTCCCTGTGGATGCCACCTCTGATGAAGTCAGGAAGAACCTGATGGACATGTTTCAGGGACAGGCA
GGCCTTCTCTGAACACACCTGGAAGATGCTCCTGTCTGTGTGCAGATCCTGGGCTGCCTGGTGCAAGCTGAACA
ACAGGAAATGGTTCCCTGCTGAACCTGAGGATGTGAGGGACTACCTCCTGTACCTGCAAGCCAGAGGCCTGGC
TGTGAAGACCATCCAACAGCACCTGGGCCAGCTCAACATGCTGCACAGGAGATCTGGCCTGCCTCGCCCTTCT
GACTCCAATGCTGTGTCCCTGGTGATGAGGAGAATCAGAAAGGAGAATGTGGATGCTGGGGAGAGAGCCAAGC
AGGCCCTGGCCTTTGAACGCACTGACTTTGACCAAGTCAGATCCCTGATGGAGAACTCTGACAGATGCCAGGAC
ATCAGGAACCTGGCCTTCTGGGCATTGCCTACAACACCTGCTGCGCATTGCCGAAATTGCCAGAATCAIAGTG
AAGGACATCTCCCGCACCGATGGTGGGAGAATGCTGATCCACATTTGCCAGGACCAAGACCTGGTGTCCACAG
CTGGTGTGGAGAAGGCCCTGTCCCTGGGGGTTACCAAGCTGGTGGAGAGATGGATCTCTGTGTCTGGTGTGGC
TGATGACCCCAACAACCTACCTGTTCTGCCGGGTGAGAAAGATGGTGTGGCTGCCCTTCTGCCACCTCCCAAC
TGTCACCCGGGCCCTGGAAGGGATCTTTGAGGCCACCCACCGCTGATCTATGGTGCCAAGGATGACTCTGG
GCAGAGATACCTGGCCTGGTCTGGCCACTCTGCCAGAGTGGGTGCTGCCAGGGACATGGCCAGGGCTGGTGT
GTCCATCCCTGAAATCATGCAGGCTGGTGGCTGGACCAATGTGAACATTGTGATGAACTACATCAGAAACCTGGA
CTCTGAGACTGGGGCCATGGTGAGGCTGCTCGAGGATGGGGACGGCAGTGGAGGATCCGGAGCCACGAACTT
CTCTCTGTAAAGCAAGCAGGAGACGTGGAAGAAAACCCCGGTCTTACCGGTGTGAGCAAGGGCGAGGAGGAT
AACATGGCCATCATCAAGGAGTTCATGCGCTTCAAGGTGCACATGGAGGGCTCCGTGAACGGCCACGAGTTCGA
GATCGAGGGCGAGGGCGAGGGCCGCCCTACGAGGGCACCCAGACCGCCAAGCTGAAGGTGACCAAGGGTG
GCCCCCTGCCCTTCGCCCTGGGACATCCTGTCCCTCAGTTTCATGTACGGCTCCAAGGCCACGTGAAGCACCC
CGCCGACATCCCGACTACTTGAAGCTGTCTTCCCGAGGGCTTCAAGTGGGAGCGCGTGATGAACTTCGAG
GACGGCGGCGTGGTGACCGTGACCCAGGACTCCTCCCTGCAGGACGGCGAGTTCATCTACAAGGTGAAGCTG
CGCGGCACCAACTTCCCTCCGACGGCCCCGTAATGCAGAAGAAGACCATGGGCTGGGAGGCCTCCTCCGAG
CGGATGTACCCCGAGGACGGCGCCCTGAAGGGCGAGATCAAGCAGAGGCTGAAGCTGAAGGACGGCGGCCAC
TACGACGCTGAGGTCAAGACCACCTACAAGGCCAAGAAGCCCGTGCAGCTGCCGCGCCTACAACGTCAACA
TCAAGTTGGACATCACCTCCACAACGAGGACTACACCATCGTGAACAGTACGAACGCGCCGAGGGCCGCCA
CTCCACCGCGGCATGGACGAGCTGTACAAGGGATATCTCAGCCATGGCTTCCCGCCGGAGGTGGAGGAGCAG
GATGATGGCACGCTGCCCATGCTTGTGCCAGGAGAGCGGGATGGACCGTACCCTGCAGCCTGTGCTTCTG
CTAGGATCAATGTGTGACTCGAGGGCGCGCTACCCGCGGTAGCTTTTCAGTCTGAGAAAAAACATTAGATCAGA
AGAACAACTGGCAACACTTCTCAACCTGAGACTTACTTCAAGATGCTCGATCCTGGAGAGGTCTATGATGACCCT
ATTGACCCAATCGAGTTAGAGGCTGAACCCAGAGGAACCCCATGTCCCAAC
```

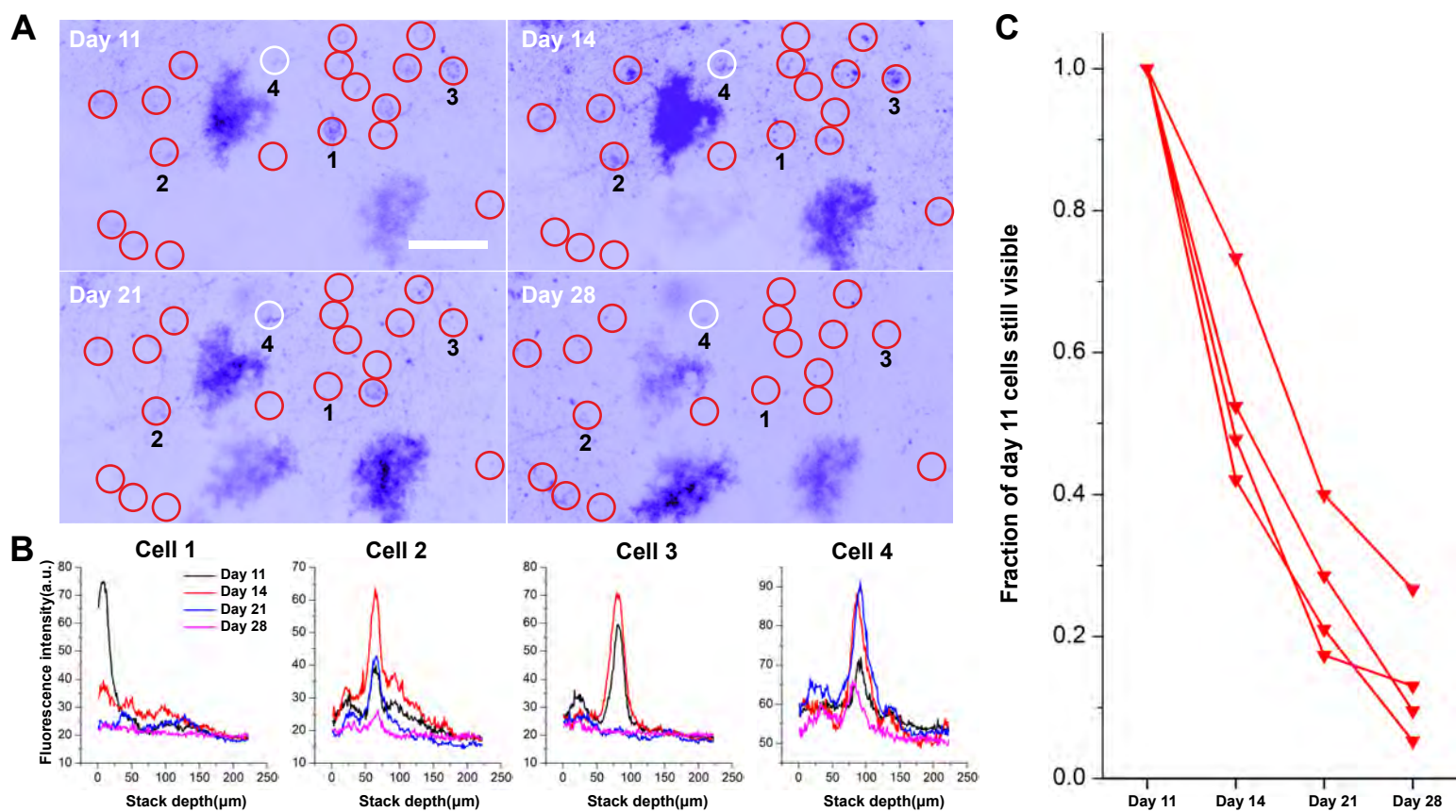
Supplementary Figure S2: 86% of SiR-CRE-labeled neurons in Arch-EGFP-ER2 reporter mice disappeared between 11 days and 28 days after injection.

A) Maximum intensity projections of the two-photon FOV shown in Supplementary Video S1 of visual cortical neurons labeled with SiR-CRE in an Ai35 mouse, 11-28 days postinjection. Images are from the same FOV at four different time points. All cells clearly visible on day 11 are circled. In this example, 18 out of 19 cells (red circles) disappeared by a subsequent imaging session. Only one cell (white circle) is still visible on day 28. Numbers below four of the circles mark the cells for which intensity profiles are shown in panel B. Scale bar: 50 μm , applies to all images.

B) Green fluorescence intensity versus depth for the four representative neurons numbered in panel A at the four different time points, showing disappearance of three of them over time.

C) Fraction of cells visibly EGFP-labeled at day 11 still visible at later time points, from four different FOVs in two Ai35 mice. Connected sets of markers indicate cells from the same FOV. 86% of SiR-CRE-labeled neurons had disappeared by 4 weeks postinjection.

Supplementary Figure S2



Supplementary Video S1 (*separate file*): Video of 95% of SiR-CRE-labeled neurons in an Arch-EGFP-ER2 reporter mouse disappearing between 11 days and 28 days postinjection.

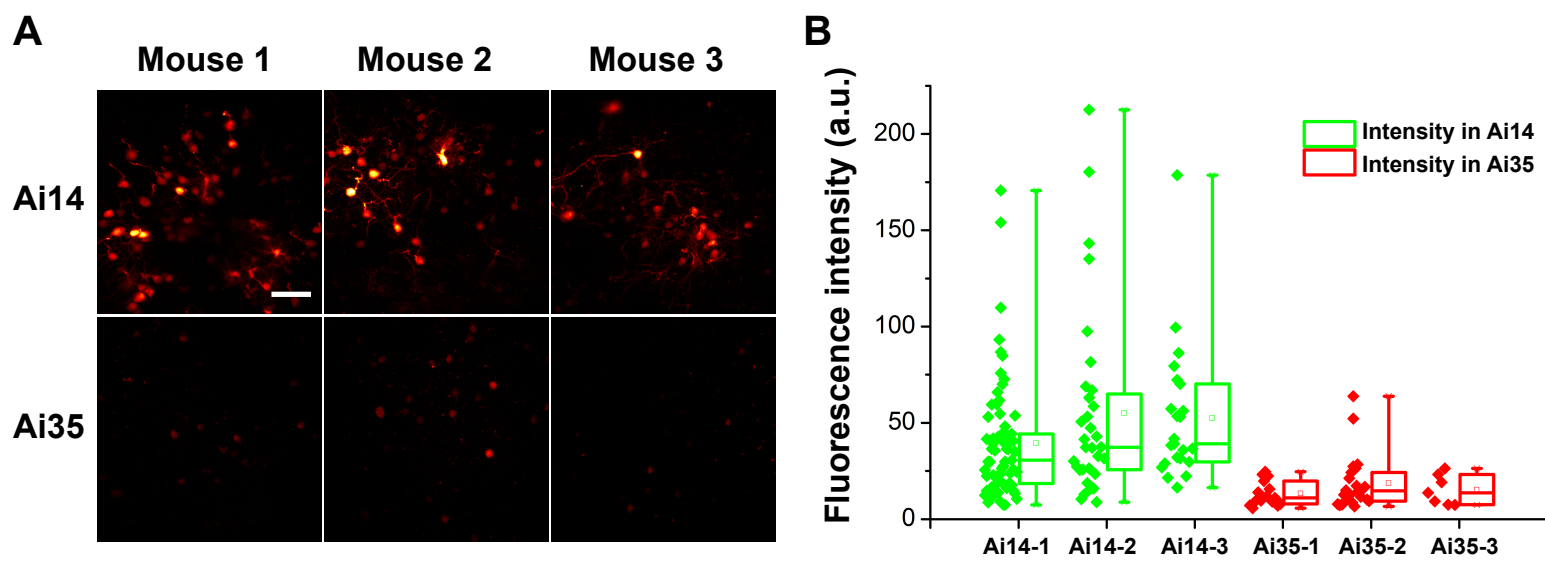
Two-photon image stacks of a single FOV of visual cortical neurons in an Ai35 mouse imaged at four different time points; time in the video represents depth of focus. Large blobs are glia. 18 out of the 19 neurons visibly labeled with Arch-EGFP-ER2 at 11 days following injection of SiR-Cre are no longer visible 17 days later. White circles indicate cells present at both 11 days and all subsequent imaging sessions; red circles indicate cells present at 11 days but gone by 28 days.

Supplementary Figure S3: mCherry fluorescence from SiR-CRE is much dimmer than tdTomato fluorescence in Ai14 mice, suggesting that the disappearance of the brighter cells in SiR-CRE-injected Ai14 mice indicates their death.

A) Representative images of red fluorescence in SiR-CRE-labeled cells in Ai14 (Cre-dependent expression of tdTomato, top row) and Ai35 (Cre-dependent expression of Arch-EGFP-ER2, bottom row). The three images for each mouse line are from 3 different mice of each line, imaged 7 days following SiR-CRE injection (see Methods), all with the same laser intensity and wavelength (1020 nm). Red fluorescence due only to mCherry (i.e., in Ai35 mice) is obviously much dimmer than that due to tdTomato (i.e., in Ai14 mice). Scale bar: 50 μ m, applies to all images.

B) Intensity of red fluorescence of SiR-CRE-labeled cells in Ai14 (left) and Ai35 (right) mice. Data point indicate intensity of individual cells in arbitrary units at the same laser and microscope settings (see Methods). Box plots indicate median, 25th–75th percentiles (boxes), and full range (whiskers) of intensities for each mouse. The average of the mean red fluorescent intensity in each mouse was 48.97 in Ai14 and 15.69 in Ai35 ($p=0.00283 < 0.01$, one-way ANOVA); the midpoint of these means, 32.33, was used as the cutoff for the reanalysis of the data in Ai14 mice to exclude neurons that could have been labeled with mCherry alone.

Supplementary Figure S3

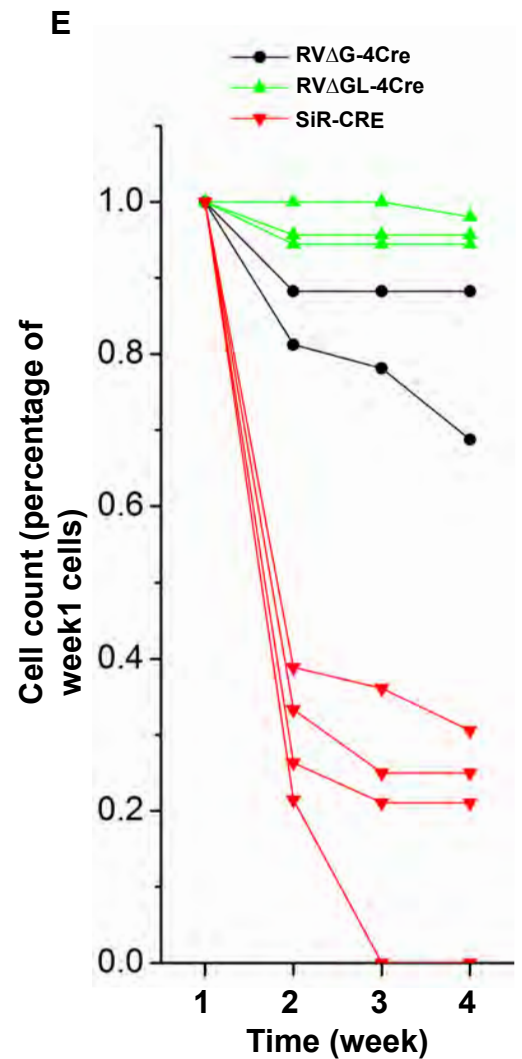
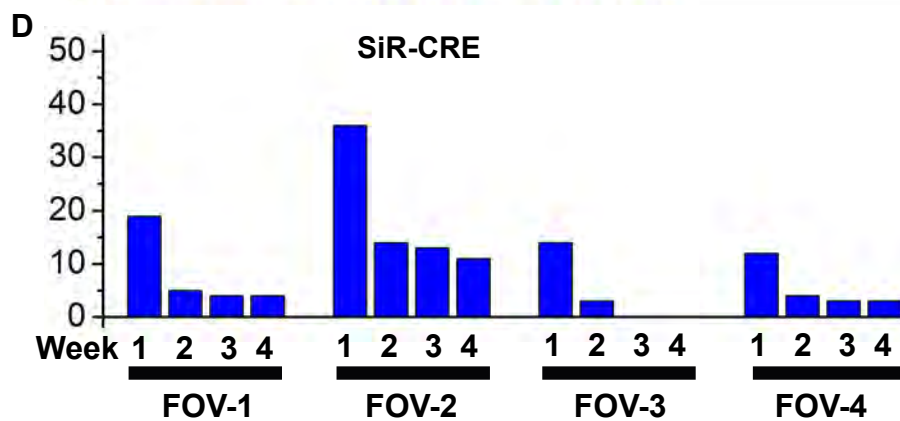
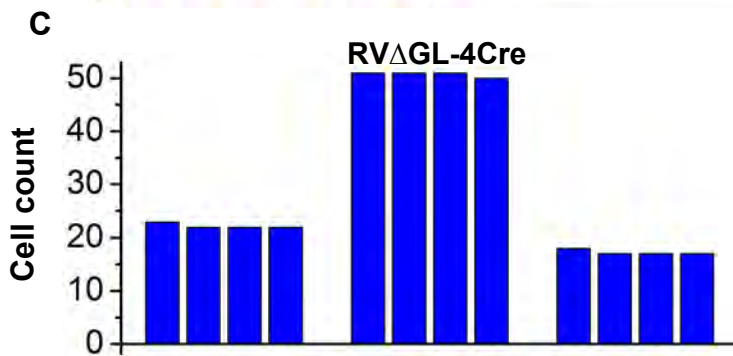
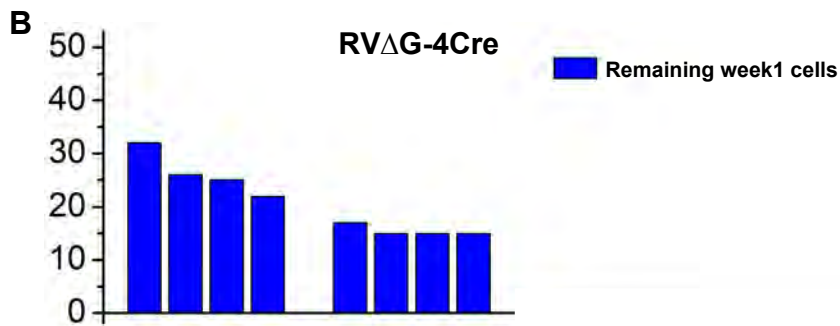
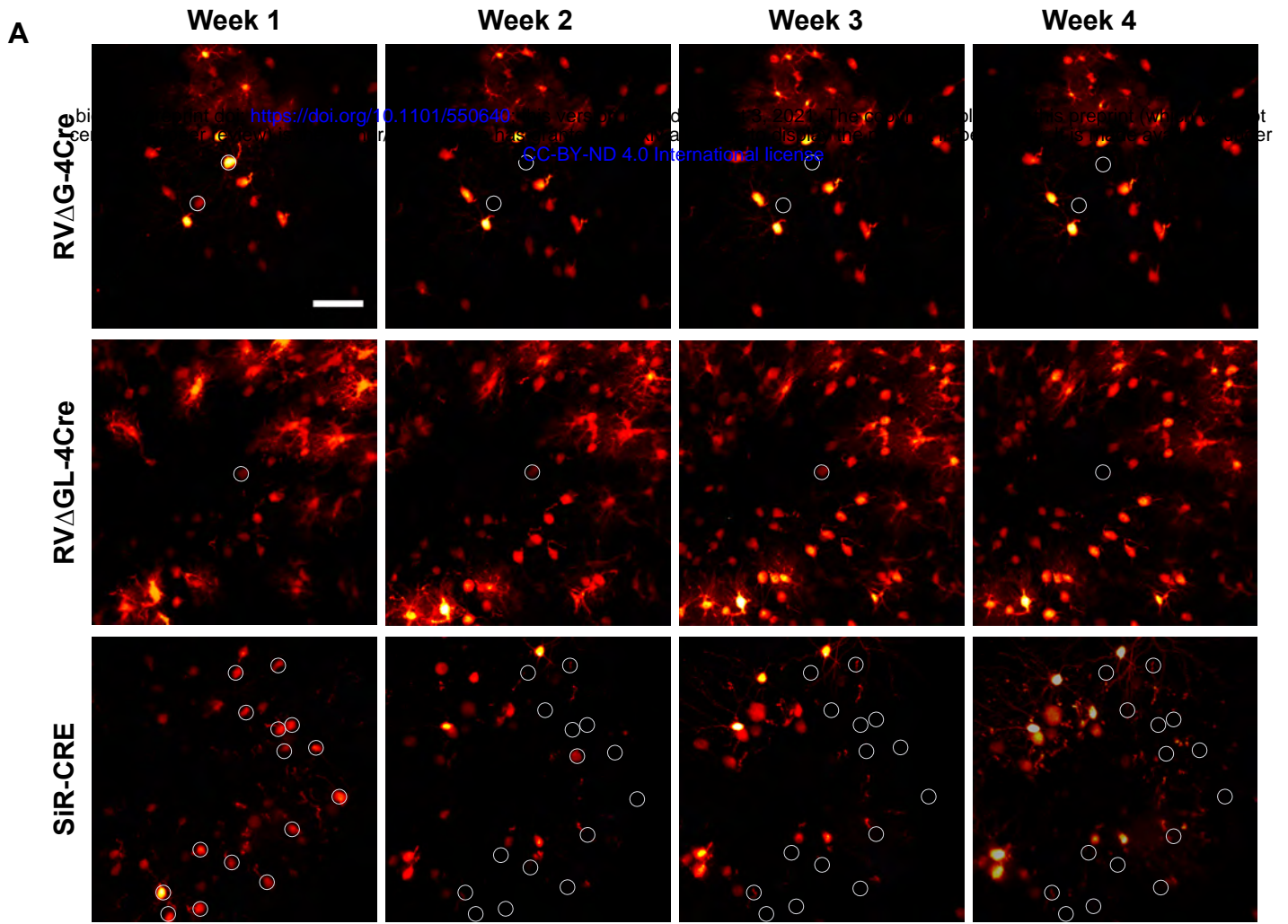


Supplementary Figure S4: 81% of SiR-CRE-labeled neurons in tdTomato reporter mice disappear within 2-4 weeks, even excluding dimmer cells that might have only been labeled with mCherry.

A) Same representative fields of view as in Figure 3 but with circles now marking only cells with intensity at 7 days of greater than 32.33 a.u. (see text and Supplementary Figure S3) that are no longer visible at a subsequent time point. Scale bar: 50 μm , applies to all images.

B-D) Numbers of cells above threshold fluorescence intensity at week 1 that were still present in subsequent weeks. The conclusions from Figure 3 are unchanged: few cells labeled with RV Δ GL-4Cre were lost, RV Δ G-4Cre killed a significant minority of cells, and SiR-CRE killed the majority of labeled neurons within two weeks following injection.

E) Percentages of cells above threshold at week 1 that were still present in subsequent imaging sessions. By 28 days postinjection, an average of only 19.2% of suprathreshold SiR-CRE-labeled cells remained.

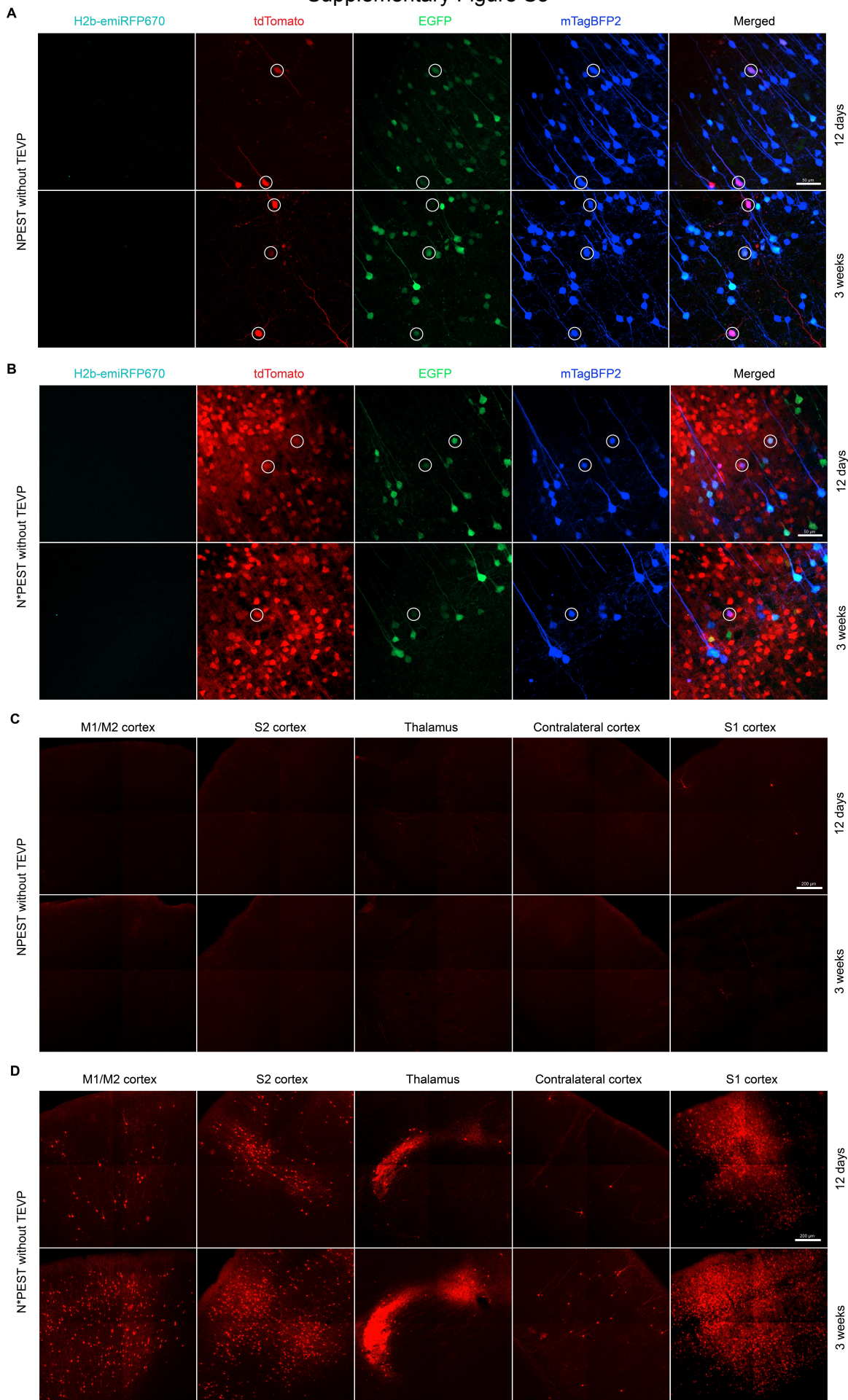


Supplementary Figure S5: Images of starter cells and input regions in the absence of TEVP.

A-B) Closeup images of virus injection sites in barrel cortex for NPEST (A) and N*PEST (B) viruses, without TEVP. Images are from the same sections as Figure 4C. The circled cells are "starter cells", defined as expressing both tdTomato (reporting Cre expressed by the rabies virus) and mTagBFP2 (coexpressed with G). Scale bar: 50 μm , applies to all images in each panel.

C-D) Images of regions presynaptic to barrel cortex for NPEST (A) and N*PEST (B) viruses, without TEVP. Red indicates tdTomato fluorescence reporting activity of the Cre-expressing rabies viruses. Scale bar: 200 μm , applies to all images in each panel.

Supplementary Figure S5



Supplementary File S7 (*separate file*): Sequencing results for RV Δ G-NPEST-4Cre(EnvA), showing that the intended 3' addition to the nucleoprotein was intact in the final stocks used for monosynaptic tracing experiments.

We sequenced the complete region of the 3' addition to the nucleoprotein region from 32 viral particles for each of the two high-titer, EnvA-enveloped preparations of RV Δ G-NPEST-4Cre(EnvA) and RV Δ G-N*PEST-4Cre(EnvA) that we made for our *in vivo* experiments. For RV Δ G-NPEST-4Cre(EnvA), none of the 32 clones had any mutations in the 3' addition; one clone had a point mutation in the intergenic region between the N and P genes (from TGTATA to TTTATA), and one other clone had a synonymous mutation in the N gene (Ser437, from TCA to TCG). For RV Δ G-N*PEST-4Cre(EnvA), 30 of the 32 clones had no mutations in the sequenced region; one clone had a synonymous mutation in the N gene (Asn436, from AAC to AAT), and one other clone had a synonymous mutation in the PEST region (Pro5, from CCG to CCA) after the stop codon.

Supplementary File S8 (*separate file*): Counts and statistical analyses of labeled neurons in transsynaptic tracing experiments.

Sheet 1: Detailed cell counts of every (6th) brain section for all mice, including tdTomato+ cell numbers from ipsilateral cortex, contralateral cortex, and thalamus, as well as counts of starter cells for each animal;

Sheet 2: Total counts of labeled cells for each mouse in each condition, as well as the ratios of tdTomato+ cells to starter cells and the average numbers for each condition;

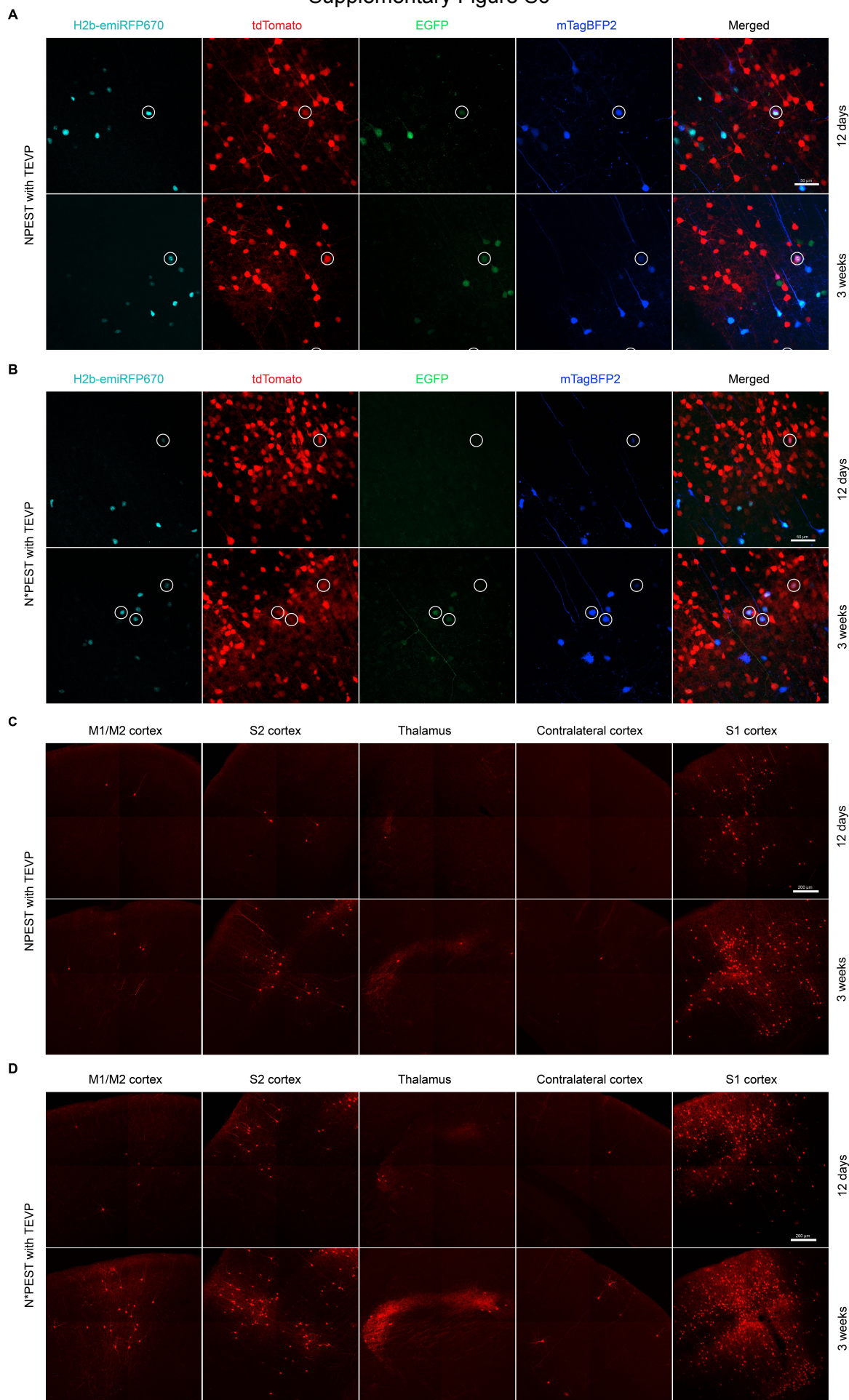
Sheet 3: P-values of comparisons using single factor ANOVAs.

Supplementary Figure S6: Images of starter cells and input regions with TEVP supplied.

A-B) Closeup images of virus injection sites in barrel cortex using NPEST (A) and N*PEST (B) viruses, with TEVP supplied in starter cells. Images are from the same sections as Figure 5C. The circled cells are "starter cells", defined as expressing both tdTomato (reporting Cre expressed by the rabies virus) and mTagBFP2 (coexpressed with G); many of these cells also express emiRFP670, coexpressed with TEVP from the third helper virus included in these cases. Scale bar: 50 μ m, applies to all images in each panel.

C-D) Images of regions presynaptic to barrel cortex for NPEST (A) and N*PEST (B) viruses, with TEVP supplied in starter cells. The NPEST virus has spread to the same input regions as has N*PEST, although to a more limited degree. Scale bar: 200 μ m, applies to all images in each panel.

Supplementary Figure S6



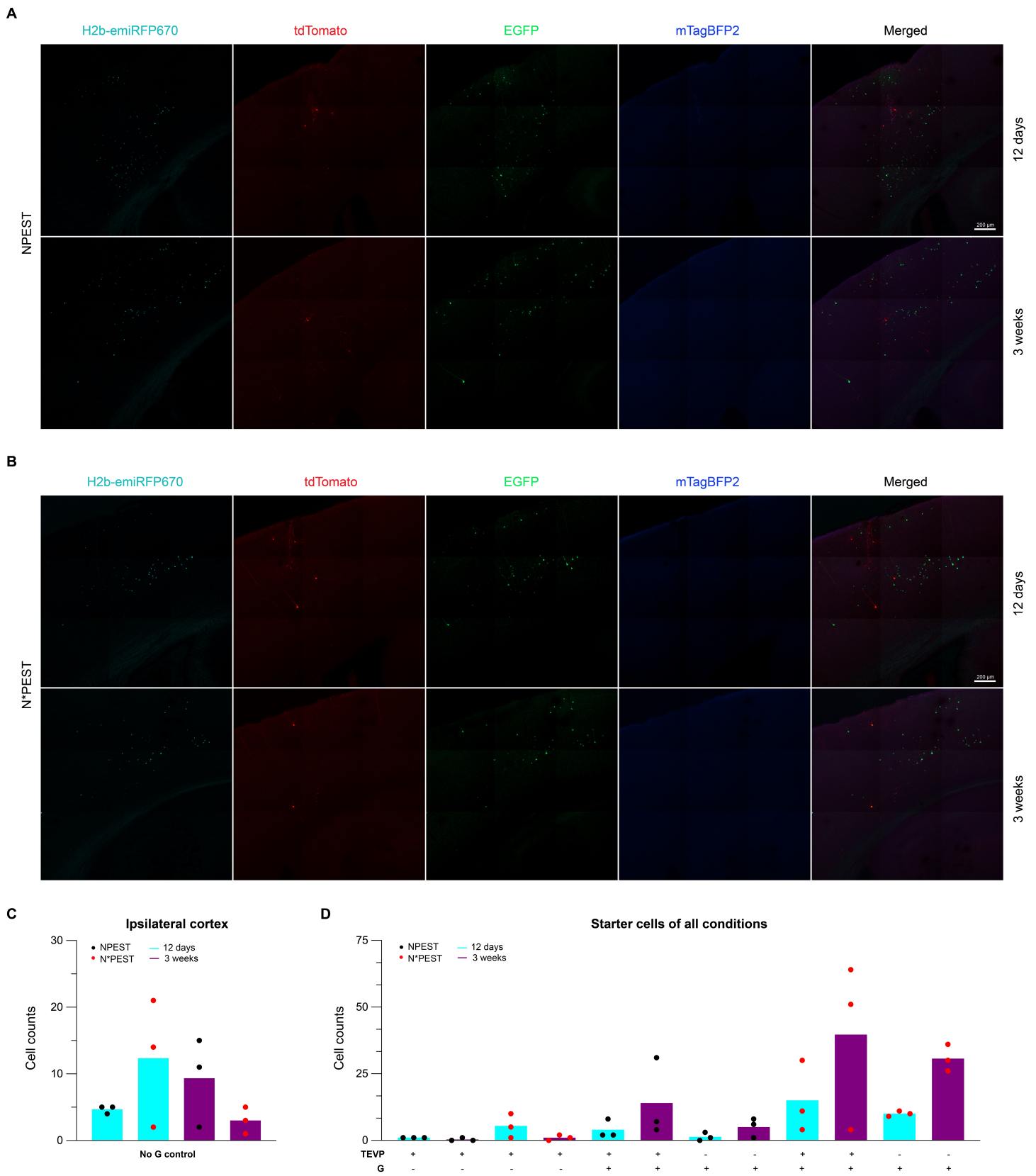
Supplementary Figure S7: Results for control experiments without G, and counts of starter cells for all conditions.

A-B) Images of injection sites for control experiments in which the helper virus expressing G was omitted (but in which the helper virus expressing TEVP was included), using NPEST (A) and N*PEST viruses. Neither virus spreads to any detectable degree without G. Scale bar: 200 μm , applies to all images in each panel.

C) Counts of tdTomato-labeled neurons in ipsilateral cortex for the controls without G.

D) Counts of "starter cells" (defined as cells coexpressing tdTomato and mTagBFP2 when TEVP was omitted, and cells coexpressing tdTomato, mTagBFP2, and emiRFP670 when TEVP was supplied) for all conditions.

Supplementary Figure S7



Supplementary Figure S8: First-generation vector RV Δ G-4FLPo appears to be toxic to most cells, unlike the comparable first-generation vector RV Δ G-Cre. Although we did not rigorously quantify the effect, our FLPo-encoding RV Δ G-4FLPo appears to kill neurons more quickly than does RV Δ G-4Cre (cf. Figure 3 and Chatterjee et al. (21)). In this example field of view, most neurons clearly visible at earlier time points have disappeared by 28 days postinjection, leaving degenerating cellular debris. See Discussion for possible reasons why a preparation of a first-generation vector encoding a recombinase may or may not preserve a large percentage of infected neurons. Scale bar: 50 μ m, applies to all panels.

Supplementary Figure S8

